HELLENIC REPUBLIC
National and Kapodistrian University of Athens
EST. 1837

School of Health Sciences
School of Medicine and Department of Pharmacy

Interdisciplinary M.Sc. course in

"Nanomedicine"

Academic year 2021-2022

"The use of gold nanoparticles for diagnostic and therapeutic approaches in ophthalmology: new developments and future perspectives"

Alexandra Kavalaraki

Supervisor: **Professor Efstathios Efstathopoulos**

Members of committee: **Scientific Collaborator Ellas Spyratou**
Assist. Professor Kalliopi Platoni

Date of Submission: *September 2022*

Acknowledgments

I would like to express my sincere gratitude to my supervisor, Prof**.** Efstathios Efstathopoulos, for giving me the opportunity to conduct my dissertation and for his continuous support and guidance throughout the research. Besides my supervisor, I would also like to thank the rest of the committee members, Scientific Collaborator Ellas Spyratou, and Assist. Prof. Kalliopi Platoni, for their support, their insightful comments, and their valuable advice in completing my dissertation.

I would also like to thank the faculty of the M.Sc. Course in Nanomedicine for their interesting lectures, which helped me delve into the fascinating field of Nanotechnology and gain a better understanding and a new perspective in Medicine.

Finally, I would like to acknowledge my family, who has always supported me through my academic accomplishments. Specifically, I would like to thank my parents, Manolis and Katerina, and my sister, Marianna, for their unconditional encouragement during my studies.

Table of Contents

Abbreviations

Akt	Protein Kinase B
AMD	Age-related Macular Degeneration
AuNcgs	Gold Nanocages
AuNPs	Gold Nanoparticles
BBB	Blood-brain barrier
bFGF	Basic fibroblast growth factor
BRECs	Bovine retinal endothelial cells
BRB	Blood-retinal barrier
BSS	Balanced saline solution
CA	Contrast Agent
CIS	Carcinoma In Situ
CNV	Choroidal Neovascularization
cSLO	confocal Scanning Laser Ophthalmoscope
CT	Computed Tomography
CTAB	Cetyltrimethylammonium bromide
DR	Diabetic Retinopathy
ERG	Electroretinogram
FFA	Fundus fluorescein angiography
FGF	Fibroblast growth factor
GNRs	Gold Nanorods
HB-GFs	Heparin-binding growth factors
HUVECs	Human umbilical vein endothelial cells
HRMECs	Human retinal microvascular endothelial cells
IV	Intravenous
LSPR	Localized Surface Plasmon Resonance
LCNV	Laser-induced choroidal neovascularization
NIR	Near-Infrared
NPs	Nanoparticles
OCT	Optical Coherence Tomography
OSSN	Ocular surface squamous neoplasia
PAI	Photoacoustic Imaging
PAM	Photoacoustic Microscopy
PAOM	Photoacoustic Ophthalmoscopy
PAT	Photoacoustic Tomography
PBS	Phosphate-buffered saline
PEG	Polyethylene glycol
ROP	Retinopathy of prematurity
RGD	Arginine-glycine-aspartic acid
SCC	Squamous Cell Carcinoma
TEM	Transmission Electron Microscopy
US	Ultrasound
VEGF	Vascular Endothelial Growth Factor

1 Abstract

Over the past few years, tremendous research concerning the possibilities of gold nanoparticles in medicine has been conducted. AuNPs are considered to be unique nanostructures due to their extraordinary chemical and physical properties. This dissertation aims to bring into light the potential applications of gold nanoparticles for both diagnostic and therapeutic purposes in ophthalmology. More specifically, attention will be drawn to the utilization of AuNPs as contrast agents (CA) in Optical Coherence Tomography (OCT) and Photoacoustic Imaging (PAI), two novel imaging modalities for the visualization of the eye. The in vitro, ex vivo, and in vivo studies investigating and supporting this concept will be presented thoroughly, to elucidate whether AuNPs are eligible for imaging enhancement owing to their optical characteristics. Then, the ability of gold nanoparticles to act as anti-angiogenic factors for the management of various ocular diseases will be presented and data from in vitro and in vivo studies will be analyzed. Finally, ocular distribution and biocompatibility of AuNPs will also be discussed. The dissertation's ultimate purpose is to overview the research work regarding the use of gold nanoparticles as contrast agents in imaging modalities and as anti-angiogenic factors against ocular neovascularization, thus improving both ophthalmic diagnosis and management. To our knowledge, this is the first work in current literature to investigate the use of gold nanoparticles as "theranostics" in ophthalmology, in hopes of unveiling potential future perspectives and encouraging further research.

Keywords: Gold Nanoparticles, Ophthalmology, Optical Coherence Tomography, Photoacoustic Imaging, Molecular Imaging, Ocular Angiogenesis, Toxicity

2 Introduction

Nanotechnology is one of the fastest advancing fields in scientific research. In 1959 *Richard P. Feynman* notably stated during the annual American Physical Society meeting that "There's Plenty of Room at the Bottom", in an attempt to present the enormous possibilities offered within this field and is therefore considered the father of nanotechnology [1]. Nevertheless, the term "nanotechnology" was first introduced by Japanese scientist *Norio Taniguchi* in 1974 and refers to the interdisciplinary branch of science dealing with the design, engineering, and application of materials and devices, whose dimensions belong in the nanoscale, namely their size typically ranges between 1-100 nm. A nanometer is equivalent to one billionth of the meter and materials belonging to this scale are associated with numerous extraordinary characteristics, which allow novel applications and revolutionary developments in a variety of sciences [2].

Nanoparticles (NPs) can be classified into different categories according to their morphological, mechanical and chemical characteristics, with the most prevalent being carbon-based NPs (fullerenes, carbon nanotubes), metal NPs (Au, Ag, Cu), semiconductor NPs, lipid-based NPs and polymeric NPs [3]. Nanomaterials present different physical, optical, chemical and electrical properties when compared to their bulk counterparts, which can be attributed to the surface and quantum effects. When the size of a material is decreased, a significant increase in the ratio of surface area to volume is to be observed. This improves the reactivity of the material's surface and affects the ability of the particle to interact with other materials and biological systems [4] [5].

The innovative applications of nanotechnology in medicine are described by the term "nanomedicine". In recent years, exponential growth in the medical field has been observed and scientific research is conducted with rapid progress. Nanotechnology has paved the way for the development of novel drug delivery systems with site-specific targeting, the design of nanovaccines, advances in tissue engineering, gene therapy, the enhancement of bioimaging, as well as the fabrication of nanobiosensors and monitoring devices [6] [7] [8]. This burgeoning in medical diagnosis and therapy can bring a positive impact on public health and improve the monitoring and management of various diseases in the following years.

Among the medicinal branches exploiting the advantages of nanomaterials and nanotechnology, Ophthalmology can also benefit from the introduction of this emerging science. According to World Health Organization, blindness and visual impairment affect more than 2.2 billion people worldwide, posing a paramount social and economic burden. The most prevalent diseases impairing visual acuity in the western world are cataract, age-related macular degeneration (AMD), diabetic retinopathy (DR), and refractive errors [9]. Therefore, it is imperative that early diagnosis and management of the above pathological entities be improved.

Nanotechnology can accelerate progress toward imaging and therapy in ophthalmology. Nanoparticles have already been employed for ocular drug delivery, due to their ability to be engineered in a way that allows them to transcend the physical and anatomical barriers of the eye [10] [11]. In this dissertation, the potential applications of gold nanoparticles will be illustrated. Gold nanoparticles present optical properties which can be advantageous for ocular imaging with Optical Coherence Tomography (OCT) and Photoacoustic Imaging (PAI). As a result, molecular imaging can be performed and allow diagnosis of the diseases at an early stage, before vision loss takes place. Gold nanoparticles also exhibit anti-angiogenic properties and could be used for the management of ocular diseases which are characterized by neovascularization. Therefore, gold nanoparticles are attractive candidates to be used as “theranostics” in ophthalmology, by combining their capacity of enhancing ocular visualization and management of neovascular conditions in the eye.

3 Theory

3.1 Imaging in Ophthalmology

3.1.1 Anatomy of the eye

Prior to attempting to study the imaging modalities currently being used in the field of ophthalmology, a brief description of the anatomical structures of the eye is required. The eye is a complex and highly specialized sensory organ, whose main functions involve the detection and focus of visual stimuli, as well as the conversion of light into electrical signals that are conveyed to the brain, in order to form an image and initiate the visual process. The ocular structures are enclosed by three layers [12].

The outermost fibrous layer consists of the sclera and the cornea, and is responsible for maintaining the rigidity of the globe of eye. The vascular layer lies beneath the fibrous layer, and is formed by blood vessels and connective tissue. It is compromised by the choroid, the ciliary body, and the iris. The third and innermost coat of the eye contains the retina, which is a light-sensitive layer of nervous tissue with the ability to transmit visual signals to central targets. The retina is structured of several layers consisting of neurons, photoreceptors cells, and blood vessels, which can be histologically divided into ten distinct layers: the inner limiting membrane (ILM), the retinal nerve firer layer (RNFL), the ganglion cell layer (GCL), the inner plexiform layer (IPL), the inner nuclear layer (INL), the outer plexiform layer (OPL), the outer nuclear layer (ONL), the external limiting membrane layer (ELM), the inner segment / outer segment layer (IS/OS), and finally the retinal pigment epithelium (RPE) [13]. The crystalline lens is located posteriorly to the iris and its primary function is to focus light on the retina. The vitreous body is a clear, semisolid gel structure that occupies the space between the lens and the retina [14] [15]. The major structures of the eye are seen in Figure 1.

The blood-retina barrier (BRB) consists of both the inner and the outer barrier. The outer BRB is formed at the level of the RPE cell layer, and its main function is the regulation of the movement of solutes and nutrients from the choroid to the subretinal space. The inner BRB is similar to the blood brain barrier (BBB) and lies in the inner retinal microvasculature,

formed by the microvascular endothelium lining these vessels. The tight junctions between these cells mediate highly selective diffusion of molecules from the blood to the retina, rendering this barrier essential in maintaining homeostasis of the retinal tissues [16] (Figure 2).

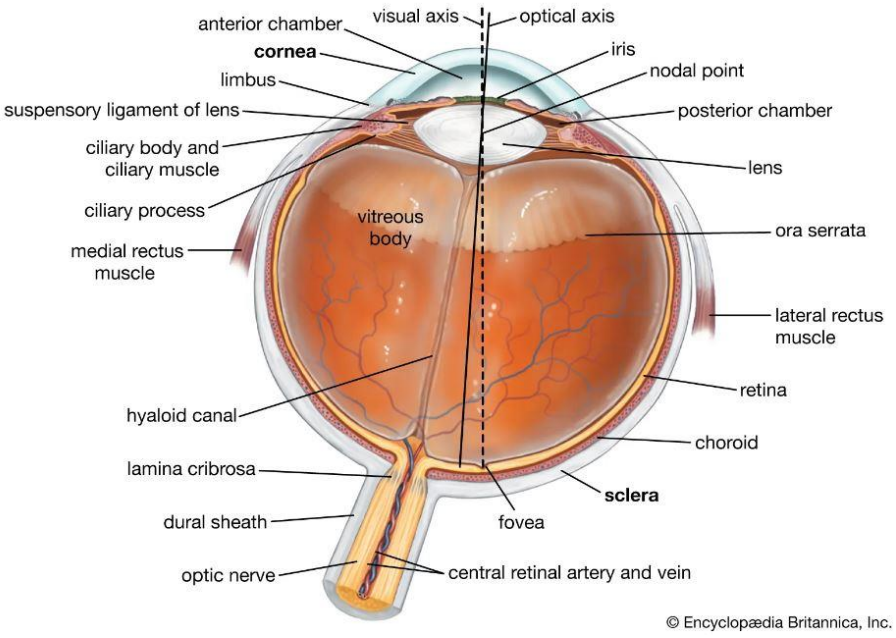

Figure 1. Anatomy of the human eye (horizontal cross section). Obtained from *Encyclopædia Britannica, Inc.*

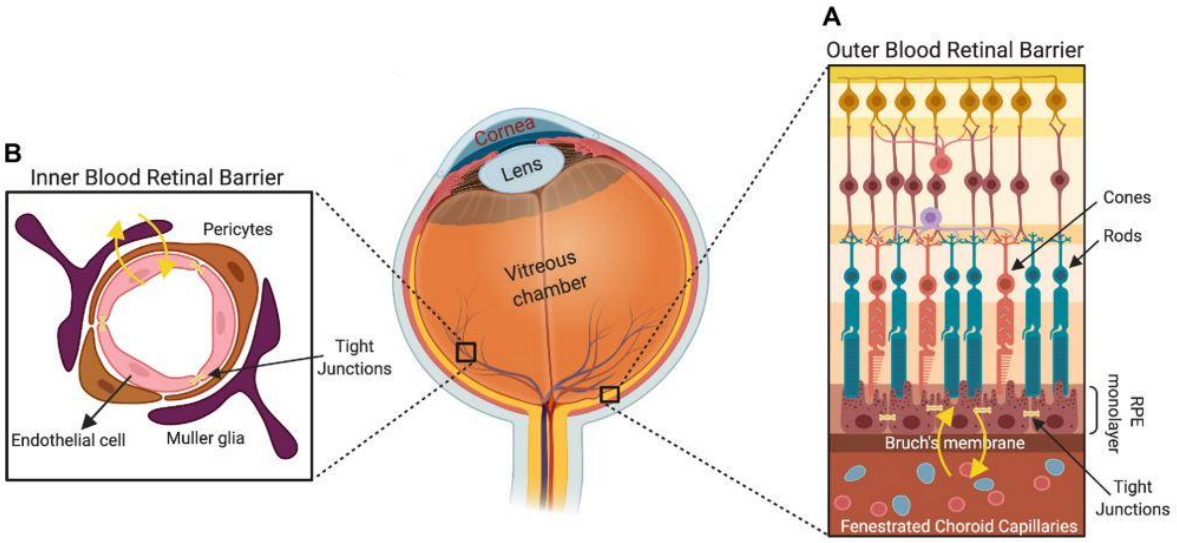

Figure 2. The retina is the innermost ocular structure and is responsible for the translation of light into electrical signals. The BRB consists of the inner and outer barrier. The outer BRB (a) consists of the RPE, whereas the inner barrier (b) includes the tight junction of between endothelial cells. Figure reprinted from *Sharma et al*. [17]

3.1.2 Novel imaging modalities in Ophthalmology

Over the last two decades, ophthalmic imaging has been gaining significant importance, becoming an indispensable part in the clinical diagnosis and management of various ocular diseases, affecting both the anterior and posterior segment of the eye [18]. The development of new imaging techniques was marked by such great advancements, that led to the shifting of their role from simple photographic documentation to highly advanced diagnostic tools, allowing the objective assessment of various ocular structures in detail, unavailable to conventional examination techniques. This progress enabled clinicians to gain a better understanding of ocular health and disease, as well as a new insight into previously undiagnosed conditions [19]. Presented below are the most commonly used ophthalmic imaging modalities in clinical practice, mainly focusing emphasis on the recent advances in eye imaging techniques and clinical applications.

Fundus fluorescein angiography (FFA) is an invasive diagnostic procedure, which allows the assessment of the structure, physiology, and pathology of the retinal circulation, by using different barrier and excitation filters. FFA involves the intravenous injection of sodium fluorescein, a small-sized molecule that can easily diffuse through the retinal capillaries forming the inner blood-retina barrier and can therefore indicate retinal areas of disrupted blood-retina barrier through leakage. However, FFA is not suitable for detailed imaging of the choroidal circulation due to profound dye leakage from the fenestrated choroidal blood vessels. Following the administration of fluorescein, a series of several normal phases can be identified in the retinal circulation. Understanding these normal phases, as well as detecting and interpreting defects in each phase, is deemed essential for the accurate diagnosis and evaluation of various ocular pathologies [19] [20] [21].

Indocyanine green angiography (ICGA) is another invasive diagnostic procedure, used for visualizing the choroidal vasculature. It incorporates the intravenous administration of indocyanine green, a larger molecule which cannot escape from the choriocapillaris, and therefore allows imaging of the choroidal circulation when combined with the use of an infrared camera. It slowly diffuses through the choroidal, staining in the choroid over the

course of 12 minutes after injection. ICGA can provide useful information in the detection and follow-up of various choroidal disorders, including central serous chorioretinopathy, polypoidal choroidal vasculopathy, occult CNV in AMD, as well as intraocular tumors and inflammatory conditions.

Ocular ultrasonography is a safe, non-invasive diagnostic tool, routinely used in clinical practice for the assessment of anatomical ocular integrity and pathology. B-scan provides two-dimensional cross-sectional images of the eye and orbit, using combined multiple A-scan echoes. It enables indirect visualization of intraocular lesions in patients with anterior segment opacities that obscure imaging i.e. corneal opacities, dense cataracts, or vitreous hemorrhage. The resolution of standard clinical US is defined by the sound wavelength in ocular tissue to about 150 μm. However, B-scan ultrasonography represents an important adjuvant in the assessment of ocular pathologies by obtaining information not accessible through clinical examination alone [22] [23] [24].

In this dissertation, emphasis will be given to two novel imaging modalities: Optical Coherence Tomography (OCT) and Photoacoustic Imaging (PAI). More specifically, interest will be focused on how nanotechnology can improve these techniques and enhance progress in ocular imaging in the future.

3.1.3 Optical Coherence Tomography

Optical Coherence Tomography (OCT) was first introduced in 1991 by *Huang et al*. [25]. They presented a non-invasive technique which uses low-coherence interferometry and achieves cross-sectional 2D imaging of internal biological structures by measuring their optical reflections. The system is based on a Michelson interferometer, which calculates the interference signal from a sample and the reference beam (Figure 3)

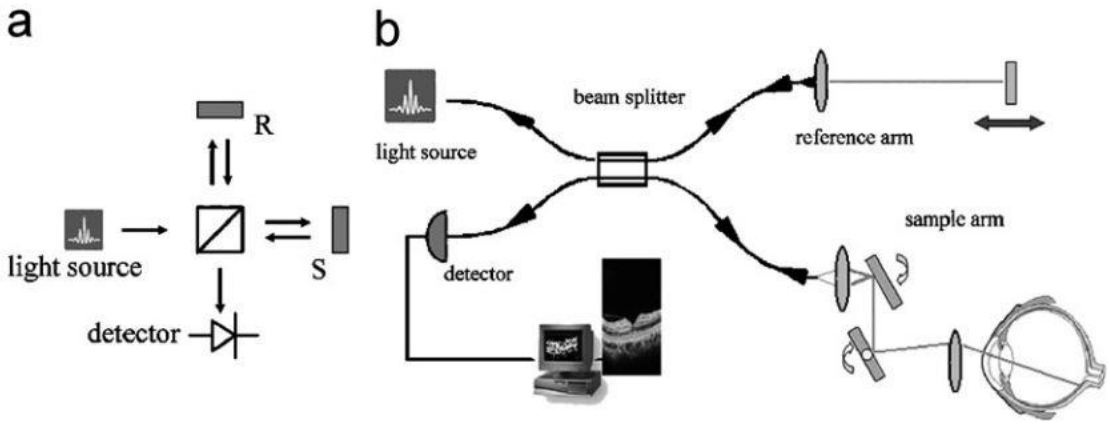

Figure 3. OCT is based on low-coherence interferometry, where the light returning from the eye interferes with light from a known path length. This is achieved with the help of a Michelson interferometer (a) and a fiber-based OCT setup (b). Light emitted from a source is divided in two directions towards two mirrors, the reference (R) and the sample (S). This interference pattern allows the establishment of the degree and depth of reflectivity in the imaging tissue. [26]

Optical signals transmitted through or reflected from tissues provide information acquired from the time-of-flight delay, which in turn offers spatial data of the tissue microstructure. It is similar to the philosophy behind ultrasound, but this time the optical reflectivity is calculated instead of the acoustic one. Most OCT systems use near-infrared (NIR) light (around 850 nm), since it has the benefit of deeper tissue penetration [27] [28]. OCT offers the advantage of longitudinal and lateral spatial resolution of micrometers and depth penetration of millimeters (10 μm). This high depth resolution is particularly useful for imaging deep tissues in the posterior segment of the eye, like the intraretinal layers [29] [30] [31] (Figures 4 and 5).

Since then, this imaging modality has become a key diagnostic tool in the field of ophthalmology and is considered to be a gold standard for the detection of a wide range of diseases and pathological conditions of both the anterior and posterior segment of the eye. Among those belong age-related macular degeneration (AMD), macular edema, choroidal neovascularization (CNV) and glaucoma [32] [33] [34] [35]. One of the most important traits of OCT over conventional imaging modalities like FA and ICG angiography is the ability of non-invasive imaging of retinal anatomy and morphology. However, one of its major disadvantages is the fact that it mainly provides us with structural information about the tissue.

In order to improve the OCT images, researchers have combined novel imaging technologies with OCT systems, known as OCT adjuncts. The OCT technique used in clinical practice is called time-domain OCT, because a sequence of samples revealing depth information are obtained over time [26]. Other adjuncts include photothermal OCT (PT-OCT), which can identify thermal changes which affect the optical path, and Spectral Domain OCT (SD-OCT) [36] [37]. With OCT angiography (OCTA) [38] we are able to image blood vessels and evaluate retinal blood flow, polarization-sensitive OCT (PS-OCT) [39] uses the birefringence of the retina to provide contrast and optical coherence elastography (OCE) [40] gives us information about the corneal mechanical characteristics. The vascular blood flow can also be measured with the assistance of Doppler-OCT, which detects phase changes [41] [42].

It is worth mentioning that aside from ophthalmology, OCT is considered to be a revolutionary imaging system in other fields of medicine for the visualization of a variety of tissues, including the gastrointestinal tract and vascular tissues [43] [44].

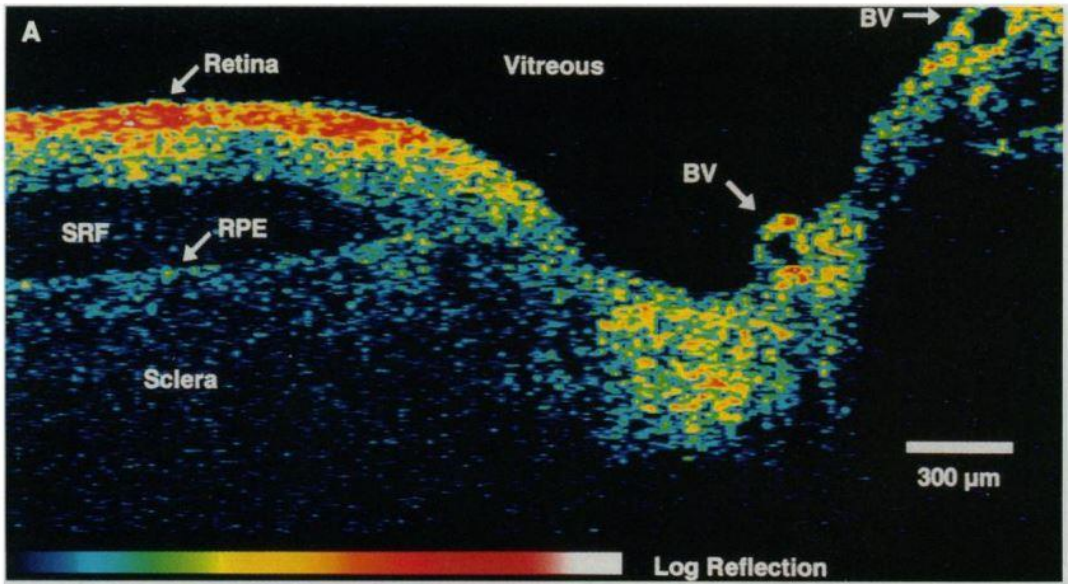

Figure 4. OCT image of the retina and the optic disk of the human eye as presented by *Huang et. al* [25] The cornea and the lens were removed and the OCT beam was focused on the retina. The structures to be seen are the vitreous, the retina, the subretinal fluid (SRF), the retinal pigment epithelium (RPE), the choroid, the sclera and blood vessels (BV). The anatomical structures visualized by OCT correlated with the histological analysis.

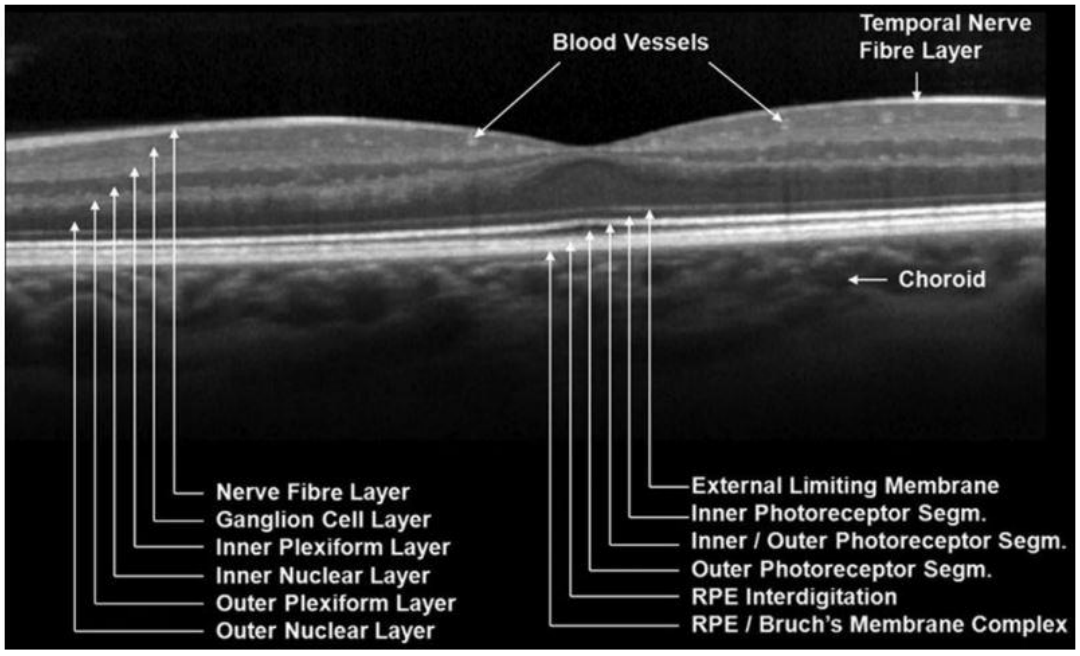

Figure 5. Cross sectional OCT images of the healthy human retina. The retinal layers are shown with arrows. [45]

3.1.4 Photoacoustic Imaging

Photoacoustic imaging (PAI), also known as optoacoustic imaging, is an emerging non-ionizing imaging modality, which is characterized by the combination of the high contrast of optical imaging as well as the high spatial resolution of the US [46] [47]. It is a non-invasive technology based on the photoacoustic effect, which was first observed by *Alexander G. Bell* in 1880 [48]. The PA effect concerns the acoustic wave production as a result of the optical irradiation of biological tissue through a pulse laser beam. Endogenous chromophores or exogenous contrast media absorb the energy of the light, and heat is released due to thermoelastic relaxation. The occurring pressure waves, named PA waves, are then detected by the US transducer, and image is reconstructed. PAI is a technology which merges light and sound and the term "Light In and Sound Out" is therefore used to describe this technique [47].

Over the last years, the interest in the use of this imaging modality has been growing rapidly [49]. Photoacoustic imaging differs from other imaging modalities like OCT and US, in the sense that it portrays optical absorption and is not influenced by the mechanical and elastic characteristics of the tested tissue [50]. Thus, it allows us to gain anatomical, structural as well as molecular knowledge concerning a tissue with a high spatial resolution (as low as 5 μm) in real-time and higher penetration depth [51] [52]. In the NIR, the tissue absorption and background scattering generated are low, therefore allowing penetration depth of several centimeters and resolution of a few hundred micrometers. This wavelength region is referred to as the "tissue transparency window" [53].

Three groups of PAI are recognized: Photoacoustic Tomography (PAT), Photoacoustic Microscopy (PAM) and Photoacoustic Endoscopy (PAE) [54]. Additionally, photoacoustic imaging can be employed in combination with OCT or other imaging technologies, using a multimodal imaging system with a different or mutual light source, to provide more information regarding the target tissue. [55].

Since *Wang et al*. [56] used PAI to view the hemodynamic responses in rat brain, the application of PAI in different medical fields has been encouraged, including cardiology and

oncology [57] [58]. The introduction of PAI in ophthalmology has also been suggested and appears to be promising, due to the presence of endogenous light-absorbing molecules within the eye; melanin and hemoglobin [59] [60]. These molecules provide intrinsic tissue contrast and enable structural and physiological imaging of blood vessels and ocular tissues containing melanin, such as the iris, the choroid and the RPE. This could be beneficial for the diagnosis and monitoring of ocular pathological conditions and diseases, which affect the presence of the aforementioned molecules. Examples include neovascularization in AMD and ocular tumors, as well as pigmentary disorders.

Even though PAI exhibits various benefits, it has not yet been implemented in ophthalmology. Research groups endeavor to design an ocular photoacoustic imaging system that could be applicable to humans, but further investigation is necessary. Photoacoustic Ophthalmoscopy (PAOM) has also been designed by research groups with the purpose to study the tissues of the posterior segment of the eye of small animals [54]. Figures 6 and 7 represent images from PAI systems that have been engineered for ocular imaging in animals in vivo.

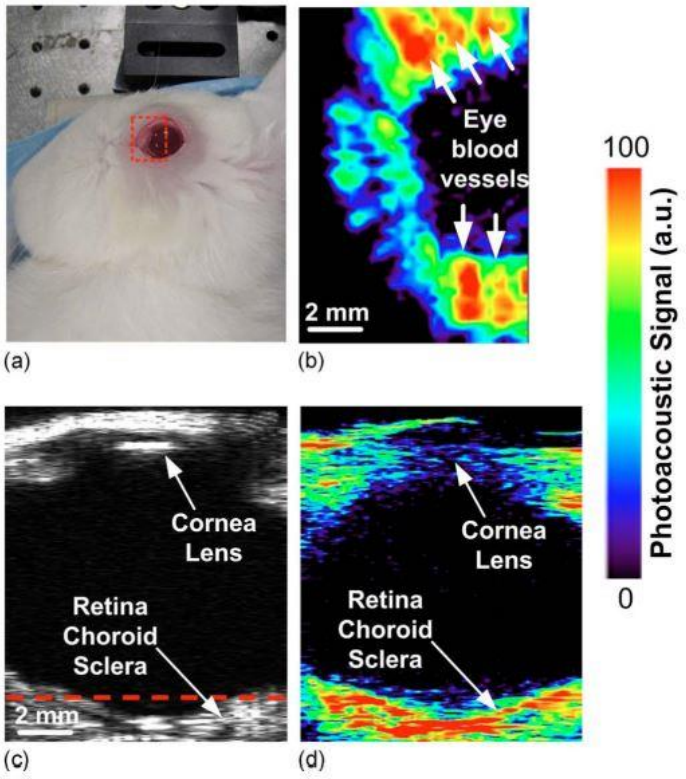

Figure 6. *De la Zerda et al*. [61] designed a PAI system for the visualization of the blood distribution in rabbit's eye in vivo. The PA image was taken at a wavelength of 740 nm. The red box in the photographic image (a) shows the region of the horizontal photoacoustic image (b). The vertical US image (c) demonstrates the depth of the horizontal image with the dashed red line. Vertical PA images (d) indicate that this system was able to detect the deeper layers of the posterior segment of the eye (retina, choroid) and achieve penetration with high depth.

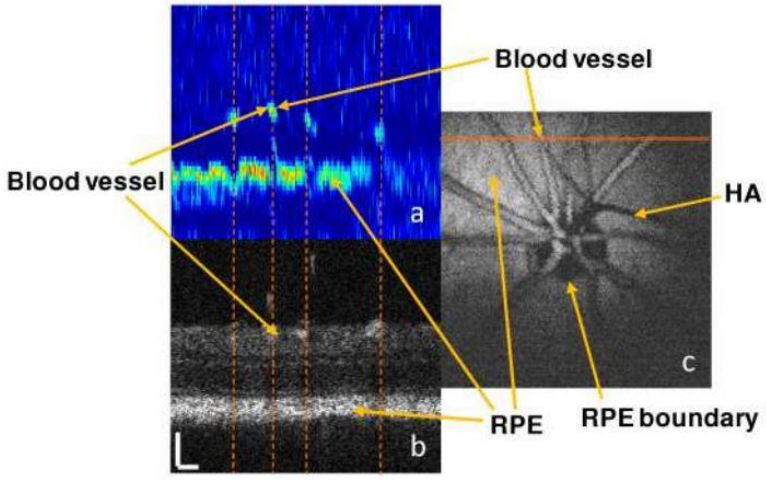

Figure 7. A photoacoustic ophthalmoscopy for in vivo imaging of the rat retina was created by *Jiao et al*. [62]. PAOM B-scan image shows regions of high PA signals which correspond to the presence of hemoglobin/blood vessels and melanin/RPE layer, which is seen as a line of high signal amplitude. The vertical lines represent the position of the vessels. OCT image was also received at the same time (b). The maximum-amplitude-projection (MAP) of the PA set (c) shows the RPE boundary.

3.2 Molecular Ophthalmic Imaging

Even though a variety of ocular imaging modalities are currently being used in clinical practice, there are still limitations to be dealt with. Morphological changes linked to diseases are often revealed and can be detected after functional and molecular changes have already manifested [63]. The disease has often developed to the point that structural damage to the tissue has already taken place. This is particularly seen in retinal diseases, which can lead to vision loss before alterations in the tissue can be visualized [64]. As a result, the early diagnosis of ocular diseases still remains a challenge for physicians, and the necessity for the advancement of molecular imaging in ophthalmology is growing. Molecular Imaging (MI) aims to detect functional as well as molecular changes in the eye and the introduction of exogenous contrast agents in traditional imaging modalities can enhance the signal and help us visualize and quantify molecular and biological processes non-invasively [26] [65]. This can allow physicians to diagnose diseases at an early stage and monitor their progression effectively.

3.2.1 Contrast Agents for OCT

OCT does not require the addition of a contrast agent to function and provide us with structural information about the eye; conventional OCT contrast is provided by the interaction between matter and light; namely optical absorption and scattering of the examined tissue. Spatial variations in the tested tissue are able to function as an endogenous source of contrast, due to the different scattering properties that they present. However the concept of using an exogenous imaging agent to improve image quality and enhance contrast has been a subject of great interest for researchers.

Designing contrast agents compatible with the OCT system can be challenging since it uses a coherent light source and therefore cannot visualize contrast agents which disrupt this technology, such as fluorophores and other dyes [66]. Contrast agents to be utilized in OCT, need to be able to absorb or reflect light in the spectral range of the system, after having

reached the tissue that needs to be imaged. Moreover, the developed contrast agents should be non-toxic, photostable, biodegradable, and able to avoid clearance by the human reticuloendothelial system (RES), to prolong circulation time [67]. Over the years, several imaging agents have been suggested for the enhancement of scattering in OCT imaging. Among those belong microbubbles [68], engineered microspheres [69] [70], melanin and near-infrared light-absorbing dyes (e.g. indocyanine green) [71] [72]. Metallic nanoparticles have also been proposed as CA, including ferrous and gold nanoparticles [73] [74].

3.2.2 Contrast Agents for Photoacoustic Imaging

Similarly, the operation of the photoacoustic imaging system also does not demand the application of an exogenous imaging agent, as it relies on the contrast produced by endogenous chromophores and intrinsic tissue contrast. This implies, that PAI offers molecular imaging without the administration of exogenous media, through the usage of various wavelengths (multispectral imaging) to obtain information from already existing molecules. To achieve high photoacoustic contrast, the utilization of imaging probes with high photothermal conversion ability is favorable [75]. However, as in the case of OCT, a variety of exogenous contrast agents have been used or suggested for the improvement of photoacoustic imaging. In the case of ocular imaging, this means that information regarding hemodynamic changes within the vessels of the eye, like blood flow and oxygen saturation, will be available to physicians.

Several agents have been tested, including small chromophores, small molecules NIR dyes (like indocyanine green, squaraines, rhodamines, Evans blue dye), and fluorescent proteins [67] [76] [77]. Nanoparticles have also been administered as contrast agents. Among the CA in use belong polymer NPs, nanomaterials made from carbon, semiconductor and plasmonic materials [78] [79] [80] [81]. Au nanoparticles are the most studied type of metallic NPs, due to their unique optical properties [82] [83] [84].

3.2.3 Gold Nanoparticles as Contrast Agents

Gold Nanoparticles (AuNPs) are one of the most studied types of nanostructures for application in bioimaging, due to their highly favorable properties for in vivo imaging. They are characterized by facile fabrication, chemical stability and biocompatibility. Furthermore, gold nanoparticles can be functionalized with antibodies, enabling the targeting of specific tissues and the design of functionalized contrast agents [85] [86]. Nevertheless, their versatile optical properties are probably their most important feature, as they allow the control of their function by changing their shape, size and other parameters. The main characteristics of gold nanoparticles and their optical properties are presented below with the aim of elucidating their potential function as contrast media in imaging modalities.

3.3 Gold Nanoparticles

Gold is a noble metal and is considered to be one of the least reactive metals. It is characterized by its high resistance to oxidation and corrosion. When gold is processed to belong in the nanoscale, it presents numerous unique physicochemical characteristics that are not seen in the bulk form or molecular scale [87]. The use of colloidal gold was first introduced during ancient times as a therapeutic and decorative means in China and Egypt. A famous example of the decorative application of gold is the Lycurgus cup (Figure 8), designed in 400 A.D., which presents color change by reflecting green light and transmitting red light, and can be found in the British Museum [88]. The optical properties of gold nanospheres and their fascinating variations in color were also exploited over a thousand years ago, to create colorful glasses in medieval European churches.

Figure 8. The vivid colors of nanoscale gold were perfectly illustrated by Romans in 400 A.D. through the design of the Lycurgus cup. The cup presents different colors when the light is reflected (a) or transmitted (b). This artwork is considered to be a milestone in the history of nanotechnology during ancient times. Obtained from *The Trustees of the British Museum / Art Resource, NY*

Apart from decorative purposes, the use of colloidal gold has been investigated and employed for the management of various diseases [89]. The oldest preserved book that describes the AuNPs medicinal applications was published at the beginning of the 17th century by *Francisco Antonii* [90]. Since then, plenty of research has been conducted in quest of the therapeutic features of gold. In 1925, the use of gold complexes against rheumatoid

arthritis was examined through clinical trials [91]. The effect on the progress and management of various other diseases has also been studied, including syphilis, tuberculosis and discoid lupus erythematosus [92].

Even though the use of gold nanoparticles in medicine has a long history, tremendous progress has been noted in the biomedical field during the last decades. Their fascinating properties explain the ascending interest in their study and their application for various medicinal purposes. More specifically, AuNPs have found appliances in bioimaging, drug delivery, photothermal therapy, gene delivery, tissue engineering, colorimetric sensing and, foremost, cancer therapy [93]. Advances in oncology with the use of AuNPs include drug delivery, photodynamic therapy, photothermal therapy, and imaging. The term "theranostics" is commonly used to describe the dual ability of gold nanoparticles to provide therapy and diagnosis simultaneously (therapeutics & diagnostics) [94] [95].

The biomedical applications of AuNPs are directly linked with their physical and optical properties, which are reported in depth below. Moreover, in vitro studies have proved the high colloidal stability as well as low acute toxicity of AuNPs and biocompatibility, which makes them even more attractive candidates for biomedical applications [96].

3.3.1 Synthesis of Gold Nanoparticles

During the 19th century, *Michael Faraday* was the first scientist to report the synthesis of colloidal gold nanomaterials in the literature [97]. He noticed that the use of phosphorus as a reduction agent for gold chloride produced particles that created a ‘‘beautiful ruby fluid’’. He realized that the color of these ‘‘fine particles’’ was due to their interaction with light. This inspired the theoretical work by a German physicist called *Gustav Mie*, who, using the Maxwell equations, explained that the ruby color of a spherical AuNP solution relates with the absorption and scattering of the light interacting with it, at the beginning of the 20th century [98].

Regarding the synthesis of nanomaterials nowadays, two different techniques can be applied: either a “bottom-up” or a “top-down” strategy. The “bottom-up” synthesis describes the use of physical or mechanical methods to “break down” bulk materials for the production of nano-sized materials. This technology includes the use of procedures like lithography, etching and mechanical grinding (Figure 9). “Top-down” protocols, on the other hand, represent the fabrication of NPs through molecular or atomic assembling. Spherical gold nanoparticles are principally synthesized with a “bottom-up” technique, using a reducing agent such as $NaBH_4$ or sodium citrate, for the reduction of Au (III) ions [87]. The concept of citrate reduction of Au (III) to Au (0) in water was first established by *Turkevitch et al*. [99] during the 20th century, and this technique is still employed nowadays. The green synthesis of AuNPs through plants’ secondary metabolites and other raw materials has also been a subject of scientific research over the last years [100].

The fabrication of AuNPs is often characterized by poor colloidal stability and aggregation. Gold nanoparticles can be stabilized with the addition of various molecules through thiol-gold interactions [101]. *Giersig and Mulvaney* [102] revealed that AuNPs can be stabilized by thiolates via a sulfur bond. The Shiffrin–Brust biphasic synthesis, which is commonly used, is based on sulfur coordination and uses $HAuCl_4$, a thiol, tetraoctylammonium bromide and $NaBH_4$ [103]. To earn better stability, surfactants like CTAB (cetyltrimethylammonium bromide) or agents that control the surface are often added [104]. Such surfactants are also used for the fabrication of anisotropic AuNPs [105]. However,

the addition of CTAB can increase toxicity and has led to cellular necrosis when tested in vitro [106]. In order to reduce cytotoxicity, achieve better stability as well as increase the ability of gold nanoparticles to conjugate with other molecules, their surface can be functionalized with PEG or silica [107].

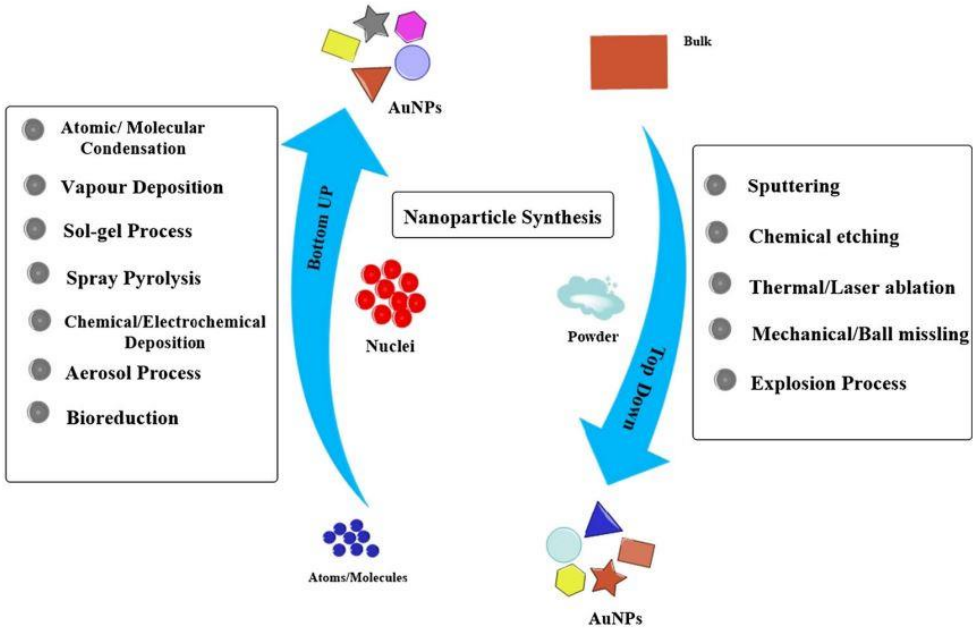

Figure 9. Physical, chemical and biological methods for Top–down and Bottom–up synthesis of AuNPs as demonstrated by *Ovais et al*. [108]

Apart from gold nanospheres, gold nanoparticles of various sizes and shapes have been engineered with appropriate methods over the years, including nanorods [109], nanoshells [110], nanocages [111], nanostars [112], nanodisks [113] and nanoprisms [114]. Figure 10 demonstrates TEM images of AuNPs with different geometries and sizes. Each of these AuNPs displays special physical and chemical properties, which will be elucidated below.

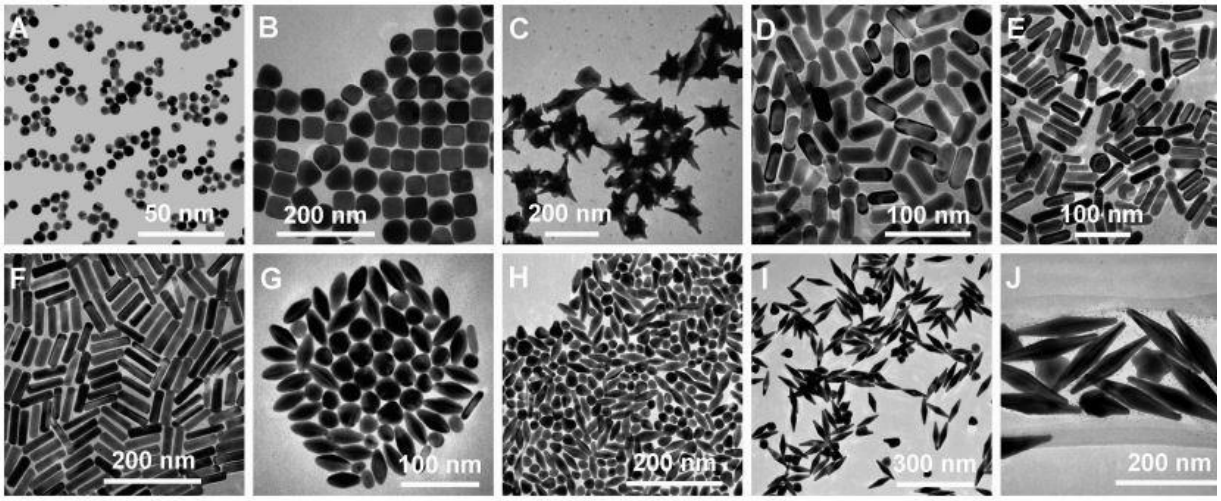

Figure 10. TEM images of AuNPs of various shapes and sizes: nanospheres (A), nanocubes (B), nanobranches (C), nanorods with aspect ratio of 2.4 ± 0.3 (D), nanorods with aspect ratio of 3.4 ± 0.5 (E), nanorods with aspect ratio of 4.6 ± 0.8 (F) and nanobipyramids with aspect ratio of 1.5 ± 0.3 (G), nanobipyramids with aspect ratio of 2.7 ± 0.2 (H), nanobipyramids with aspect ratio of 3.9 ± 0.2 (I) and nanobipyramids with aspect ratio of 4.7 ± 0.2 (J). Figured obtained from *Chen et al*. [115]

3.3.2 Localized Surface Plasmon Resonance

Noble metals, like gold, are characterized by the collective oscillation of the conductive electrons when an electromagnetic field is applied. This means, that the oscillation of the free electrons is driven by an alternating electric field at an eigenfrequency (ω_p), which is relative to the lattice of positive ions [116]. This phenomenon is commonly known as Localized Surface Plasmon Resonance (LSPR), as it leads to the formation of the localized surface plasmon, which can be characterized as a "negatively charged cloud" (Figure 11). This process involves two types of interactions between light and matter: scattering, which results in the light being re-radiated in different directions, but at the same frequency, and absorption, which causes the conversion of light to heat [87]. Metal particles that belong to the nanoscale are capable of intensifying the electromagnetic field applied near their surface and their optical absorption lies in a spectrum with a maximum at the plasmon resonance frequency [117].

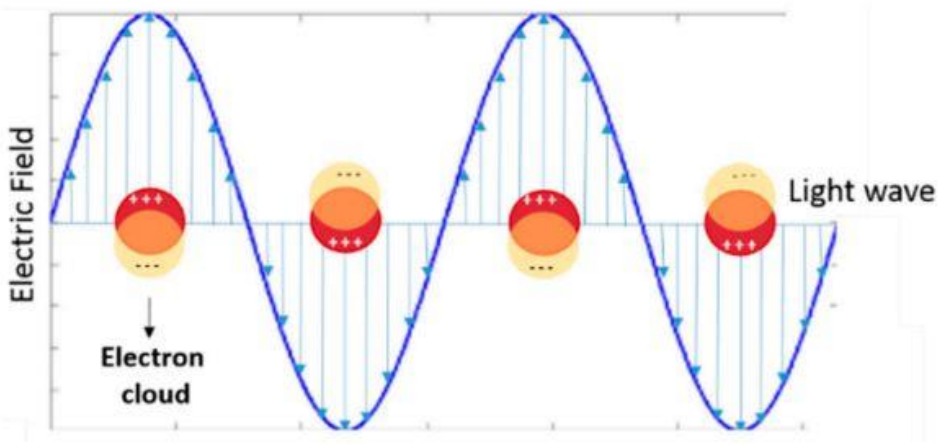

Figure 11. Graphical illustration of Localized Surface Plasmon Resonance (LSPR) band as presented by *Kohout et al*. [117]. The yellow circle represents the negative electron cloud and the red one the positive electron cloud.

The collective oscillation of the conductive electrons results in photon absorption at different wavelengths, a phenomenon depending on a number of parameters, such as shape

and size. The way gold nanoparticles interact with light explains the intense colors that gold nanoparticles present, as opposed to the yellow color of gold in its bulk form (Figures 12 and 13) The LSPR parameters of a gold nanostructure (peak position and scattering to absorption ratio) are highly dependent on a variety of parameters such as its size, shape, aggregation, morphology, and surrounding environment [96] [118]. The interaction of gold nanoparticles with light explains the different colors. It should be noted that the plasmon resonance of gold nanoparticles cannot be detected if their diameter is less than 3 nm, because molecular orbitals are created rather than conduction bands [119].

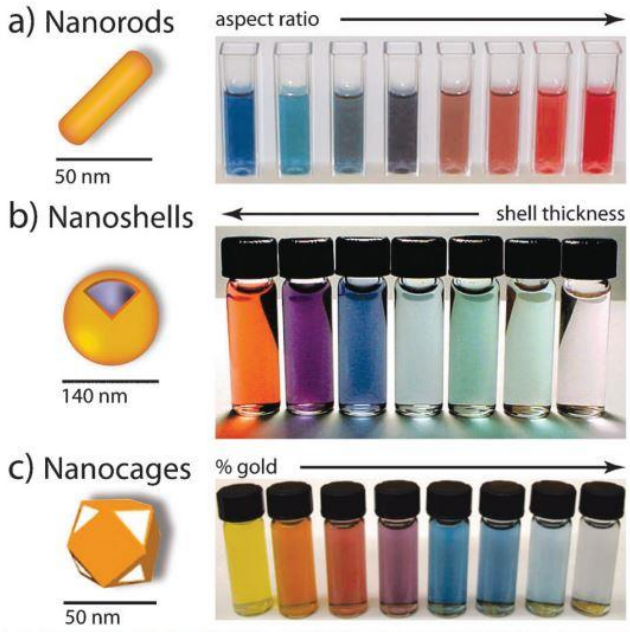

Figure 12. Au nanoparticles commonly used for biomedical purposes exhibit different colors due to their interaction with the light at various wavelengths. This phenomenon can be explained by the shift in the LSPR peak, depending on the morphology of the gold nanoparticles.
Gold nanorods are affected by the aspect ratio (a), gold nanoshells are affected by the shell thickness (b) and gold nanocages are affected by the galvanic displacement by gold (c).
Photo obtained from *Dreaden et al*. [120].

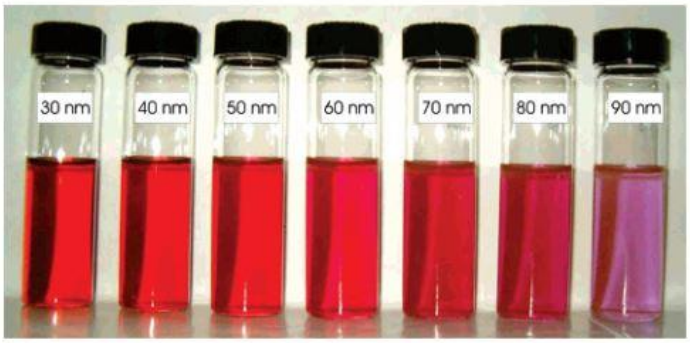

Figure 13. Vials containing Au nanospheres with diameters ranging from 30 to 90 nm exhibit different colors. Thus, size alone is capable of changing the optical properties of AuNPs. Photo obtained from *Njoki et al*. [121]

The alteration of the above factors strongly affects the LSPR and enables the shift of the absorption band within the visible to the near infrared region (NIR). The electromagnetic spectrum and the types of electromagnetic radiation can be seen in Figure 14. The NIR is distinguished into two regions: the NIR I (650 nm–950 nm) and NIR II (1000–1350 nm). This range of the spectrum is considered to be beneficial for optical imaging in medicine because it allows light to penetrate deeper tissues [122] [123]. This can be explained by the fact that light absorption by tissue components, including hemoglobin, water and intrinsic chromophores, is minimum in this region of the electromagnetic spectrum [28]. Therefore the term “tissue transparency window” or “optically clear window” is often used to characterize the NIR [124].

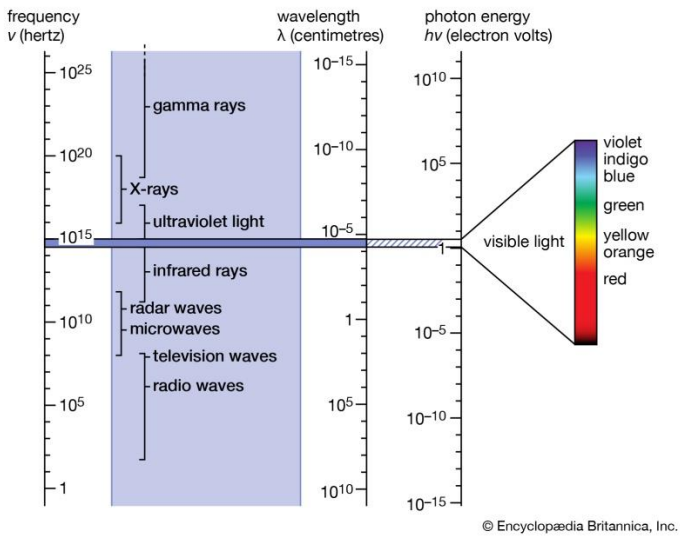

Figure 14. The electromagnetic spectrum. The narrow range of visible light is depicted on the right.
The first near-infrared (NIR-I) window corresponds to 650–950 nm and the second near-infrared (NIR-II) to 1000–1350 nm.
Obtained from *Encyclopædia Britannica, Inc.*

Regarding the absorption band of gold nanostructures, the shift to the NIR can be achieved either through the interaction between spherical nanoparticles, such as aggregation, or by designing nanoparticles with a non-symmetrical morphology, which are named anisotropic NPs.

The absorption peak of Au nanoparticles can be tuned within the broad range of 520–1415 nm [63]. Gold nanospheres with a diameter of 50 nm have an LSPR peak of around 520 nm, which is too limited to be suitable for in vivo imaging (Figure 15a). The peak absorption

at this wavelength (green color) interprets the ruby red color which Faraday noticed in the Au colloid samples, taking into account that it is the complementary color of green. However, when the diameter of the Au nanospheres is raised to 100 nm, the LSPR peak displays a small red- shift to 550 nm, which is still not appropriate for in vivo application [125]. This indicates that it is not feasible to regulate the peak in the range of 700− 900 nm and at the same time keep the size below 100 nm when it comes to gold nanospheres (Figure 15b).

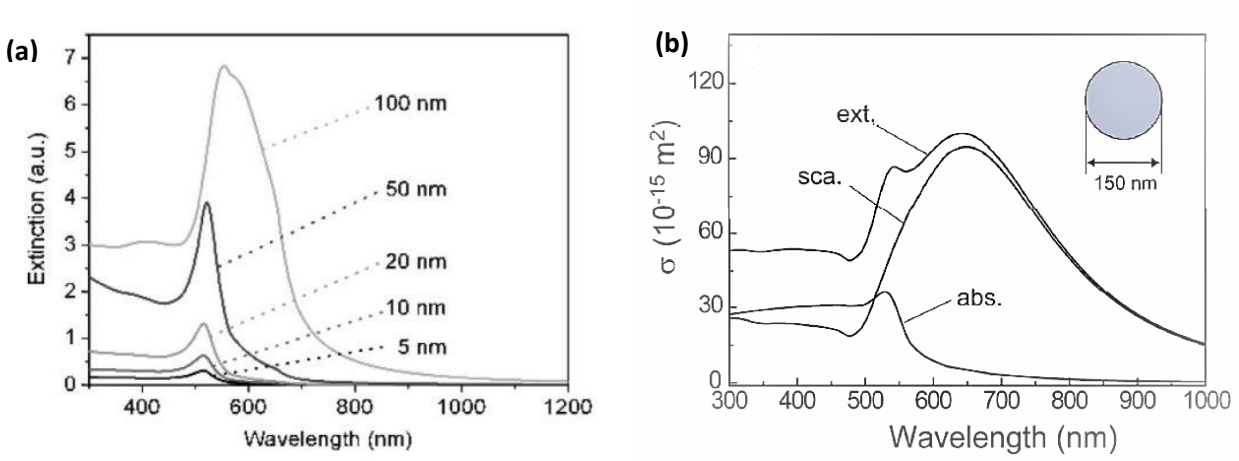

Figure 15. The extinction spectra (scattering and absorption) for gold nanospheres of various diameters were calculated using the Mie theory (a). The LSPR absorption peaks are detected at ca. 520 nm. The increase in the size of Au nanospheres creates a small red shift of the LSPR, which also appears broader [126].
The LSPR spectra compare the ratios of scattering to absorption for gold nanospheres. It can be noted that the LSPR peak is below 700 nm for Au nanospheres with a diameter of 150 nm (b).
Abbreviations: ext.: extinction; abs.: absorption; sca.: scattering. [127]

Consequently, by altering the size of spherical AuNPs alone, the LSPR peak remains out of the NIR spectrum and thus other parameters such as shape, morphology and structure of the NP need to be adjusted to achieve the desirable LSPR tunability [128] [120]. This phenomenon can be explained by the ability of these parameters to modify the conditions of the Maxwell equations, which were solved by *Mie* and are still used nowadays in a modified way to predict the scattering and absorption of nanoparticles [126]. Thus, LSRR shifts to the NIR region can result from small variations of these parameters and this adjustability has brought great interest toward anisotropic/non-spherical AuNPs for biomedical applications

[90].

Among the anisotropic NPs that have been studied for their LSRP properties in the NIR, gold nanorods are probably the most examined type of AuNPs. The first synthesis was reported in 1977 and was performed through electrochemical reduction and the use of CTAB [129]. Due to their morphology, the conductive electrons of gold nanorods are able to oscillate in two different directions resulting in a transverse and longitudinal LSPR peak, with the latter tuning into the NIR [130]. As a result, the aspect ratio (the ratio of the length of the long axis to the short axis) is a determinant parameter for the adjustment of the two separate bands that control the optical properties of gold nanorods. The longitudinal band is shifted from the visible to the NIR when the aspect ratio is raised, whereas the transverse band undergoes small blue-shift variations (Figure 16).

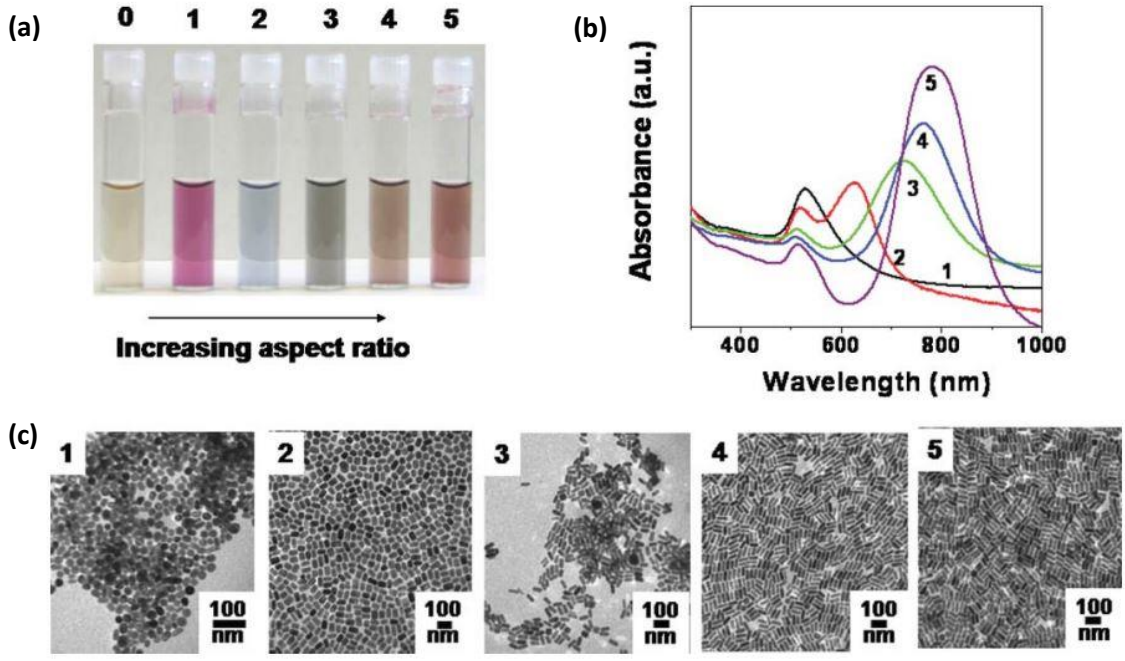

Figure 16. The aspect ratio of gold nanorods determines their optical properties. Vials containing aqueous solutions of gold nanoparticles are seen in (a). Vial 0 contains gold nanospheres with a diameter of 4 nm and the vials 1-5 contain gold nanorods with increasing aspect ratio. The absorption bands of the gold nanorod solutions are seen in (b) and the transmission electron micrographs of the particles are presented in (c). The scale bars are 100 nm. [131]

Gold nanoshells, which consist of a metallic shell and a dielectric core, also present interesting LSPR shifts, depending on their geometry [132] [133]. More specifically, the LSPR tunability can be accomplished by tailoring the ratio of shell thickness to diameter (Figure 17). The LSPR properties of gold nanoshells are very sensitive to even small changes in the morphology of the nanoparticles and a NIR shift can be achieved when increasing the shell thickness [134].

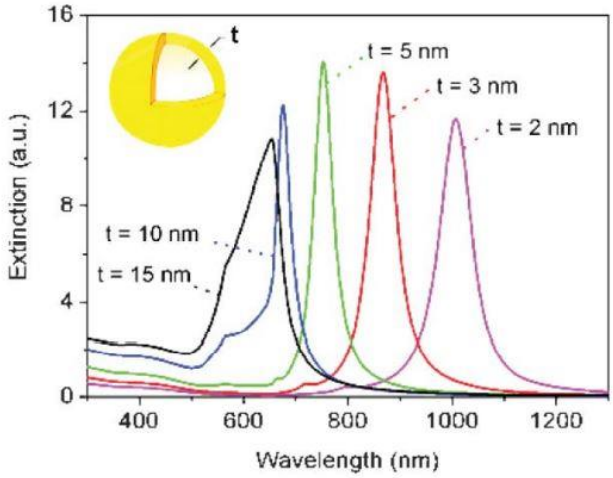

Figure 17. The extinction spectra of gold nanoshells with a fixed diameter of the silica core at 60 nm and shell thickness (t) ranging from 2 nm to 15 nm. Small variations in shell thickness lead to significant alterations in the plasmonic properties of Au nanoshells [126].

Gold nanocages represent a recently designed type of gold nanostructures, which present hollow interiors or porous walls. These nanoparticles also exhibit morphology-dependent plasmonic characteristics, which can be attained through adjustments in the thickness and porosity of the walls [135] [136]. The morphology of the designed nanocages is determined by the fabrication method, by adjusting the molar ratio of silver nanocubes to $HAuCl_4$ [126]. Varying the molar ratio enables the tunability of the extinction spectra in a wide range of 400 to 1200 nm (Figure 18) [137]. Furthermore, the hollow morphology of Au nanocages allows them to load molecules for drug delivery as well as magnetic nanoparticles, adding to the extraordinary properties of this novel class of gold nanostructures.

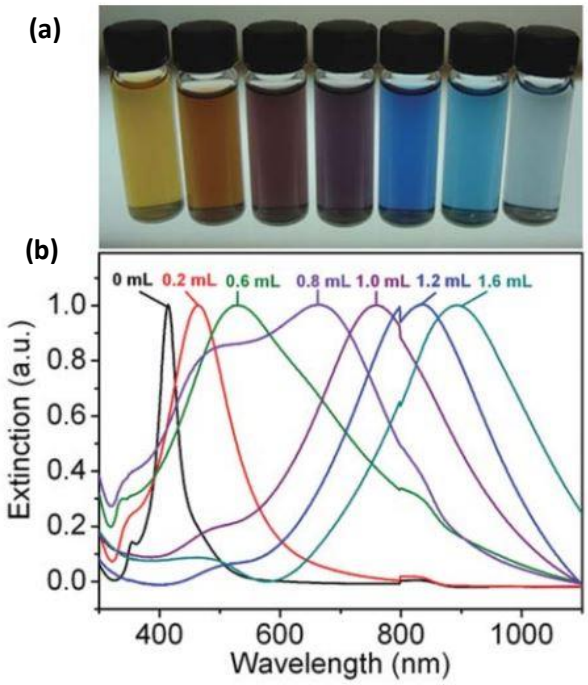

Figure 18. Vials with Au nanocages suspended in water, designed by titrating silver nanocubes with $HAuCl_4$ solutions of different volumes (a) and extinction spectra of these Au nanocages (b). The volumes of the $HAuCl_4$ solutions are noted above each curve [126].

Similarly, gold nanoparticles of other shapes present plasmonic properties which are controlled by their geometry and dimensions. For example, gold nanostars are highly anisotropic nanostructures and present plasmon resonances from the hybridization of plasmons which depend on the morphology of the core and the individual tips of the particle [138]. These properties of gold nanostructures are undoubtedly of great interest for many biomedical applications in both diagnosis and therapy. Among those is the enhancement of medical imaging through their function as contrast agents in modalities such as OCT and PAI.

3.3.3 How can Gold Nanoparticles function as Contrast Agents?

The exceptional physical properties of AuNPs, in combination with their facile fabrication and functionalization, render them appropriate for in vivo bioimaging applications [93]. The ability to customize their optical properties and extinction band, as described previously, has brought attention to their use in various imaging techniques, including X-ray computed tomography, dark field microscopic imaging, magnetic resonance imaging, and fluorescence imaging [139] [140] [141]. The high LSPR tunability of gold nanostructures makes them more suitable for these imaging modalities when compared to organic fluorophores or quantum dots [142] [143].

Aside from the above modalities, gold nanoparticles are also considered to be attractive candidates for the enhancement of imaging using techniques such as OCT and PAI, due to their ability to be precisely tuned at a specific wavelength by morphology [144] [145] [146]. As explained previously, OCT images result from the detection of backscattering of light from biological tissues. Gold nanoparticles present excellent light scattering ability, which is many times stronger than the one generated by conventional fluorophores. Therefore, imaging enhancement can be achieved by tuning the optical properties of gold nanoparticles in the wavelength, in which the OCT system operates.

Furthermore, gold nanostructures can effectively act as imaging adjuvants in photoacoustic imaging. Cross-sectional photoacoustic images of biological tissues are based on the principles of optical and ultrasonic/acoustic waves, which means that acoustic waves are generated after the absorption of optical energy. The operation of this system, therefore, requires the presence of light-absorbing molecules. Gold nanoparticles can effectively absorb light in a tunable manner, based on their LSPR properties, and can consequently serve as exogenous contrast agents for this imaging modality [144]. Au nanostructures can result in an optical absorption significantly higher compared to organic dyes [147].

In short, AuNPs show great potential as exogenous contrast agents for both OCT and PAI. Their optical properties allow high backscattering of light and strong light absorption, which is beneficial for imaging with OCT and PAI, respectively. Figures 19 and 20 are

schematic representations of the application of gold nanoparticles as contrast agents for these novel imaging techniques, as illustrated by *Chen et al*. [63] and *Nguyen at al*. [148].

In the following chapters, the in vitro, ex vivo and in vitro studies which investigate the use of gold nanoparticles as contrast agents in the above modalities will be analyzed in detail. The ex vivo and in vivo studies that are presented are performed in ocular tissues or animal eyes. It should be noted that studies which include an in vitro as well as in vivo experiment, have been included in the in vivo studies. Research concerning other tissues and organs has also been carried out, but is out of the scope of this dissertation and will not be discussed.

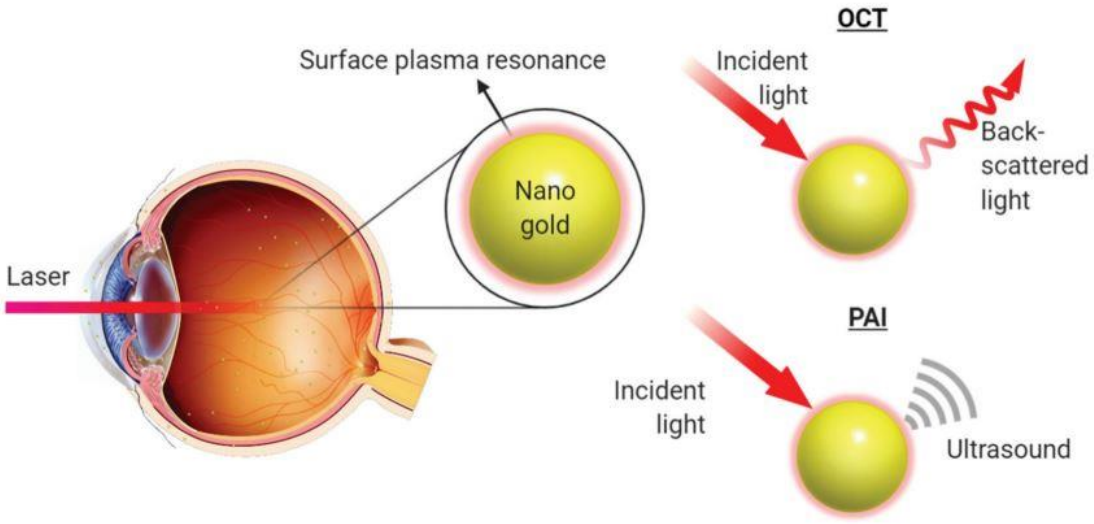

Figure 19. Schematic illustration of the use of Gold Nanoparticles as Contrast Agents in Optical Coherence Tomography and Photoacoustic Imaging for the visualization of the eye. After the stimulation with incident light, gold nanoparticles can create back-scattered light for the detection by the OCT camera or an ultrasound signal to be detected by the PAI system [63]. Plasmons convert a part of the oscillation energy into heat, which is then detected by the PAI system.

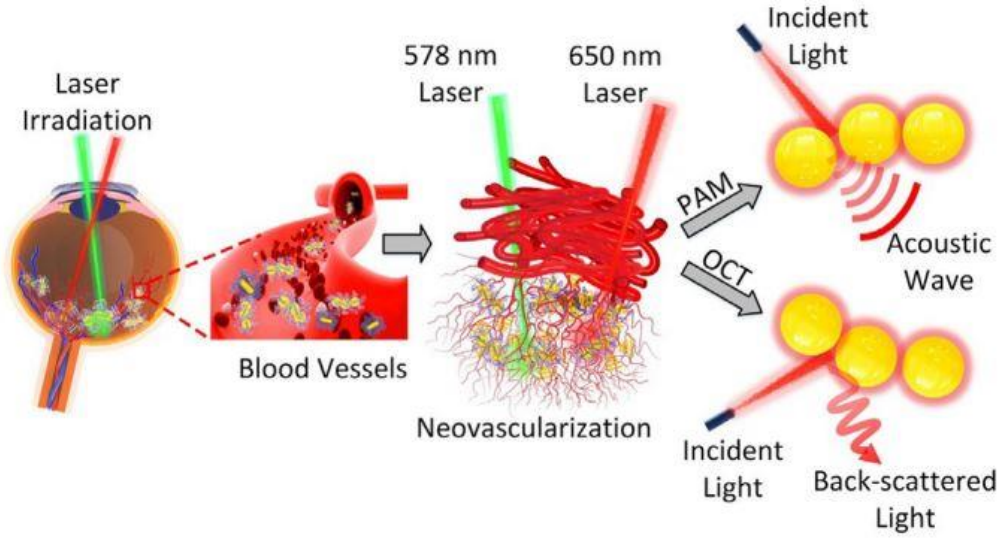

Figure 20. Application of gold nanoparticles as a CA for a multimodal CA for PAM imaging system for ophthalmic molecular imaging, as proposed by *Nguyen et al*. [148]. AuNPs can be administrated with or without targeting molecules. Using a laser beam with a specific wavelength, gold nanoparticles are capable of producing strong back-scattered light or acoustic signal, which can then be detected by an OCT image or by ultrasound to create a PA image, respectively. It should be noted that the wavelength of 578 nm is selected in order to detect hemoglobin in the vessels and 650 nm to detect extravasation of AuNPs at the vessels, with the purpose of distinguishing neovascularization.

4 Methods

This review inspects publications of the recent literature, which analyze the features of gold nanoparticles and their potential applications in ophthalmology. For this purpose, various search engines were utilized, with the most prominent being PubMed, Google Scholar and Elsevier. To detect the most related articles to the subject of this dissertation, a number of keywords were chosen, such as “Gold Nanoparticles AND Ophthalmology”, “Gold Nanoparticles AND molecular imaging”, “Gold Nanoparticles AND Optical Coherence Tomography”, “Gold Nanoparticles AND Photoacoustic Imaging”, “Gold Nanoparticles AND Angiogenesis”, “Gold Nanoparticles AND Toxicity”, “Gold Nanoparticles AND ocular distribution” and more. The results were screened based on titles and their abstracts. Articles discussing the use of AuNPs in medical fields other than ophthalmology were excluded and the articles selected were those related with ocular applications of gold nanoparticles. More specifically, attention was focused on articles publishes during the past two decades, which investigated the applications of gold nanoparticles as contrast agents for ocular imaging through OCT and PAI and articles demonstrating their anti-angiogenic effects, with a view to highlight their potential as both diagnostic and therapeutic tools in ophthalmology.

5 Results

5.1 Studies investigating the use of Gold Nanoparticles as Contrast Agents for OCT & PAI

5.1.1 Gold nanoparticles as Contrast Agents for Optical Coherence Tomography

5.1.1.1 In vitro studies

Gold Nanorods (AuNRs/GNRs) are generally considered to be beneficial as possible contrast agent candidates for in vivo imaging, due to their plasmonic properties in the near-infrared wavelength. They present an intense and narrow LSPR absorption band in the NIR, which can be easily tuned depending on their aspect ratio [128].

Troutman et al. [149] created cylinder-like shaped gold nanorods (GNRs) with an average diameter of 20 nm and tested their application as backscattering contrast agents in a time-domain OCT, using tissue phantoms. The nanorods exhibited a plasmon resonance peak at 750 nm or at 912 nm, which was close to the spectral distribution of the OCT, and therefore produced a much stronger signal. They furthermore noticed that both suspensions enhanced the signal contrast compared to water, indicating that gold nanorods effectively worked as contrast agents for OCT imaging.

AuNRs absorbing in the second near-infrared wavelength (1000-1200 nm) were engineered by *Chen et al*. [150], using a seedless method in order to achieve small dimensions. These miniature Au nanorods (smallest GNR: 8 ± 2 nm by 49 ± 8 nm) were tested as CA for PAI and their performance was compared with the one using Au nanorods of regular sizes (18 ± 4 nm by 120 ± 17 nm), which were synthesized through a seed-mediated method. The experiment took place in vitro, using phantom tubes. It was seen that miniature GNRs not only produced a ∼ 3.5 fold stronger photoacoustic signal, but were also characterized by better photothermal stability than large nanorods under nanosecond irradiation. *Chen and co-workers* attributed this signal enhancement to the greater surface to volume ratio of the miniature nanoparticles, which boosts heat transfer.

Jia et al. [151] conducted in vitro experiments to determine the effectiveness of gold nanorods as CA for imaging via a Fourier-domain OCT system. For their study they chose intralipid tissue phantoms to mimic the retinal tissue as well as cultured RPE cells for labeling.

The OCT system functioned at a center wavelength of ~ 840 nm and the NPs (diameter: 10 nm) were coated with PEG and Tat peptide. The OCT images from the intralipid alone were compared with those obtained by the GNR (SPR= 870 nm) sample and the intralipid mixed with GNRs, and it was seen that the presence of GNRs caused a red shift. Next, images of 1 % gelatin, unlabeled RPE cells, and GNR-labeled (10 × 50 nm) RPE cells were taken. The spectral shift allowed the visualization of the RPE cells that were labeled. The purpose of this study was to design a cellular CA, with the purpose of finding a way to track stem cells for the management of retinal diseases in the future.

The use of gold nanorods in a dual-band OCT system with two separated bandwidths (830 and 1220 nm) was discussed by *Rawashdeh et al*. [152]. GNRs of different dimensions were studied using a highly scattering agar phantom. Their idea was to exploit and measure the different contrast that is produced when the nanoparticles used are only resonant to one wavelength of the dual system. The strongest differential contrast at both wavelengths was produced with the aid of nanorods large (NRL) sample, which had an average length of 75 nm. The optimal concentration to create this contrast was measured to be 100-500 μg Au/mL. Regarding the gold nanorods with the smallest dimensions (length: 48 nm), the signal intensities were not detectable

Apart from regular gold nanorods, *Liba et al*. [153] [154] proposed the use of large gold nanorods (LGNRS) as spectral OCT contrast enhancers. Their larger dimensions (~ 100 × 30 nm) offer advantages compared to smaller gold nanorods, due to their ability to produce stronger backscattered and spectral signals. Through their in vivo study, they discovered that these LGNRs presented a 30-fold higher OCT intensity and were able to produce a spectral signal per particle more than 100 times stronger when compared to conventional GNRs.

Gold Nanoshells have also been proposed as OCT contrast agents, due to their high scattering and low absorption efficiency, which are considered to be desirable properties [155].

Gold Nanoshells with a core radius of 100 nm and shell thickness of 20 nm were fabricated by *Loo et al*. [156] and their prospect for OCT imaging was tested in vitro. The

scattering properties of these nanoparticles at a concentration of 10^9/mL in water, were evaluated and compared to solutions of saline and scattering microspheres. The average grayscale intensity for the saline solution was 247, whereas for the cuvette walls with the nanoshells solution, it was found to be 160.

Agrawal et al. [157] performed in vitro quantitative measurements to investigate the OCT contrast enhancement with the use of gold nanoshells. Their intention was to elucidate the effect of the relative dimensions of the Au nanoshells on the image quality and fabricate NPs with high-backscattering properties and low absorption at a specific wavelength. For this purpose, OCT imaging was conducted at 1310 nm, in water and tissue-simulating phantoms. Mono-layered nanoshells of different concentrations, core diameter and shell thickness were tested, to understand the influence of the geometry of the NPs on the signal strength. Results revealed a monotonic elevation of the OCT signal intensity and attenuation when the shell and core size were enlarged. Moreover, the NP leading to the strongest backscattering was found to have a core diameter of 291 nm and shell thickness of 25 nm and the threshold concentration to produce a signal elevation (intensity gain of 2 dB or more) was measured at 10^9 nanoshells/mL. Gold nanoshells can, therefore, be promising CA for the improvement of the OCT image by optimizing the dimensions of the core and the shell and consequently modulating their optical resonance for molecular imaging.

An OCT system operating at 900 nm was utilized by *Zagaynova et al*. [158] to evaluate the contrasting abilities of silica-gold nanoparticles as contrast media. The nanoshells exhibited a silica core size of 150 nm and gold shell thickness of 25 nm and agar bio-tissue phantoms were chosen for the experiment. OCT imaging proved that gold nanoshells penetrating the phantoms caused the intensification of the signal.

Gold nanoshells were also tested as an exogenous CA for a phase-sensitive OCT imaging system in vitro by *Adler et al.* [74]. The Au nanoshells that were chosen had a core of 120 nm and shell thickness of 16 nm. Photothermal modulation was induced by an 808 nm laser diode, with the purpose to study the modifications in the optical path length caused by temperature oscillations. An OCT phase microscopy was used on pure deionized water and an Au nanoshell solution. Results illustrated a high contrast between the phantoms with and

the phantoms without NPs. Consequently, gold nanoshells are also prospective candidates as contrast agents in a phase-sensitive OCT system.

Gold Nanocages are gold nanoparticles with a hollow and porous morphology. They are usually fabricated through the galvanic replacement reaction between silver nanocubes and $HAuCl_4$ in solution and have also been suggested as CA [111].

Gold nanocages were proposed as potential contrast media for spectroscopic OCT in vitro, using gelatin-made tissue phantoms, by *Cang and co-workers* [159]. The monodispersed NPs demonstrated an average edge length of ~ 35 nm and resonant peak at ~ 716 nm. It was observed that using nanocages, the absorption cross section presented a ~ 5 orders larger magnitude than conventional dyes.

Gold nanoparticles with a star-like morphology, also referred to as gold nanostars (GNSs), have also been engineered to be studied as contrast agents.

Ponce-de-Leon et al. [160] fabricated gold nanoparticles of different geometry and size and analyzed their ability to enhance imaging using an OCT system in the wavelength region of 1325 nm in vitro. The morphology of the produced AuNPs was either spherical-, cubic- or star-like-shaped. Among these, the AuNPs with a morphology resembling a star and sizes less than 150 nm were the ones producing the best contrast in water as well as in agarose phantoms. This was the first time that gold nanostars were introduced as potential contrast materials for the enhancement of OCT imaging.

The use of gold nanostars as contrast adjuvants for OCT and Doppler OCT at 930 nm was evaluated by *Bibokova et al*. [161] in vitro. Through the seed-mediated method, GNSs of various sizes and numbers of spherical seeds were used for this purpose (50, 82, 100 and 120 nm) and their plasmon resonance peaks were in the range of 690-830 nm. The GNSs presented different scattering/absorption ratios at the LSPR wavelengths (being 0.12, 0.25, 0.30, 0.35 respectively). The nanoparticles showing the most promising results as a CA for OCT and Doppler OCT were found to be the 120 nm- sized nanostars, due to their prominent scattering properties leading to improved contrast. Therefore, by changing the number of

seeds and consequently the size of the Au nanostars, it was possible to adjust their scattering properties to the appropriate wavelength, rendering them appealing as imaging agents.

5.1.1.2 Ex vivo studies

Wang and co-workers. [162] performed GNR-enhanced Doppler OCT scans to image the intrascleral aqueous humor outflow. The aqueous flow, which normally does not produce a Doppler signal, determines intraocular pressure and is therefore related to the development of glaucoma [163]. The dimensions of the nanoparticles used were ~ 40 x 10 nm and their peak resonance wavelength 850 nm. A solution of gold nanorods with concentration of 1 x 10^{12} GNRs/mL was injected into porcine eyes with mock aqueous (n=2) and the control group was injected with Barany's mock aqueous (n=6). The use of Au nanorods produced a measurable signal and the anterior chamber outflow was visualized.

In a study by *Prabhulkar et al*. [164], antibody-conjugated Au nanorods were examined as backscattering OCT contrast adjuvants for molecular histopathology on an ocular surface squamous neoplasia (OSSN) model. Anti–glucose transporter-1 (Glut-1), which is normally expressed by erythrocytes and overexpressed in OSSN lesions, was selected as a molecular target for the NP functionalization [165]. The term OSSN describes a variety of pathological entities and types of lesions, including dysplasia of the cornea and conjunctiva epithelium, carcinoma in situ (CIS), and invasive squamous cell carcinoma (SCC) [166]. Furthermore, fluorescent-tagged secondary Abs were applied and immunofluorescence and OCT imaging of human conjunctiva tissue specimens took place.

The OCT images taken from the control specimens (presenting no epithelial atypia) revealed a minimal background signal in the epithelium, since there was no binding of the functionalized NPs and therefore no Glut-1 overexpression. However, an enhanced signal derived from the sub-epithelial region (substantia propria), correlated to the foci detected on immunofluorescence, due to the presence of capillaries. The OCT imaging of the conjunctival specimens with CIS disclosed a weak background signal within the epithelium, even though immunofluorescence showed intense staining due to atypical epithelial cells. In the three cases of SCC that were studied, the OCT of only two showed increased signal which matched with the immunofluorescence-positive regions. No OCT enhancement was seen in the third case, even though there was moderate staining in immunofluorescence.

The above research findings suggest the presence of a minimum concentration of

GNRs for the generation of a detectable OCT signal. In the six cases of OSSN studied, only SCC cases were characterized by a strong Glut-1 overexpression, and only two of them exceeded the threshold for detection. Despite the limitations of this study, it is the first reported application of Au-enhanced imaging for this purpose and it broadens the scope of research for the use of molecular markers in ocular imaging.

Faber et al. [167] discussed the use of nanoshells as contrast agents for OCT in an attempt to develop nanoparticle-assisted optical molecular imaging (NAOMI). In their study, they used nanoshells with a core radius 290 nm thick and a gold shell 33 nm thick and injected them ex vivo in porcine eyes, subretinally, after removing the lens and the iris. These nanoshells had contrast features in the wavelength region of 800 nm. The withdrawal of the syringe created a "cloud" of nanoshells, which appeared to sediment onto the retina and create a reflective layer. These observations supported the idea of using gold nanoshells as an OCT contrast agent.

Ozone (O_3) has oxidizing effects and can be harmful when penetrating the damaged corneal epithelium of the eye [168]. To study and visualize the penetration of O_3 into the anterior chamber of the eye, *Jiang et al*. [169] used gold triangular nanoprisms as CA for 3D OCT imaging, using an isolated crucian carp eye. The idea to use GTNPs as signal-modulation contrast agents arose from the blue shift of the plasmon peak that takes place as a result of their morphological changes in the presence of O_3 [170]. Exposure to O_3 can be considered as an alternative method for tailoring the plasmon mode of gold NPs, in an uncomplicated and controllable process. More specifically, after O_3 exposure, the morphology of the GTNPs changed into circular nanodisks, which have stronger scattering properties at 830 nm and caused a higher contrast enhancement. In this way, the ozone penetration can be assessed by measuring the contrast enhancement that results from this morphology transformation.

The OCT images of the crucian carp eye with the use of GTNPs can be seen in Figure 21. After the Au nanoparticle- injection (~ 0.0228 mg/mL) in the anterior chamber of the eye, contrast enhancement was noticed. The crucian carp eye with a damaged cornea was exposed to ozone to study its distribution and OCT images were obtained at several time points. It was noted, that the area around the wound had enhanced contrast due to the

morphological change of the nanoparticles (Figure 22). These results indicated that gold nanoprisms could serve as a promising CA for the detection of ozone in the eye using OCT imaging.

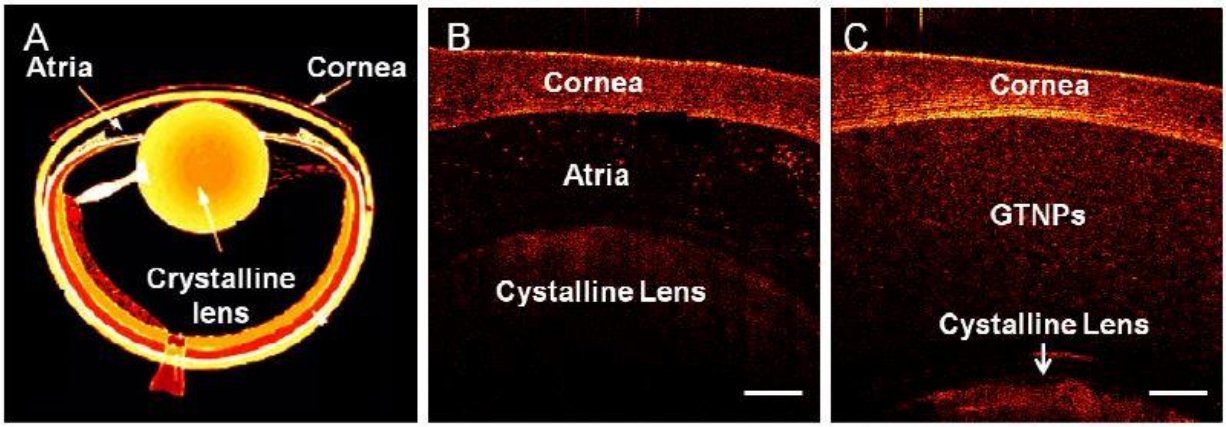

Figure 21. Cross-sectional OCT images of the crucian carp eye before and after the NP injection: A schematic diagram showing the structure of a fish eye. (A) OCT image of a crucian carp eye before the injection (B) and after the injection (C) into the anterior chamber. The scale bars represent 300 μm.

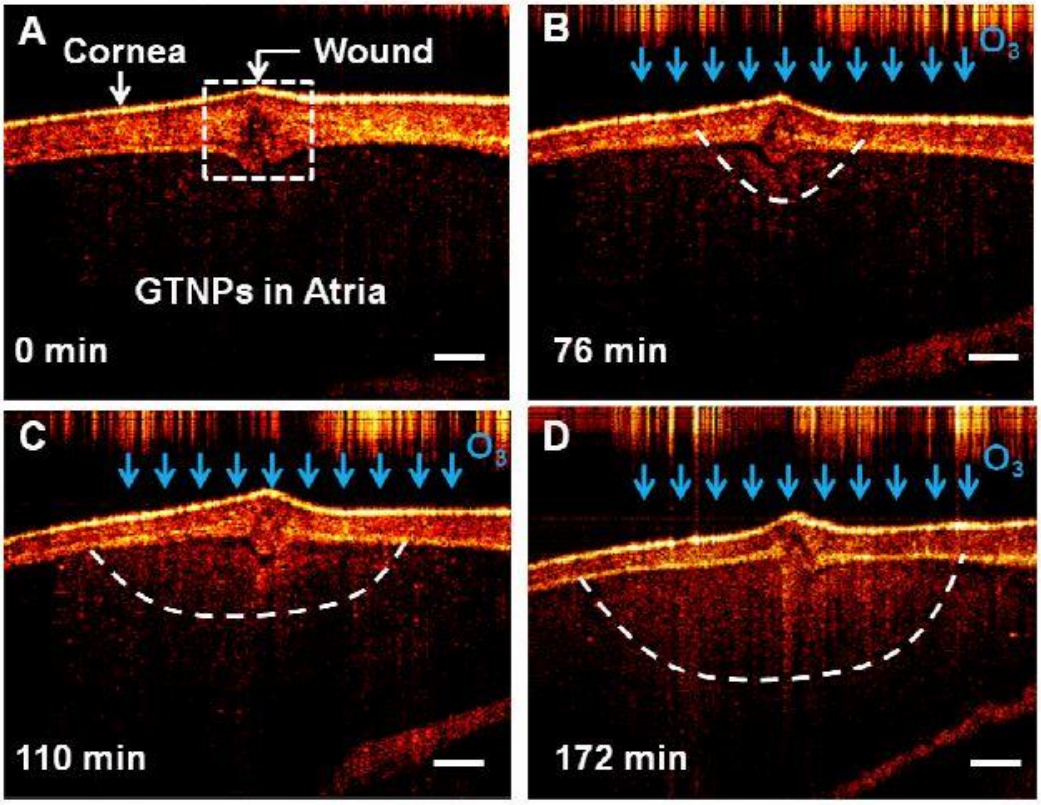

Figure 22. OCT images of an isolated crucian carp eye after the GTNPs - injection under ozone exposure: 0 min (A), 76 min (B), 110 min (C), and 172 min (D). The scale bars represent 300 µm.

5.1.1.3 In vivo studies

De la Zerda et al. [171] investigated the use of gold nanorods as optical coherence contrast agents in vivo, in mice eyes. For their study, they constructed GNRs with an absorbance peak at 780 nm and 850 nm. To avoid aggregation, these particles were suspended in cetyltrimethyl-ammonium bromide (CTAB) during the manufacturing process, and were then coated with thiol-terminated polyethylene glycol (PEG) in order to replace the potentially cytotoxic CTAB and achieve stealth properties. Corneal and anterior chamber injections of two different sizes of GNRs at different concentrations took place: GNRs corresponding to a peak absorbance wavelength of 780 nm (GNR-780: length = 43 ± 4.22 nm; axial diameter = 12 ± 0.25 nm) and 850 nm (GNR-850: length = 49.31 ± 6.9 nm; axial diameter = 12.09 ± 1.63 nm) were utilized.

Results indicated that the signal produced by GNR-850 was higher than the one by GNR-780 for each of the concentrations that were tested and the lowest concentrations to detect were 230 pM and 750 pM respectively. Regarding GNR-850, concentrations of 120 pM or above resulted in a significantly different OCT contrast ($P < 0.05$) (Figure 23). Furthermore, the signal from corneas injected with GNR-780 was 3 times stronger compared to mice corneas injected with balanced saline solution (BSS) and 7.5 times stronger compared to naïve mice corneas. GNR-850 injected at a concentration of 0.5 nM led to a clear contrast and when the concentration was 5 nM or above the contrast was even higher (Figure 24).

Overall, this study led to the conclusion that GNRs can be characterized as high-sensitivity contrast agents for OCT in living animals and are capable of creating an OCT signal stronger than the background signal of tissues in the eye. Their sensitivity limit in living corneas of mice was found to be 120 pM.

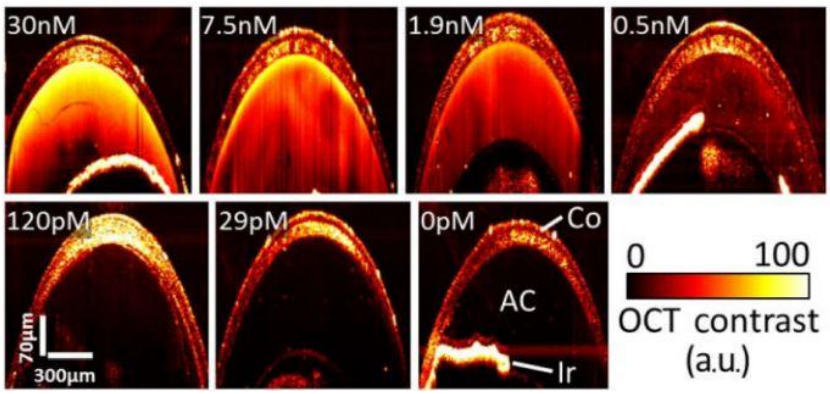

Figure 23. 3-5 µL of GNR-850 at concentrations from 30 nM to 0 nM were injected at the ACs of mice (N=12) The control group was injected with Matrigel. Mice injected with 29 pM of GNR-850 showed similar contrast to control mice, whereas concentrations ≥ 120 pM led to distinct detectable OCT signal.

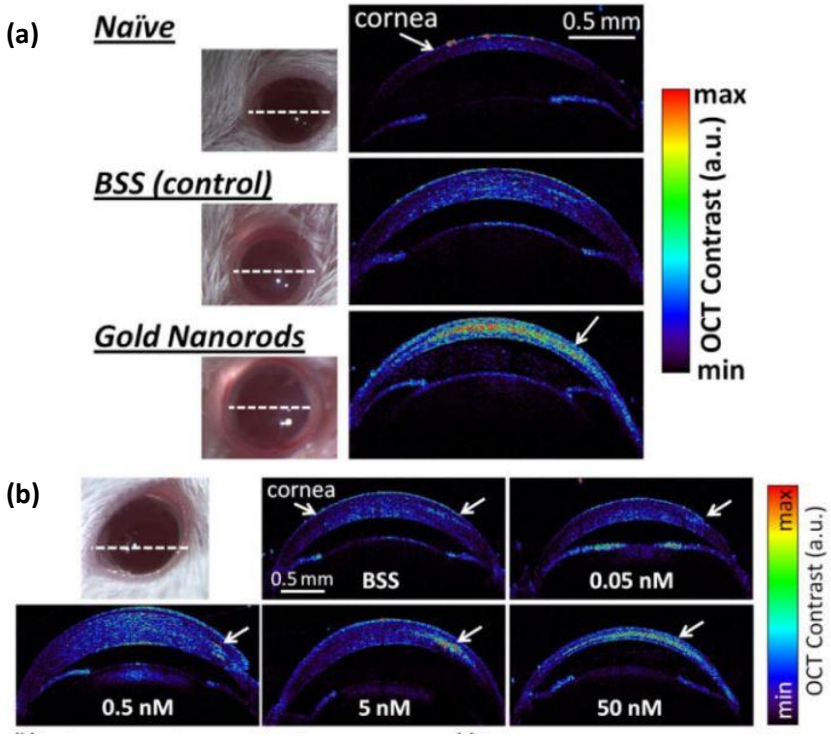

Figure 24. Mice corneas injected with 10 µL GNR-780 at 50 nM (bottom) compared to control mice corneas injected with 10 µL of BSS (middle) and mice corneas not injected at all (upper). OCT cross sectional images showed the high contrast by GNR-780 in the cornea. (a) Mice corneas (N=4) injected with 5 µL of GNRs at concentrations from 50 nM to 0.05 nM and control mice injected with BSS. Concentration of 0.05 nM had a contrast similar to control mice, whereas concentration of ≥ 0.5 nM created a distinct detectable signal. (b)

Bioconjugated GNRs (~110 x 32 nm, peak absorbance wavelength: 824 - 830 nm) were used as exogenous OCT CA to image single cells and vessels in vitro and in vivo, in mice retinae, by *Sen et al*. [172]. GNRs functionalized with anti-mouse CD45 (GNR^{CD45}) were used

to label mouse leukocytes (taken from blood and spleen) and mPEG-GNRS (GNR^{mPEG}) were used to determine the in vivo sensitivity inside retinal vessels.

In vitro, the GNR^{CD45}-labeled leukocytes were imaged with OCT and had a significantly higher scattering intensity compared to the unlabeled cells. To investigate the detection sensitivity of the NPs inside the retinal vessels in vivo, 200 µL of GNR^{mPEG} (10 nM) were injected intravenously into living mice. An increase in OCT intensities could be detected at a GNR concentration as low as 0.5 nM and GNR^{mPEG} circulated in the blood for ~4 h. (Figure 25) These results indicate that GNRs can effectively be used as a contrast agent for the imaging of the retina using OCT and can be detected at a sensitivity of ~0.5 nM after being injected intravenously.

(a)

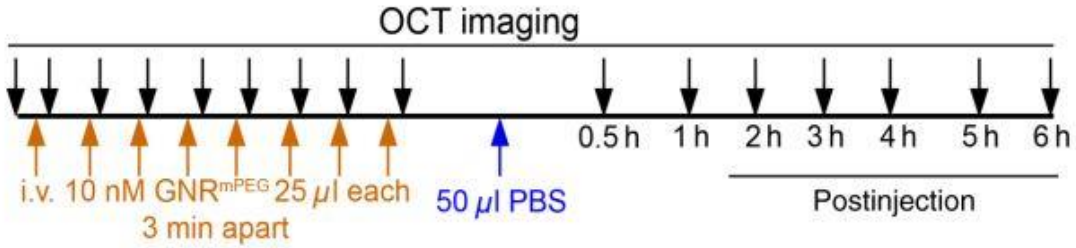

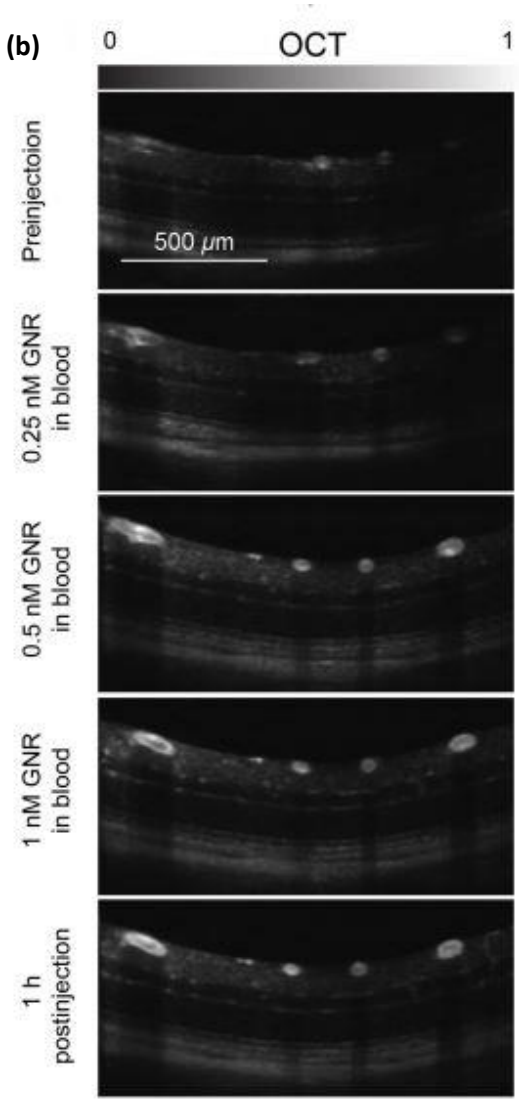

Figure 25. OCT images of the retinal vessels after GNR^{mPEG} injection in living mice.
200μL of GNR^{mPEG} (10 nM) were injected via a tail vein catheter progressively with an interval of 25μL. Images were taken 3 min after each injection. Orange arrows show the time of injection and black arrows the time of OCT imaging. (a)
OCT images of mice retinae pre- and post-GNR^{mPEG} intravenous injection. The concentrations achieved each time are shown on the left of the bar. The scale bar is 500 μm. It can be noticed, that the nanoparticles can be detected at a sensitivity of ~ 0.5 nM. (b)

Sandrian et al. [173] performed intravitreal injections of gold nanorods to determine their eligibility as CA for OCT, as well as their potential ocular inflammatory effects on the eyes of mice. The OCT images were received with a spectral-domain OCT (SD-OCT) operating at 870 nm. C57Bl/6 mice were selected (N=14, 25 eyes) and the images were taken approximately 30 min and 24 h after the AuNR (aspect ratio: ~3.4) injection, as well as before the intravitreal injection, for the purpose of using them as baseline images. Unconjugated PSS-AuNR (Au nanorods coated with poly(strenesulfate)) and Ab-AuNRs (Au nanorods coated with Anti-CD90.20. (Thy1) antibodies were chosen for the intravitreal injections. Thy1 was selected because it is expressed by retinal ganglion cells. Phosphate-

buffered saline (PBS) injections were used as sham injections. As seen in Figures 26 and 27, the enhanced backscattered signal was noted in the vitreous of the AuNR-injected mice, when compared to baseline images and images obtained from mice which received PBS injection. A day after the GNR injection, the increased contrast could still be observed. These results indicated that gold nanorods can function as contrast agents and be imaged within the vitreous of the eye using OCT and the presence of GNRs was verified via TEM. Nevertheless, the intravitreal injection of bare GNRs resulted in the creation of opacities of unknown nature, which hindered retinal imaging due to the shadowing effect caused by the vitreal signal. This optical effect was attributed to the immunological response from the GNR injection. Results regarding the immune response and inflammatory effects are discussed in "Ocular distribution and safety of gold nanoparticles"

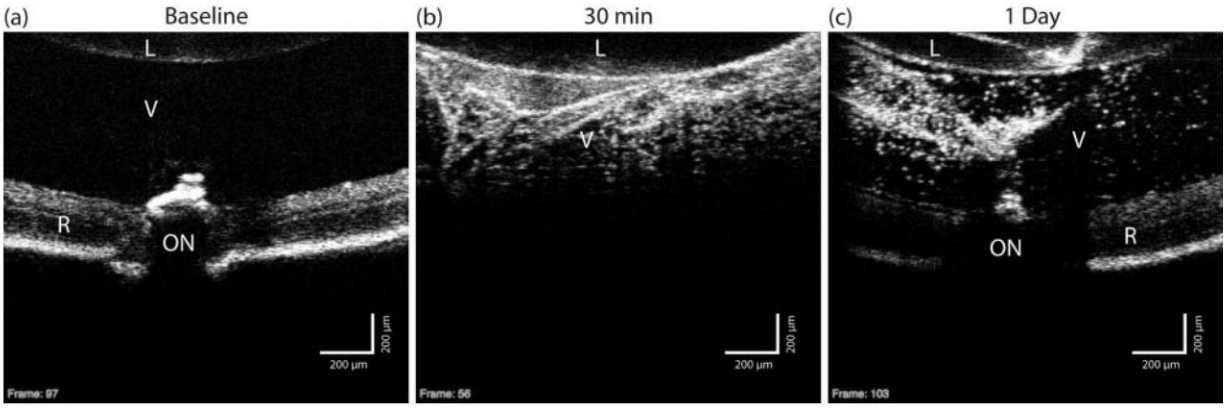

Figure 26. Single cross-section OCT images (a-c) of a single living mouse, before and after PSS-AuNR-injection in the vitreous. Signal increase is to be noted. However, 30 min after the injection, the imaging of retina is unclear.
The lens (L), the optic nerve (ON), the retina (R), and the vitreous (V) are visible in the images.

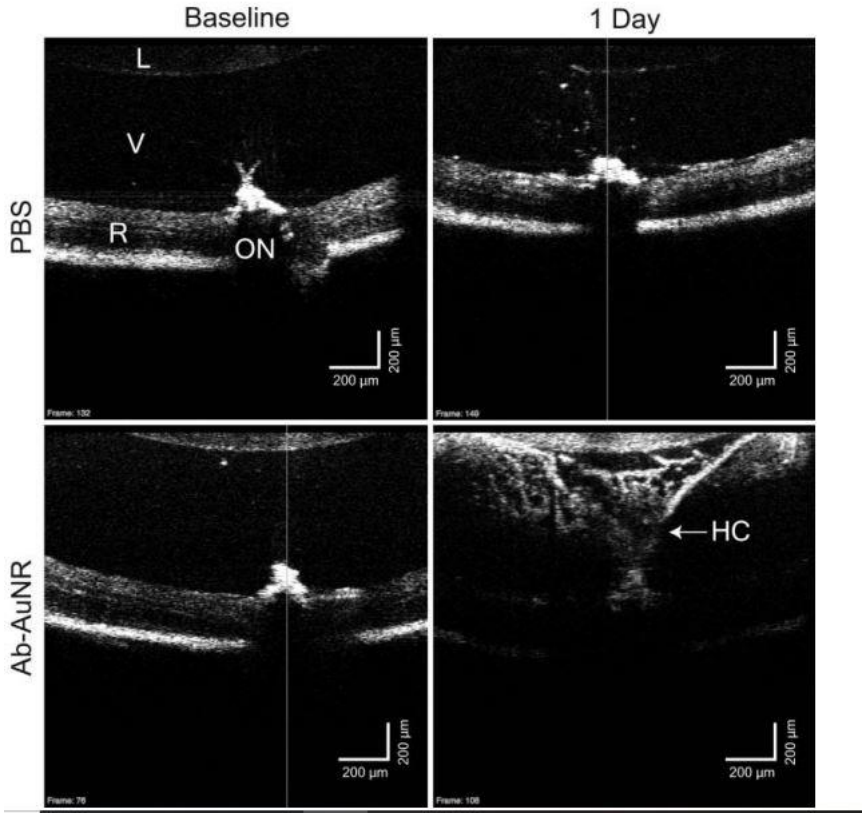

Figure 27. Baseline and 1 day post-injection OCT images from PBS and Ab-AuNR injected mice. After the gold nanorod injection, significant signal enhancement can be seen in the vitreous in comparison to pre-injection and the sham injection images. The shadow occurring from the strong vitreous signal reduces the signal from the retina.
The hyaloid canal (HC), the lens (L), the optic nerve (ON), the retina (R) and the vitreous (V) are visible in the above images.

The formation of opacities in OCT images and this "shadowing effect" was also observed by *Gordon et al.* [174], who performed intravitreal injections of bare gold nanorods (CTAB-coated) in wild-type (C57BL/6) mice. Within a few minutes of injecting the nanorods, this amorphous opacity became apparent and the visualization of the retina was obscured (Figure 28). Considering the above reaction, the surface CTAB was then displaced with PEG, to attain better stability and biocompatibility. In this case, the Au nanorod injection did not cause the morphological changes described above. Even though PEG-coated GNR seemed to be viable agents for in vivo imaging experiments, they were not able to reach the retina through the vitreous, due to their size (Figure 29).

In view of the results from intravitreal injections, *Gordon et al*. continued their studies with GNR intravenous injections via the tail vein of mice, to enable retinal imaging. For this purpose, they decided on the use of the laser-induced choroidal neovascularization (LCNV) model [175]. Five days after being treated with the LCNV model, mice were injected with PBS (n=10 eyes) (phosphate-buffered saline) or targeted GNRs (n=10 eyes), aiming to estimate the GNR accumulation in the lesions and the potential target effect via functionalization. OCT images were taken 8, 24 and 28 hours after the injection. Even though GNRs reached the LCNV lesions and the functionalization was effective for targeting, they were not able to be detected using OCT due to the background noise of the tissue.

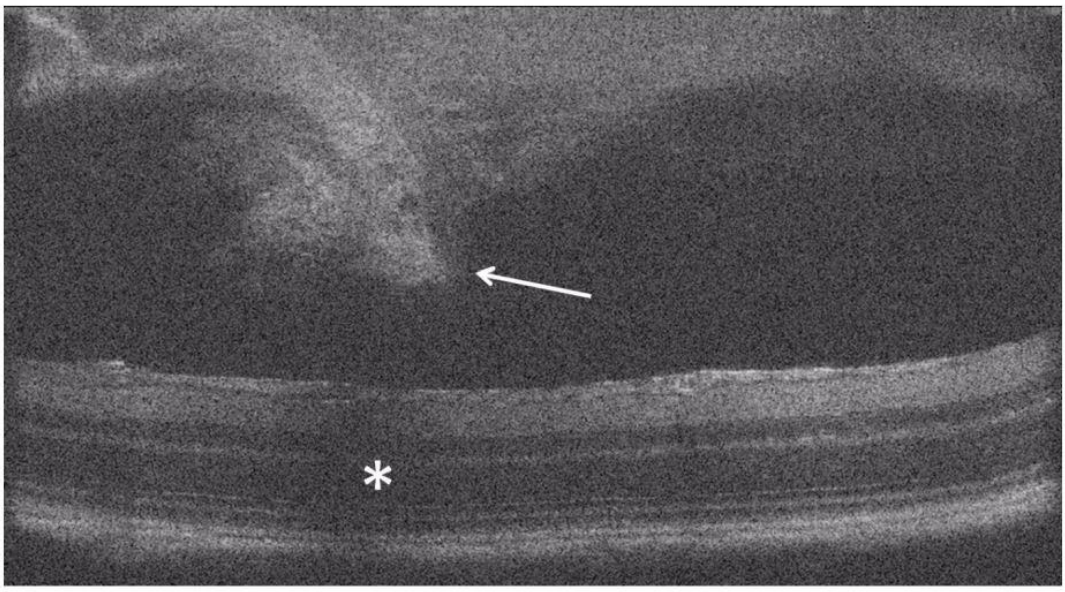

Figure 28. In vivo OCT imaging after CTAB-coated GNR intravitreal injection. The arrow indicates the amorphous opacity throughout the vitreous. The asterisk shows the "shadowing effect" caused on the retina.

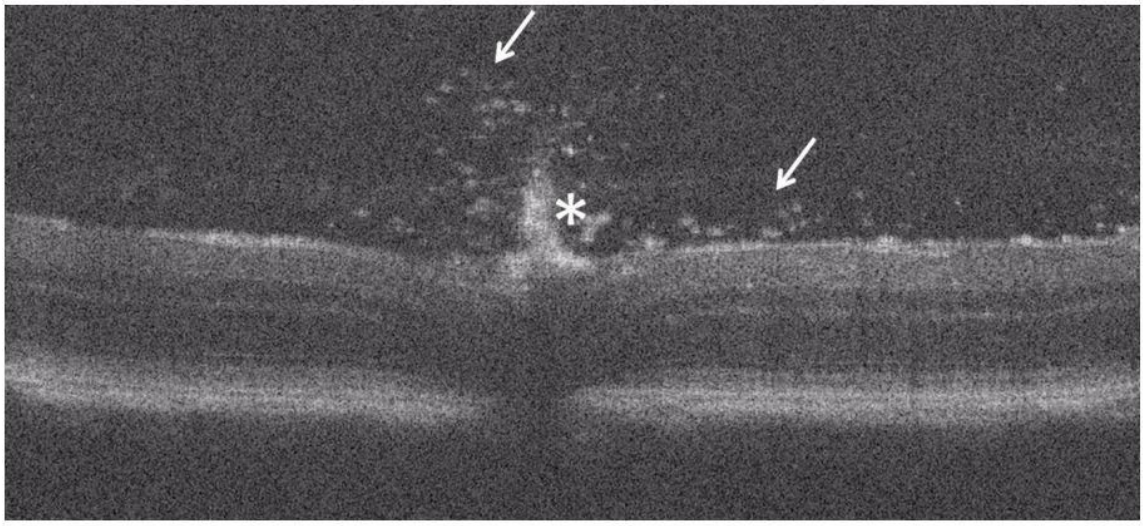

Figure 29. In vivo OCT retinal imaging after PEG-GNR intravitreal injection. The asterisk shows the optic nerve and the arrows show the discrete scatterers in the tissue near the inner retina. The opacities seen with the bare GNR injections are no be seen in this case.

Lapierre-Landry et al. [176] proposed the use of photothermal OCT (PT-OCT) to image endogenous (melanin) and exogenous (Au nanorods) absorbers in the eyes of pigmented (C57BL/6, n = 6 eyes) and albino mice (BALB/c, n=6 eyes). Pigmented mice have melanin in the retinal pigment epithelium (RPE) and choroid. First, OCT and PT-OCT images without the injection of a CA were taken by both types of mice, in order to separate the signal generated by melanin. In this case, a potent signal was generated from the RPE and choroid of the pigmented animals and no signal from the albino ones.

For the PT-OCT imaging of the Au nanorods, pigmented mice were first subjected to laser-induced choroidal neovascularization. Gold nanorods coated with PEG or saline (control group) were injected intravenously via the tail vein five days after the photocoagulation and the images were received 6 h later. A statistically significant ($p < 0.05$) enhancement in the PT-OCT signal was observed in the LCNV lesions of the group injected with the Au nanorods in comparison to the control group (Figure 30). This study showed that gold nanorods can accumulate in these lesions and identified with an OCT-based system.

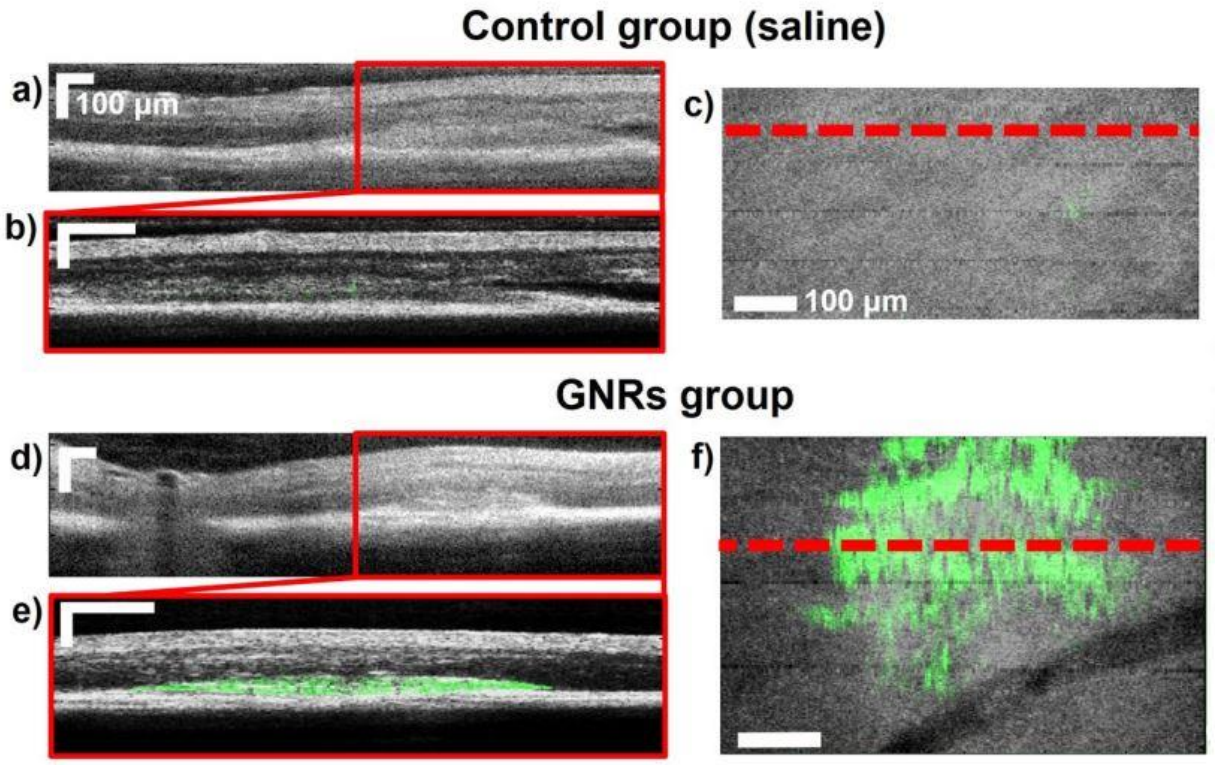

Figure 30. OCT B-scans of the retina for the control group (a) and the GNRs group (d), with the LCNV lesion marked by the red box. PT-OCT scans of the boxed area were taken, which are seen in green on top of the OCT B-scans (grayscale) in (b) and (e) respectively. The control group presents minimal PT-OCT signal. En face images of the lesion are shown in (c) and (f). The dashed red line indicated the location of the B-scan.

Through a top-down process*, Song et al.* [177] synthesized 160-nm-sized gold nanodisks with a resonant wavelength of 830 nm, to evaluate them as OCT CA for retinal imaging in mice eyes. The spectral domain OCT system had a central wavelength at 849 nm. Gold nanodisks were chosen because they are considered to have a better scattering ability compared to gold nanorods, as their signal does not depend on the direction and polarization of the light source [178]. The threshold concentration for an OCT signal following the intravitreal injections was found to be as low as 1 pM, whereas concentrations of 0.1 pM showed a minimal signal, similarly to when distilled water was administered. At higher concentrations (10 pM), the signal in the mice vitreous bodies was even stronger (Figure 31)

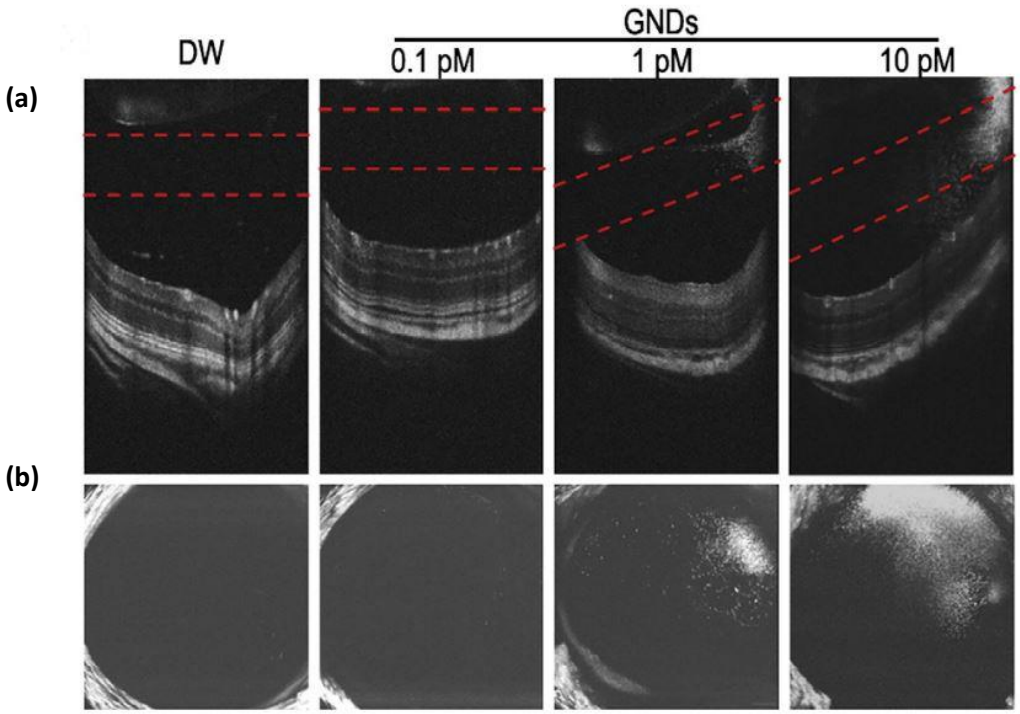

Figure 31. Cross-sectional OCT images after intravitreal injections of distilled water and GND solutions of various concentrations (0,1 pM, 1 pM, 10 pM) in mice eyes (a). Projectional images of the regions between the red dotted lines were also obtained (b).

The use of gold nanoparticles was also proposed for the monitoring of transplanted cells using multimodal imaging in vivo [179]. Cell replacement therapy has been presented as a method to restore vision in retinal degenerative diseases, such as AMD and retinitis pigmentosa [180]. Photoreceptor precursors (PRPs) are transplanted subretinally and tracking of the cells is essential for the assessment of the transplantation, but can often be challenging.

For this purpose, *Chemla and co-workers* suggested the use of AuNPs for non-invasive multimodal monitoring of PRP cells through CT, OCT, and fluorescence fundus imaging. More specifically, AuNP- and fluorescently labeled PRPs were transplanted in the vitreous and subretinal space of wild-type pigmented rats and were monitored in vivo at 24 h and 7 and 30 days after the transplantation. The gold NPs that were used were coated with PEG, presented a spherical shape, and had an average diameter of 20 nm. OCT imaging at 24 h was able to detect PRP clusters of cells subretinally. At 7 and 30 days, the imaging of small

cellular clusters that migrated from the subretinal space toward the inner layers of the retina was possible, indicating the ability of prolonged monitoring. Moreover, gold nanoparticles showed no toxicity to PRP cells when tested in vitro. Altogether this study demonstrated that gold nanoparticles can enhance ophthalmic imaging and achieve longitudinal and high-resolution tracking of the transplanted PRPs using multimodal imaging technology.

5.1.2 Gold Nanoparticles as Contrast Agents for Photoacoustic Imaging

5.1.2.1 In vitro studies

Gold nanostars have been tested for contrast enhancement in photoacoustic imaging using phantoms (2 % agarose in water, 1 % intralipid). *Raghavan et al*. [181] designed multibranched star-like AuNPs, which present dual plasmon peaks, one longitudinal (1000-1150 nm) and one transverse (~ 700 nm). The distance between opposite tips of the Au nanostars was found to be 120 - 150 nm and the length of the braches at 35 – 40 nm. Using a 1064 nm laser, PA images of the tissue phantoms with and without the addition of the NPs were compared. An enhancement in the signal was observed when the concentration of the Au nanostars was also increased, and the same phenomenon was to be seen when using a 700 nm laser. Of particular importance was the fact that gold nanostars were able to produce a potent signal in the wavelength of 1064 nm, which belongs in the NIR-II. This region is where deeper tissue penetration is achieved and background signal from the tissue is minimized, allowing better contrast in vivo.

In vitro studies were also conducted by *Bayer et al*. [182], who designed silica-coated gold nanorods for molecular PAI. The SiO_2-AuNPs (thickness: 40 nm) were functionalized with monoclonal antibodies, which targeted specific proteins/cell-receptors over-expressed by cells within the tissue phantoms. The NPs presented separate peak absorption wavelengths at 780 and 830 nm. Results showed increased PA signals, which represented the presence of gold nanorods in cell inclusions. *Bayer et al*. were able to identify the separate cell inclusions of the tissue phantom with the use of this multispectral PAI system, due to the different wavelengths of the SiO_2-AuNPs used to label the cell types. Therefore, the silica-coated Au nanorods were proved to promote molecular imaging through a multiplex photoacoustic system.

5.1.2.2 Ex vivo studies

Raveendran et al. [183] examined the function of gold nanocages (AuNcgs) as contrast agents for PAI using enucleated porcine eye models with the purpose of improving the diagnosis of ocular diseases, such as uveal melanoma – an intraocular cancer. The AuNcgs were fabricated with an ultra-fast microwave assisted method, enabling synthesis in just a few seconds, and the dimensions of the NPs were: wall thickness: 5±2 nm and average edge length: ∼65 nm. In this study, AuNcgs were used for the first time as contrast agents for ophthalmic imaging and separate tubings filled with solutions of AuNcg at different concentrations were used to obtain PA and US images and understand the effect of the concentration on the signal. It was found that the amplitude of the photoacoustic waves was directly proportional to the concentration of the AuNcgs solution and that the signals were produced by the nanocages under pulsed optical excitation. Furthermore, PA and US images were obtained and compared with images before the injection of the nanocages. The results showed that there was an increase in the PA signals from 17.6 % to 81.4 % after the injection of AuNcgs into the eye models. Therefore, the idea of using quickly synthesized gold nanocages for ocular photoacoustic imaging produced encouraging results, as it was demonstrated that have the capacity to enhance contrast for the diagnosis of ophthalmic disease.

5.1.2.3 In vivo studies

Kim et al. [184] investigated the potential of AuNPs to work as both a therapeutic and diagnostic means for intraocular tumors using New Zealand White rabbits (N=24). Gold nanoparticles coated with fucoidan (Fu) and conjugated with doxorubicin (Dox), which is a chemotherapeutic drug, were able to act as anti-tumor agents due to their chemo-photothermal properties in vitro and in vivo. Using rabbit models with VX2 tumor, the feasibility of Dox-Fu@AuNPs to function as CA for photoacoustic imaging was tested. Imaging before and after the intratumoral injection of 100 µl of Dox-Fu@AuNPs at a concentration of 200 µg/µl was performed in vivo. The tumor which had received the injection produced stronger PA signals in comparison to the image taken before the injection, which presented an obscure signal. Moreover, the post-injection image allowed visualization of the than two folds of deeper tissue ($p < 0.001$), and the margins of the tumor were clearly viewed (Figure 32). This study was able to prove that AuNPs can be useful as tools for both the treatment and imaging of intraocular tumors, as they increase the PA contrast and aid to determine the tumor margins.

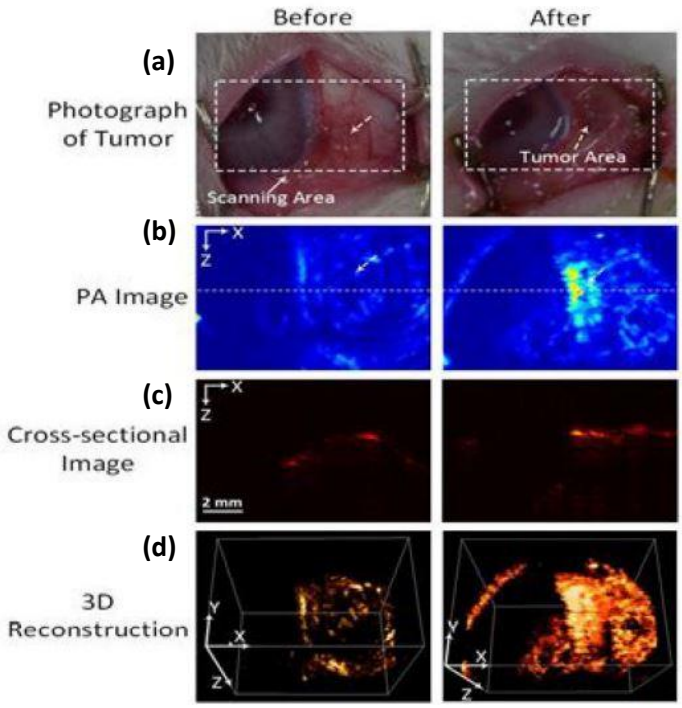

Figure 32. Intratumoral injections of Dox-Fu@AuNPs were performed in rabbit eyes. On the top panel, photographs of the tumor are visible before and after the injections (a). Photoacoustic images (b) disclosed enhanced signal after the injection ($p < 0.05$). The lower panels exhibit cross-sectional images (c) and 3D reconstructions (d).

5.1.3 Gold Nanoparticles as Contrast Agents for a multimodal OCT & PAI system

5.1.3.1 In vitro studies

Two different-sized nanodisks were physically synthesized in a stacked form by *Wi et al*. [185] and were assessed as CA for a bimodal PA and OCT system. The smaller nanodisk (80 nm) was placed on top of the larger one (180 nm) and due to their different size they presented a localized surface plasmon resonance of two separate wavelengths, at 630 nm and 850 nm. Gold nanodisks with small diameters (< 100 nm) are more appropriate for light absorption and therefore can be utilized in OCT imaging, whereas the ones with larger diameters (> 100 nm) are more appropriate for light-scattering and can be effectively used in PAM [186]. Thus, the stacked Au nanodisks could be applied as a bimodal contrast agent for both OCT and PAM.

For their study, *Wi and co-workers* used four silicon tubes which contained: aqueous solutions of a black-colored ink (blood phantom), gold nanorods (PAM-CA, resonant wavelength: 650 nm), stacked Au nanodisks (bimodal CA), and gold nanospheres (OCT-CA, resonant wavelength: 850 nm). Quantitative measurements showed that only the stacked Au nanodisks were detected by both OCT and PAM, and furthermore the PAM intensity of a single stacked Au nanodisk was 2-folds larger than that of a gold nanorod. Therefore, Au nanodisks in a stacked form with different sizes and consequently a different SPR can effectively function as sensitive contrast media and improve PAM and OCT image.

5.1.3.2 In vivo studies

In 2019, *Nguyen et al*. [148] synthesized PEGylated AuNPs and tested their capability to serve as CA for multimodal imaging with PAM and OCT in vivo, aiming to achieve vasculature visualization. Colloidal AuNPs (20.0 ± 1.5 nm) were fabricated by femtosecond laser ablation and their surface was functionalized with PEG. Their absorption peak was found at 520 nm. The NPs were intravenously injected in living rabbits (N= 16: 13 New Zealand white rabbits, 3 Dutch Belted pigmented rabbits) and their retinal and choroidal microvasculature was examined.

The PAM operated at the wavelength of 532 nm, close to the absorption peak of the produced NPs. Images of the retinal and choroidal vessels were obtained before (control group) and after the injection of 0.8 mL PEG-AuNPs (2 mg/mL) and were then reconstructed in 2D and 3D images. The maximum intensity projection (MIP) of the retinal vessels before the PEG-AuNP injection and at 1, 3, 5, 9, and 11 minutes after injection was presented. The rabbits injected with PEG-AuNPs led to a stronger signal compared to control animals and the PA signal of the vessels reached an increase of 52 % over the one without injection. To examine the dynamic changes, PEG-AuNPs concentration was raised at 5 mg/mL and PAM images were acquired every minute for 14 minutes and the increase of the signal reached 82 % compared to the one before the injection. Furthermore, to examine whether melanin can affect the PA signal, PEG-AuNPs (0.5 ml, 5 mg/ml) were injected into Dutch Belted pigmented rabbits (N=3) in vivo, and a 62 % increase of the signal at 1-minute post the injection was noted. Finally, *Nguyen and co-workers* tested the ability of PEG-AuNPs to function as CA for OCT and found that the rabbit injected with AuNPs demonstrated ∼ 45 % greater OCT intensity than the control. Overall, this study demonstrated that PEG-AuNPs can function as a multimodal CA for PAM and OCT in vivo in rabbits to visualize retinal and choroidal microvasculature.

In another study by *Nguyen et al*. [187], they used gold nanostars functionalized with arginine-glycine-aspartic acid (RGD) peptide as a CA for multimodal imaging with OCT and PAM in vitro and in vivo, in living rabbits with choroidal neovascularization model. The purpose of this study was to test whether the use of GNS-RGD (average diameter of 30 nm,

absorption peak of 650 nm) can help distinguish neovascularization from the surrounding retinal vasculature, which remains a challenge for ocular imaging. (Figure 33)

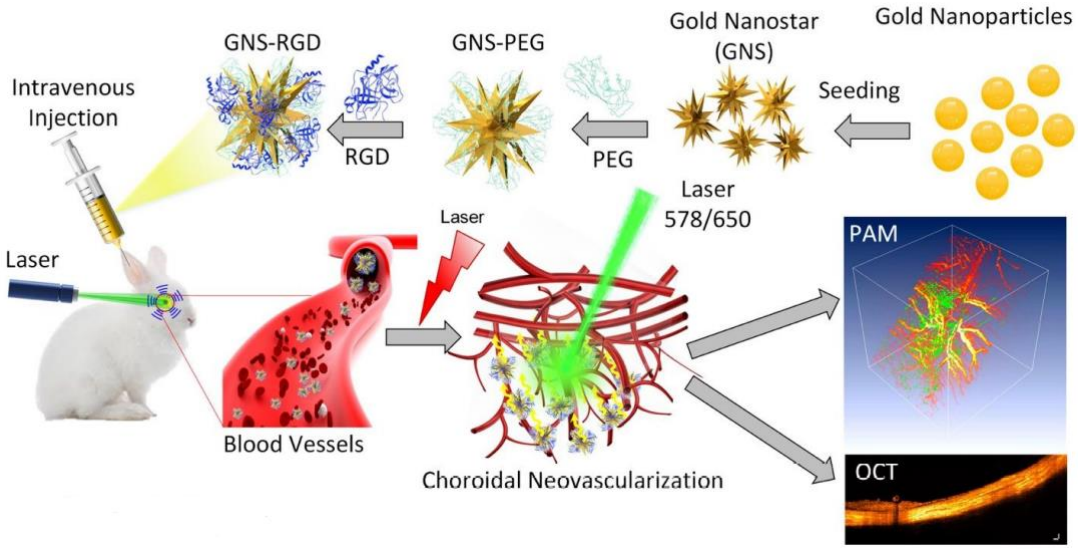

Figure 33. *Nguyen et al*. fabricated gold nanostars functionalized with RGD peptide and examined their function as contrast agents for a multimodal OCT and PAM imaging system in living rabbits, using a laser-induced choroidal neovascularization (CNV) model.

Quantitative measurements using silicon tubes filled with GNS suspension of different concentrations showed a linear relationship between the PA signal and the GNS concentration in vitro. Moreover, in vitro OCT analysis with capillary glass tubes indicated a linear relation of the OCT signal and the GNS concentration.

The in vivo studies were carried out using a laser-induced choroidal neovascularization (CNV) model in six rabbits. The rabbits were injected with 400µL of GNS (5 mg/mL). PAM images were obtained at two different wavelengths (578 nm and 650 nm) and the contrast in CNV and the microvasculature of the retina were measured. OCT images were obtained as well after the injection. The PAM images presented CNV distinctively against the choroidal vessels.

On the same rabbit, sequential images at 0 h, 2 h, 48 h, 72 h, and 5, 7, 9, 11, and 14 days post-injection showed that GNS can create contrast between CNV and the adjacent vasculature (Figure 34). There was a 17- fold increase in the PA signal inside the CNV after the GNS injection. GNS were also tested as CA for OCT and images were taken pre- and post-

injection at 2h. It was noted that CNV was depicted with better contrast after the injection and the OCT signal reached ~ 167 % higher intensity compared to pre-injection ($p < 0.001$) (Figure 35)

In conclusion, this study showed that gold nanostars can function as high-sensitivity contrast agents for OCT and PAM and allow CNV to be differentiated from the surrounding microvasculature.

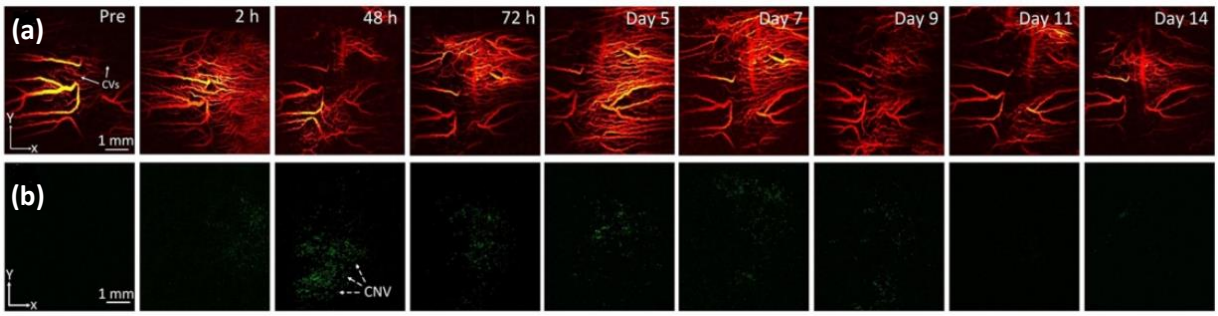

Figure 34. Longitudinal in vivo PAM images at different wavelengths: 578 nm (a) and 650 nm (b) before then GNS injection and 2 h, 48 h, 72h, 5d, 7d, 9d, 11d and 14d after the GNS injection (0.4 mL, 5 mg/mL). White arrows show choroidal vessels (CVs) and white dotted arrows show Choroidal Neovascularization (CNV)

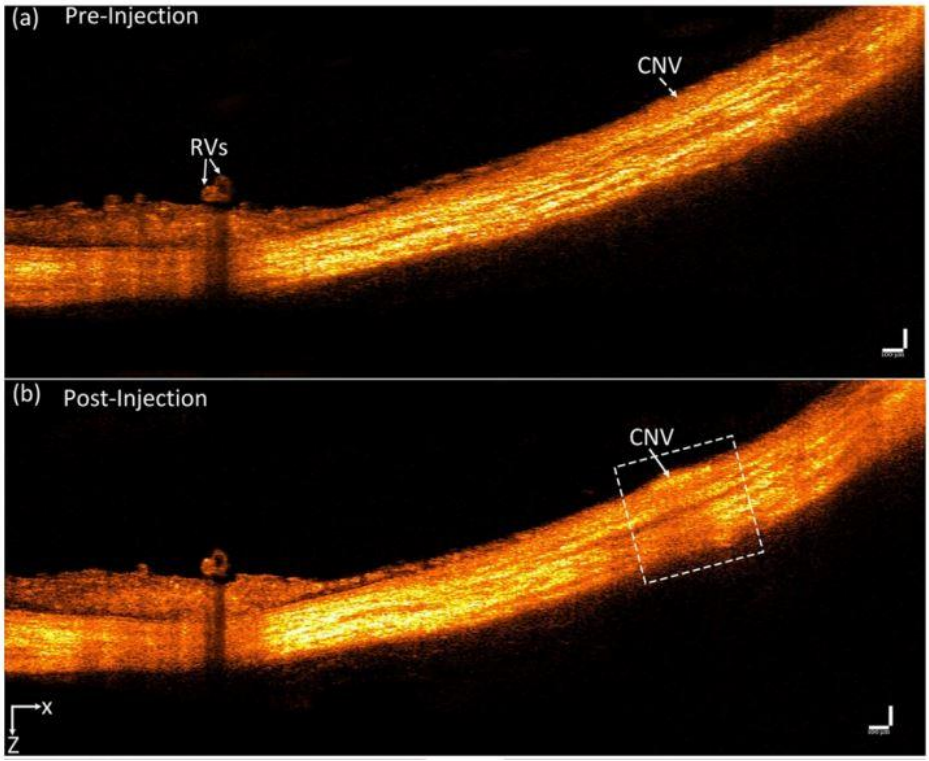

Figure 35. OCT image enhanced with GNS in vivo: B-scan OCT images obtained before (a) and 2 h after IV injection of GNS (b). The white arrows indicate the position of Choroidal Neovascularization (CNV).

Recently, the same research team created chain-like gold nanoparticle (CGNP) clusters and tested them as CA for a multimodal PAM and OCT imaging system in vitro and in vivo, in living rabbits (N=12) [188]. The nanoparticles (average diameter: 20 nm) were functionalized with arginine-glycine-aspartic acid (RGD) peptides (CGNP clusters-RGD) and exhibited peak LSPR features at 650 nm. The purpose of this study was to elucidate whether these functionalized nanoparticles can visualize choroidal neovascularization (CNV) and retinal vessels, with the hypothesis that RGD peptides target $\alpha_v\beta_3$ integrin, which is expressed in CNV (Figure 36).

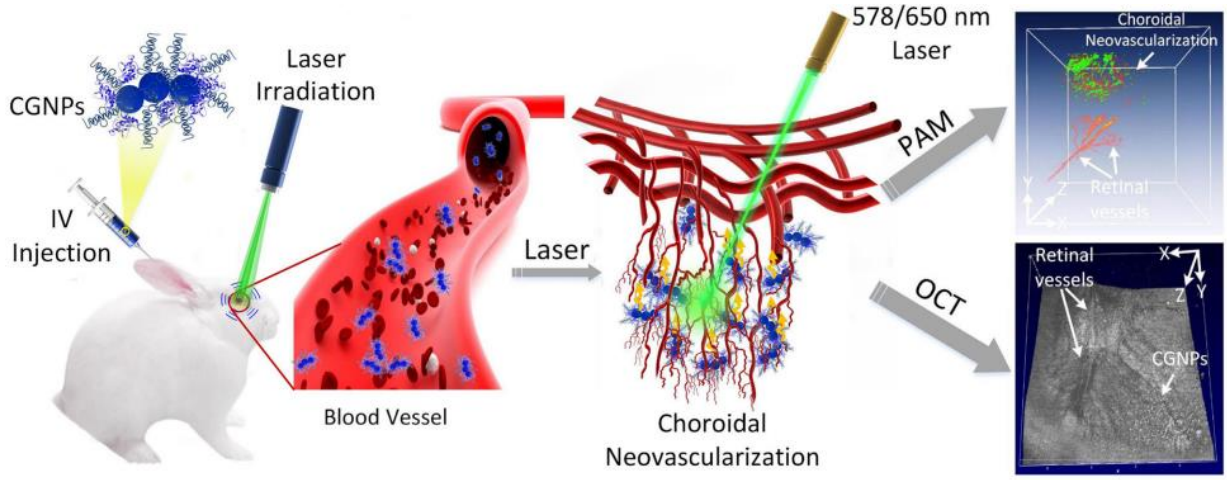

Figure 36. In vivo imaging with OCT and PAM using CGNP clusters-RGD. CGNP clusters-RGD were intravenously injected into the rabbit through the marginal ear vein. PA signals were produced with the use of nanosecond pulsed laser illumination at a wavelength of 578 or 650 nm.

For the in vitro part of their experiments *Nguyen and co-workers* used silicone tubes filled with CGNP clusters-RGD solutions at different concentrations. A linear increase (R^2 = 0.9947) of the PA signal produced was noted when raising the concentration of the nanoparticles in the solution and the threshold concentration to be detected was 0.01 mg/mL. A linear relation was also to be seen between the OCT signal and the CGNP clusters-RGD concentration (R^2 = 0.9938) and the lowest perceivable concentration was calculated at 0.005 mg/mL.

For the in vivo study, 0.4 mL CGNP clusters-RGD (5 mg/mL) was administered intravenously to rabbits with laser-induced CNV (N=3) and PA images were obtained before and after the injection at wavelengths of 578 nm and 650 nm. 2D and 3D PA images were reconstructed at several time points after the injection. The PA signal of CNV at both wavelengths was significantly elevated compared to the images before the injection. At the wavelength of 650 nm, the optical absorption from the blood vessels is decreased and therefore CNV was imaged distinctly from the surrounding vasculature. When CGNPs were administered without RGD, the signal at 650 nm was not as strong. Overall, the peak signal showed a 17-fold increase (0.11 ± 0.01 to 1.89 ± 0.1) at 24 h after the injection.

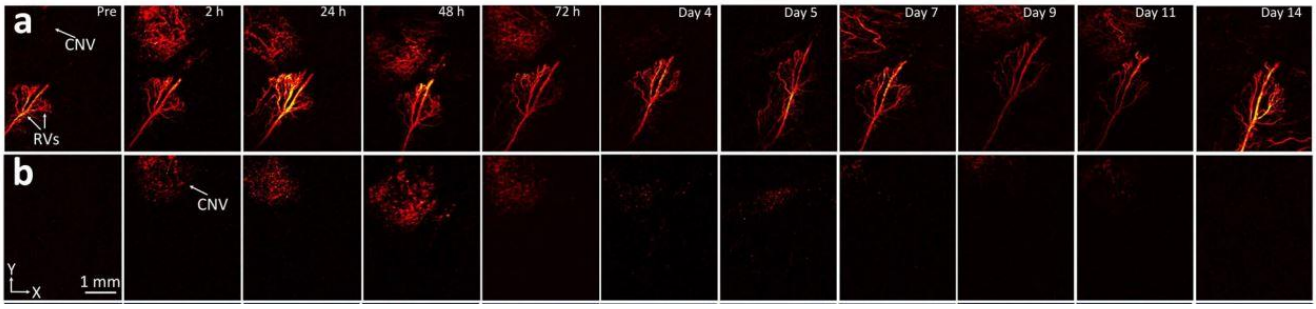

Figure 37. PAM images of CNV before and at 2 h, 24 h, 48 h, 72 h, 5, 7, 9, 11, and 14 days after injection of 0.5 mL CGNP clusters-RGD (2.5 mg/mL) acquired under nanosecond pulsed laser illumination at wavelengths 578 nm (a) and 650 nm (b) . The increase in the signal after the injection can be noticed.

OCT images were also taken before and after the IV-injection of CGNP clusters-RGD at different time points. Peak OCT signal was noticed at 48h and the contrast to noise ratio improved from 1 to 1.76. (Figure 38).

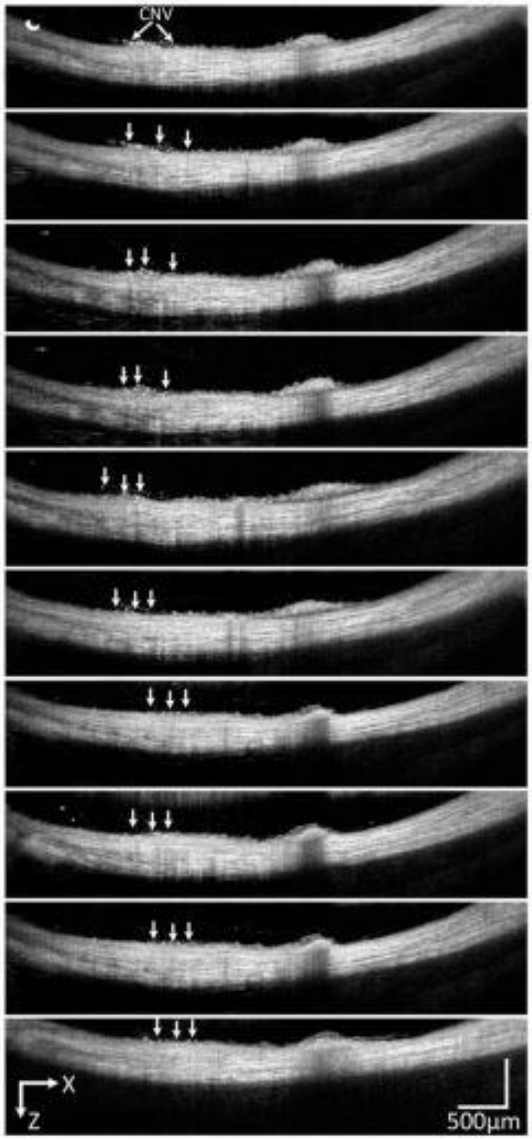

Figure 38. Cross-sectional B-scan OCT images after the injection of CGNP clusters-RGD at 2 h, 24 h, 48 h, 73 h, days 4, 5, 7, 9, 11, and 14, in vivo. White arrows indicate the location of CNV. Rabbit injected with CGNP clusters-RGD showed an increase of 176 % in the OCT amplitude compared to the pre-injection.

Table 1. In vivo studies investigating AuNPs as CA for OCT, PAI or a multimodal OCT/PAM system

Imaging Modality	AuNP Type	Dimensions	LSPR peak	Concentration / Dose	Administration	Subject Type	Results	References
SD-OCT	PEG-coated nanorods	GNR-780: length: 43 ± 4.22 nm; diam.: 12 ± 0.25 nm GNR-850: length: 49.31 ± 6.9 nm, diam.: 12.09 ± 1.63 nm	780 nm & 850 nm	GNR-780: 50 nM / 5–10 µL (corneal stroma) GNR-850: 29 pM-30 nM / 3–5 µL (AC)	Anterior chamber (AC) (GNR-850) & corneal injections (GNR-780)	Wild-type C57BL/6 mice	GNR-780: injected corneas: x3 stronger signal vs BSS-injected and x7.5 vs naïve mice; concentrations > 5 nM lead to clear contrast GNR-850 : Threshold concentration for significantly enhanced signal > 120 pM	De la Zerda et al. [171]
SD-OCT	mPEG-coated nanorods	~ 110 x 32 nm	824-830 nm (longitudinal)	10 nM/ 200 µL (in steps of 25 µL)	Intravenous injections	Nu/nu mice	Images of the retinal blood vessels showed that AuNRs were perceived at a sensitivity of ~ 0.5 nM	Sen et al. [172]
SD-OCT	Nanorods coated with poly(strenes ulfate)/ (PSS-AuNRs) or anti-CD90.2 antibodies/ Ab-AuNRs	Aspect ratio: ~ 3.4	PSS-AuNRs: 850 nm Ab-AuNRs: 857 nm	2 µL	Intravitreal injections	C57BL/6 mice	Enhanced backscattered signal in the vitreous of the mice vs control group, even after 24 h	Sandrian et al. [173]
OCT	CTAB-coated nanorods, PEG-coated nanorods, Targeted nanorods (ICAM2)	Diameter: 10 nm	808 nm	100 uL of the AuNR solution for iv injections	Intravitreal & Intravenous Injections	Wild-type C57BL/6 mice, LCNV model	Images after Intravitreal CTAB-AuNRs inj. showed amorphous opacity, PEG-AuNPs intravitreal inj. had no shadowing effect, IV inj. of targeted NPs caused unclear results due to retinal background noise	Gordon et al. [174]
PT-OCT	PEG-coated nanorods	diameter: 10 nm, length: 35 nm	750 nm	1.66 nM/ 100 µL	Intravenous injections	Pigmented mice C57BL/6, LCNV model	Statistically significant ($p < 0.05$) increase in the PT-OCT signal in the LCNV lesions	Lapierre-Landry et al. [176]

							vs the control group	
SD-OCT	Nanodisks	160 nm	830 nm	0.1 pM-10 pM	Intravitreal injections	C57BL/6 J mice	Threshold concentration for significant OCT enhancement vs the control group was found 1 pM, Signal increases in a dose-dependent manner	Song et al. [177]
OCT	PEG-coated nanospheres	Average diameter: 20 nm	532 nm	PRPs incubated with AuNPs at a concentration of 0.2 mg/ml	AuNP- & fluorescently labeled PRPs transplanted intravitreally & subretinally	Long-Evans pigmented rats	Prolonged monitoring of the transplanted AuNP-labeled cells was possible even after 1 month	Chemla et al. [179]
PAI	Doxorubicin-coated nanospheres loaded with fucoidan (Dox-Fu@AuNPs)	101.5 ± 23.2 nm	532 nm	200 µg/µL / 100 µL	Intratumoral injection in the rabbit eye VX2 tumors	New Zealand white rabbits	Dox-Fu@AuNPs-injected tumors showed stronger PA signals vs pre-injection, X 2 deeper image depth ($p < 0.001$)	Kim et al. [184]
Multi-modal PAM & OCT	PEG-coated nanospheres	20.0 ± 1.5 nm	520 nm	5 mg/mL / 0.8 mL	Intravenous injections	New Zealand white rabbits	The OCT & PAM signal from retinal and choroidal visualization was increased by 45 % and 82 % respectively vs control group	Nguyen et al. [148]
Multi-modal PAM & OCT	Nanostars conjugated with RGD peptide	Average diameter: 30 nm	650 nm	5 mg/mL / 400 µL	Intravenous injections	New Zealand white rabbits, CNV model	Photoacoustic performance raised x 17 and OCT intensities were elevated by 167 %	Nguyen et al. [187]
Multi-modal PAM & OCT	Chain-like gold nanoparticle (CGNP) clusters conjugated with RGD peptide	Average diameter: 20 nm	650 nm	5 mg/mL / 400 µL	Intravenous injections	New Zealand white rabbits, CNV model	Photoacoustic performance raised x 17 and OCT intensities were elevated by 176 %	Nguyen et al. [188]

5.2 Anti-angiogenic properties of Gold Nanoparticles

5.2.1 Mechanism of Angiogenesis

Angiogenesis describes the physiological process of formation of new blood vessels from vasculature that already exists [189]. Early stages of this process include proliferation and migration of endothelial cells as well as tube formation [190]. Pathological angiogenesis/ neovascularization plays a critical role in a number of diseases and pathological entities, such as age-related macular degeneration (AMD), ischemic heart disease, rheumatoid arthritis and cancer [191].

Vascular endothelial growth factor (VEGF) is the leading cytokine in the cascade of angiogenesis [192]. VEGF 165, an isoform of VEGF, is a heparin-binding protein, which binds to the tyrosine kinase receptor KRD (also named VEGFR-2) and is responsible for the initiation of signaling cascades and the activation of VEGFR-2/PI3K/Akt/eNOS pathway in endothelial cells [193] [194]. This results in endothelial cell proliferation, which in turn leads to migration and angiogenesis [195]. VEGFR-2 has been recognized as the key signaling VEGF receptor [196] [197]. Fibroblast growth factor (FGF) is another essential element in the pathophysiological process of angiogenesis and also binds to cell receptors with tyrosine kinase function [198].

Angiogenesis is a process controlled by the balance between pro-angiogenic growth factors like VEGF and anti-angiogenic factors. This equilibrium can be disrupted by the presence of hypoxia, which can promote neovascularization through pathways that increase pro-angiogenic factors, such as VEGF, epidermal growth factor (EGF) and transforming growth factor β (TGF-β) [199] [200].

5.2.2 Angiogenesis in ocular diseases

Pathological neovascularization is the hallmark of various diseases of the posterior segment of the eye, with the three most typical being age-related macular degeneration (AMD), diabetic retinopathy (DR), and retinopathy of prematurity (ROP). These types of retinopathy are associated with a high risk of vision loss.

Age-related macular degeneration is the leading cause of blindness in the elderly population of the Western world [201]. Two types of AMD have been recognized: “wet” AMD, which occurs through exudative neovascularization, and “dry” AMD, which concerns non-exudative geographic atrophy. In “wet” AMD, the neovascularizations pass through Bruch’s membrane and reach the RPE [202]. Diabetic Retinopathy (DR) is a manifestation of diabetes mellitus and can also appear in a proliferative and non-proliferative form [203]. In the neovascular condition, the neovascularizations pass through the inner limiting membrane and reach the vitreous cavity [204]. Retinopathy of prematurity (ROP) is a blinding condition which appears in premature infants and is characterized by abnormal development of the retinal vasculature and high sensitivity to VEGF. This disease is the primary cause of blindness in children around the globe [205].

There are two classes of neovascularization that can arise in the retina: retinal neovascularization (RNV), where new vessels grow from retinal capillaries and reach the vitreous and neural layers of the retina, and subretinal or choroidal neovascularization (CNV), where the vessels grow from the choroidal vasculature and enter the subretinal space [206] (Figure 39). However, both types of retinal neovascularization are a result of the same molecular mechanisms. VEGF is the driving force for the development and molecular pathogenesis of these retinopathies [207] [208]. Retinal neovascularization is seen in ROP, proliferative DR, and retinal vein occlusions, which are diseases characterized by the presence of an “ischemic retina”, promoting the up-regulation of VEGF and therefore the progress of retinal neovascularization. Choroidal neovascularization, on the other hand, is primarily seen in AMD cases [209]. Neovascularization in ocular diseases leads to hemorrhage in the retina and eventually in retinal detachment as well as photoreceptor

degeneration. Visual impairment or even blindness is the final result of these diseases [210] [211].

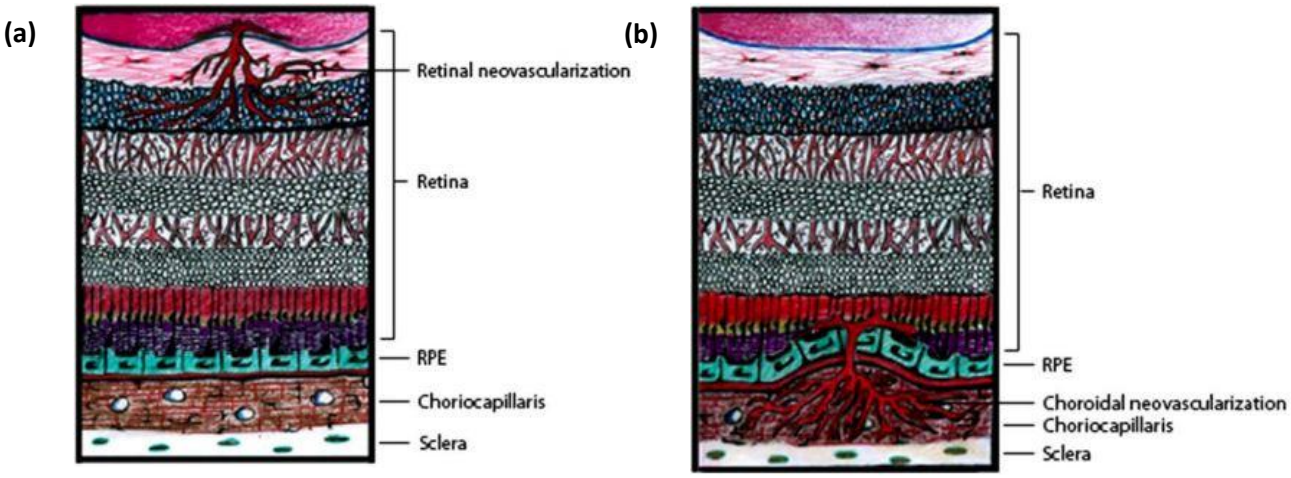

Figure 39. Schematic representation of the pathological neovascularization in retinal diseases. Retinal neovascularization (a) shows retinal capillaries invading the retinal tissue and choroidal neovascularization (b) describes choroidal capillaries passing penetrating Bruch's membrane and reaching the subretinal area [206].

Neovascularization can also appear in the cornea, which is normally avascular and transparent. This process involves the growth of new vessels from the pericorneal plexus into the corneal tissue. This sight-threatening condition can be induced by various ocular insults, such as inflammation, trauma, infection and hypoxia from the wear of contact lenses [212]. The pathophysiological mechanism of corneal neovascularization is associated with the disequilibrium between pro-angiogenic and anti-angiogenic molecules, and the production of VEGF is again of paramount importance [213]. This pathological state eventually leads to reduced visual acuity and disruption of corneal transparency [214].

For the management of the conditions described above, intravitreal injections of an anti-VEGF monoclonal antibody (bevacizumab) are performed [215]. However, these injections have been associated with a variety of implications, including inflammation, hemorrhage, endophalmitis, detachment of the retina as well as macular edema [216]. Moreover, many patients experience discomfort due to the injection frequency and are not able to comply with this method of treatment. Therefore, there is an emerging need to

develop alternative therapeutic approaches to suppress ocular neovascularization, prevent vision loss and at the same time avoid these adverse events.

A number of reports have suggested that gold salts have the ability to suppress the progression of rheumatoid arthritis, a disease which is also characterized by angiogenesis [217]. These findings encouraged scientists to delve deeper into the investigation of the anti-angiogenic potential of gold nanoparticles. Many research groups have conducted in vitro experiments to determine the mechanism through which the inhibition of neovascularization takes place and which pathways are involved. In vivo studies using Choroidal Neovascularization (CNV) models have also been performed to elucidate whether AuNPs can produce a therapeutic effect against ocular diseases characterized by angiogenesis [218]. These in vitro and in vivo studies are presented below to assemble the existing data regarding neovascularization with an emphasis on ocular applications.

5.2.3 In vitro studies

Bhattacharya et al. [219] were the first to demonstrate the capacity of gold nanoparticles to bind and inhibit vascular permeability factor/ vascular endothelial growth factor 165 (VPF/ VEGF-165). For their study they utilized gold nanospheres with a diameter of ~ 5 nm and human umbilical vein endothelial cells (HUVECs) to test their proliferation.

First, the effect of AuNPs (67, 335, 670 nM) on VEGF 165-induced cell proliferation was evaluated. The pre-incubation with AuNPs showed a statistically significant suppression in the proliferation of the cells ($p < 0.001$). On the other hand, when the proliferation of HUVECs was induced by VEGF 121, which is a non-heparin binding growth factor, AuNPs did not have a suppressing effect on the proliferation of the cells. This led to the suggestion that the inhibitory effect of gold nanoparticles is dependent on the presence of a heparin-binding domain. Therefore, AuNPs bind to VEGF 165 through its heparin-binding domain, which was proved by using XPS analysis.

Mukherjee et al. [220] inspected the potential of AuNPs (~ 5 nm) to obstruct the pro-angiogenic function of vascular endothelial growth factor/vascular permeability factor (VEGF/ VPF)-165, basic fibroblast growth factor (bFGF), VEGF 121 and endothelial growth factor (EGF). VEFG/VPF and bFGF are both heparin-binding factors, whereas VEGF 121 and EGF are non-heparin-binding growth factors.

HUVECs were selected for this experiment as well and were treated with VEGF 165 or VEGF 121 (10 ng/mL) and pre-incubated with AuNPs. Results showed that AuNPs were capable of inhibiting VEGF 165- but not VEGF 121-induced proliferation. Similarly, NIH3T3 fibroblasts were treated with bFGF or EGF (10 ng/mL) and pre-incubated with AuNPs. The inhibition of bFGF-induced proliferation of the fibroblasts was observed, but the same effect was not seen on EGF-induced cell proliferation. No toxicity was noticed in any of the two cell lines. This study, therefore, supported the idea that AuNPs require a heparin-binding domain to be effective as anti-angiogenic factors. Their studies were continued, by further searching for the inhibition mechanism involving the pathway of VEGF 165. They were able to prove

that AuNPs bind to the heparin-binding domain and block the phosphorylation of VEGFR-2 by VEGF 165.

The effect of AuNPs (50 nm) on the VEGF-induced tube development and proliferation of Bovine retinal endothelial cells (BRECs) was evaluated by *Kalishwaralal et al*. [221]. Cell proliferation assay showed that treatment with gold nanoparticles (500 nM) impeded the VEGF-induced cell proliferation. Apart from that, AuNPs were able to inhibit the migration of BRECs, with the maximum result seen at a concentration of 500 nM. Matrigel assay was used to figure out whether AuNPs impede the development of tubules in the endothelial cells, which is a key step in the process of angiogenesis. Tube formation of BRECs was inhibited at a percentage of 80 % when AuNPs were used with VEGF, which was proven to be the stimulus responsible for the presence of the tubules.

Vascular leakage is another principal pathophysiological process which characterizes the retina in various diseases, resulting from cell permeability. A dose-dependent effect of AuNPs on the prevention of VEGF-induced permeability was perceived. Lastly, *Kalishwaralal and co-workers* discovered that gold nanoparticles inhibit the phosphorylation of VEGF-induced VEGFR2 and Src, which are involved in the angiogenic pathways. In short, gold nanoparticles can, in the presence of VEFG, prevent cell proliferation, migration and tube development in BRECs in vitro.

Pan et al. [222] carried out in vitro studies on HUVECs to elucidate the mechanism through which AuNPs obstruct cell proliferation and angiogenesis. More specifically, HUVECs were treated with VEGF165 or VEGF121 (20 ng/mL) and pre-incubated with AuNPs (500 µL) at a concentration of 1,000 nmol/L. The nanoparticles had a mean diameter of 10 nm. Results from MTT and BrdU assay indicated that gold nanoparticles did not affect cell proliferation when VEGF was not present. AuNPs were capable of suppressing VEFG 165-induced endothelial cell proliferation; however, no inhibition was notable on VEGF 121-induced proliferation. These findings supported conclusions from previous studies, showing that AuNPs have a heparin-binding ability. Moreover, no cytotoxic effects were observed on HUVECs.

They continued their experiments by evaluating the relationship between AuNPs and VEGF 165-mediated phosphorylation of VEGFR2 and AKT, important steps in the angiogenesis pathways. VEGF 165 and VEGF 121 are both factors which increase the phosphorylation of these receptors. *Pan and co-workers* proved that gold nanoparticles can inhibit phosphorylation mediated by VEGF 165, but not VEGF 121. Then, near-field scanning optical microscopy/quantum dot (NSOM/QD) imaging was utilized to search for possible changes in the nanostructure of VEGFR2 caused by AuNPs. It was seen that the NPs can block VEGFR2/VEGF 165 interaction and affect the shaping of nanodomains and microdomains on VEGFR2.

The same research group proceeded with the in vitro investigation of the anti-angiogenic effects of gold nanoparticles [223]. This time, their goal was to determine their effect on endothelial cell migration and the formation of tubes. For the testing of migration, wound-healing and Transwell assays were used. HUVECs were treated with VEGF 165 (20 ng/mL) with or without gold nanospheres (diameter of 15 nm) at a concentration of 125 or 250 nM. When pre-incubation with AuNPs took place, a statistically significant reduction in the VEGF-induced cell migration was observed in a dose-dependent way.

Matrigel assay was employed to determine the effect on tube formation. The development of tubes by VEGF 165 was strongly inhibited by the presence of AuNPs. Furthermore, the function of Akt was examined with Western blotting and pre-incubation with gold nanoparticles showed limited phosphorylation in the HUVECs in a dose-dependent manner.

The inhibitory ability of AuNPs (3–5 nm) on VEGF-induced choroid-retina endothelial (RF/6A) cell migration was studied by *Chan et al*. [224] in vitro. Transwell migration assays were utilized for the evaluation of RF/6A cell migration. The migration of cells was induced by the presence of VEGF and they noticed that when VEGF was pre-incubated with AuNPs, migration was prevented accordingly to the dose. This effect was not visible, without VEGF treatment.

The effect of AuNPs on the attachment of RF/6A cells to fibronectin was also tested, to understand whether it could affect the migration process. However, no such interference

was found to be responsible for the suppression of cell migration. Furthermore, the possibility of a cytotoxic effect was excluded as a factor in the results on cell migration, through MTT assays. AuNPs of different concentrations (1, 2, and 4 ppm) did not decrease the viability of RF/6A cells. The effect of AuNPs on the phosphorylation of protein kinase B (Akt) and endothelial nitric oxide synthase (eNOS), whose pathways are related to angiogenesis, was also evaluated. Western blot results indicated the decrease of VEGF-induced phosphorylation in a dose-dependent way. The above results suggest that gold nanoparticles hinder the migration of endothelial cells via the pathways of Akt/eNOS, without affecting the viability of the cells or the adhesion to fibronectin.

Arvizo et al. [225] were able to prove that the angiogenesis inhibitory ability of gold nanoparticles is dependent on their size and surface charge. Using AuNPs of different sizes (5, 10, and 20 nm) to stimulate HUVEC cells pre-incubated with VEGF 165, they showed that they inhibited heparin-binding growth factors (HB-GFs), such as VEGF 165 and basic fibroblast growth factor (bFGF). The nanoparticles with the larger diameter (20 nm) exhibited the strongest effect and it was also proved that a naked NP surface is essential for the inhibition process.

5.2.4 In vivo studies

The anti-angiogenic properties of gold nanoparticles were evaluated by *Roh et al*. [226], who conducted in vitro and in vivo studies using a choroidal neovascularization model in mice.

For their in vitro studies, they used human umbilical vein endothelial cells (HUVECs) to explore the effect of AuNPs on the development of a capillary network induced by VEGF treatment. The cells were treated with AuNPs at different concentrations (0.1, 1, and 10 μM) and a concentration-dependent decrease in the tube formation was noted. Using an MTT assay it was also found that the proliferation of HUVECs was hindered when treatment with AuNPs took place. Moreover, treatment with AuNPs suppressed the phosphorylation of ERK1/2, Akt, and FAK in HUVECs, which takes place in angiogenesis and is induced by VEGF. Lastly, using an RPE cell line (ARPE-19), no increase in apoptosis and no cytotoxic effects caused by the presence of AuNPs were observed with flow cytometry.

For the in vivo part of their study, C57BL/6 mice were chosen (N=40) and CNV occurred by the rupture of Bruch's membrane via laser photocoagulation. A day later, gold nanoparticles with a neutral charge and size of 20 nm were injected within the vitreous of the mice (n=10) at a concentration of 10 μM and a total dose of 1 μL. The control group received a PBS injection of the same dose instead (n=10). Images of choroidal flat-mount preparations obtained by the two groups showed suppressed CNV progress in the AuNP-treated group. The decrease in the mean CNV area of the lesions in the treated group was calculated to be 67.9 % ($P < 0.001$) in comparison to the untreated one (Figure 40). Immunofluorescence staining with the use of markers, such as isolectin B4, to label endothelial cells was performed 14 days after laser coagulation. Less staining in the CNV regions which were treated with AuNPs was seen in comparison to the control group.

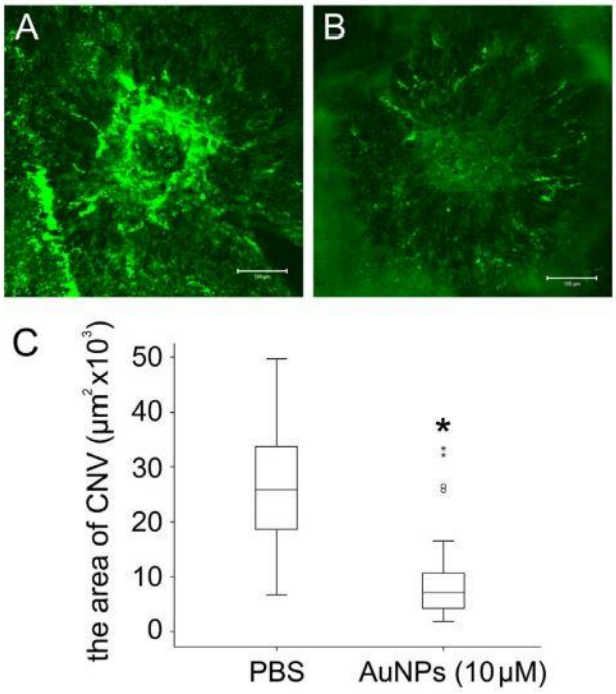

Figure 40. Images of choroidal flat-mount preparations of the mice treated with PBS intravitreal injections (A) and the mice treated with AuNPs intravitreal injections (B). *Roh and co-workers* calculated that the mean CNV region of each lesion was about 26,160.9 and 8400.8 respectively. This means that the development of CNV was decreased by 67 % in the treated group. The length of the scale bar (C) represents 100 μm. The difference in the CNV formation between the two groups was statistically significant ($P < 0.001$).

Song et al. [177] used gold nanodisks to investigate their anti-angiogenic effect both in vitro and in vivo in C57BL/6 J mice. After calculating the concentration of VEGF bound to GNDs at concentrations of 1 pM and 3 pM via ELISA, in vitro angiogenesis assays took place. They noticed that GNDs were able to suppress migration of human retinal microvascular endothelial cells (HRMECs) when their concentration was 3 pM, but were not as successful at 1 pM.

For their in vivo study, they selected a mouse model with oxygen induced retinopathy. Intravitreally injected gold nanodisks caused inhibition of the neovascularization at concentrations 1 pM and 3 pM, with the larger concentration having a stronger effect. To assess the potential toxic effect, histological examination, TUNEL assay as well as an electroretinogram (ERG) took place 5 weeks post-injection of NPs at 10 pm. No inflammation or apoptosis was observed and changes on ERG were of no significance.

The therapeutic effect of systematically delivered AuNPs in a laser-induced CNV animal model was monitored by *Singh et al*. [227] with the use of OCT imaging and confocal scanning laser ophthalmoscope (cSLO) in vivo. CNV lesions were induced in pigmented wild

type (C57BL6/J) mice (N=18) via laser. All animals received intravenous injections (50 μL) of either the nanoparticle solution (average diameter of 50 nm) at a concentration of 4.37 × 10^{10} nps/mL or Phosphate -Buffered Saline (PBS) through the tail vein on days 0 and 4 after the laser injury.

Fluorescein angiography (FA) images were obtained at days 7, 14 and 21 after the laser injury from both the experimental and the control group. Dye leakage was calculated and compared between the two groups of mice. The FA images showed that the AuNP-treated group was characterized by a statistically significant decrease in the leakage area when compared to the PBS-injected group on all testing days. OCT imaging at the same time points indicated a reduced lesion volume in the treated animals in a statistically significant manner. The decrease was calculated at ∼ 53 % on days 7 and 14 and ∼ 35 % on day 21, due to the intrinsic healing that took place in both groups (Figure 41).

After the FA and OCT imaging on day 21, the mice were euthanized and the eyes were enucleated and the choroid was isolated. Samples were stained with the endothelial cell marker Isolectin B4. Images of the retinal flat mounts showed reduced CNV area (∼ 75 %) in the treated group. TEM images confirmed the presence of AuNPs in the CNV lesions and the junctions between RPE and the photoreceptors. In conclusion, the longitudinal evaluation of CNV lesions through in vivo imaging highlighted the therapeutic potential of gold nanoparticles against neovascularization after systemic administration.

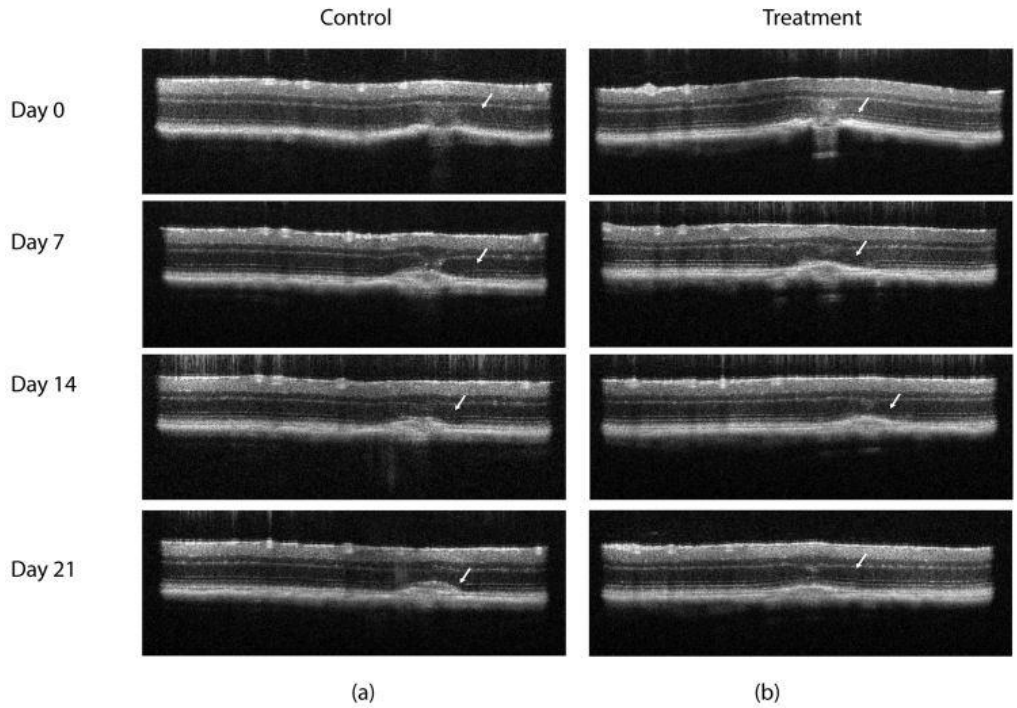

Figure 41. OCT – CNV volume representative images of PBS-injected mice/control group (n=17) (a) and AuNP-treated/treatment group (n=24) (b) at various time points (day 0, 7, 14, 21) after the laser injury. A statistically significant reduction was observed at each time point.

Shen et al. [228] presented autophagy as another mechanism which explains the anti-angiogenic ability of gold nanoparticles. Initially, in vitro experiments took place to measure the proliferation of HUVECs when treated with AuNPs. EdU kit measures DNA replication and can subsequently provide information about cell growth. Data showed that AuNPs decreased HUVEC proliferation in a dose-dependent way. Cell migration was another factor that was evaluated and results indicated a dose-dependent suppression of HUVECs migration after treatment with AuNPs, compared to the control group. Moreover, Matrigel assay was utilized to study tube formation. Data revealed that the presence of gold nanoparticles diminished capillary formation.

For the in vivo experiment, 0.4 μL of AuNPs at a concentration of 1.2 μg were injected into the vitreous of C57BL/6 mice, which served as the treatment group, whereas the control group was PBS-injected. Oxygen-induced retinopathy model was chosen to assess the effect of gold nanoparticles on retinal angiogenesis, and the retinas were stained with

isolectin B4. This retinopathy model exhibits avascular and neovascular regions. However, in the AuNP-treated mice group a reduction in these regions was observed suggesting the therapeutic properties of gold nanoparticles against oxygen-induced retinopathy. In an effort to elucidate the mechanism explaining these therapeutic effects, *Shen and co-workers* used confocal microscopy to determine the accumulation of LC3, a marker of autophagy. While the fluorescent green dots and red dots were scattered evenly in the control group, the number of the dots was increased in the treatment group, proving the induction of autophagy. Western blotting confirmed alteration in the expression of autophagic markers after AuNP treatment. Overall, the research group supported the concept that gold nanoparticles inhibit retinal angiogenesis through the activation of autophagy.

Aside from choroidal neovascularization, the corneal neovascularization model has also been investigated upon exposure to AuNPs. *Cho et al*. [229] administrated gold nanoparticles (20 nm) topically in Balb/c mice, after the induction of inflammatory corneal neovascularization through alkali burns. The treatment group (n=15) received AuNPs at a dose of 5 mL per drop, whereas the control group (n=15) received PBS drops of the same dose.

The presence of corneal neovascularization between the border and the limbus was confirmed with a digital camera 7 days after the alkali burns. It was observed that the AuNP-treated mice group exhibited a statistical reduction in corneal neovascularization in comparison to the control group ($P = 0.002$). The neovascular region was calculated to be 34.2 % ± 7.8 % of the total corneal area in the treated mice and 56.8 % ± 11.6 % in the control group (Figure 42). *Cho and co-workers* utilized Western blot analysis to evaluate VEGFR2 and p-ERK1/2 expression and determine the mechanism leading to neovascularization inhibition. The increase in VEGF expression in the treated group was smaller than the one of the control group when compared with corneal areas which did not receive alkali burns ($P = 0.029$). Moreover, AuNPs suppressed the ERK phosphorylation induced by the burns ($P = 0.029$). These results disclosed that the mechanism of corneal neovascularization suppression is due to inhibition of the ERK pathway.

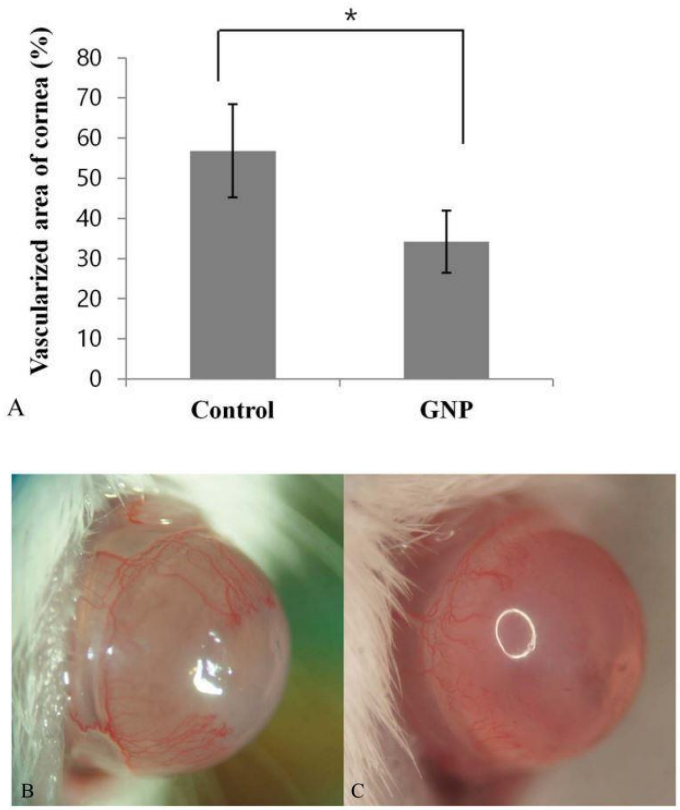

Figure 42. Topical administration of gold nanoparticles in mice model of corneal neovascularization. One week after the alkali burns, images taken from the PBS-treated/control group (a) and AuNPs-treated/treatment group (b) showed a reduction in the area of corneal neovascularization in the treated group. This suppression was calculated to be 39.8 % when the two groups were compared and was statistically significant (*P , 0.05)

The in vivo studies exploring the anti-angiogenic properties of AuNPs are summarized in Table 2.

Table 2. In vivo studies investigating the use of Gold Nanoparticles as anti-angiogenic factors

AuNP type	Size	Concentration / Dose	Administration	Subject Type	Pathology	Results	References
Nanospheres	20 nm	10 μM / 1 μL	Intravitreal	C57BL/6 mice	Laser-induced CNV	CNV growth presented a 67 % reduction in AuNP-treated mice vs control group	Roh et al. [226]
Nanodisks	160 nm	1 pM, 3 pM	Intravitreal	C57BL/6 J mice	Oxygen-induced retinopathy	Inhibition of neo-angiogenesis in a dose-dependent manner	Song et al. [177]
Nanospheres	50 nm	4.37×10^{10} nps/mL / 50 μL	Intravenous	C57BL6/J mice	Laser- induced CNV	OCT & cSLO imaging showed statistically significant reduction in CNV lesion areas in AuNP-treated vs control group	Singh et al. [227]
Nanospheres	26.2 ± 2.8 nm	1.2 μg / 0.4 μL	Intravitreal	C57BL/6 mice	Oxygen-induced retinopathy	AuNPs exhibit therapeutic effects on oxygen-induced retinopathy & inhibit retinal angiogenesis by inducing autophagy	Shen et al. [228]
Nanospheres	20 nm	5 mL/drop	Topical	Balb/c mice	Alkali burns-induced corneal neovascularization	AuNP-treated group demonstrated a reduction of 39.8 % in the neovascular corneal region vs control group	Cho et al. [229]

5.3 Ocular distribution and safety of gold nanoparticles

5.3.1 Factors affecting distribution and safety of gold Nanoparticles

Even though gold nanoparticles offer unique properties and are promising candidates for diagnostic and therapeutic purposes in Ophthalmology, it is of paramount importance to test their bio-distribution and potential bio-accumulation and toxicity, in order to introduce them in clinical practice. They are generally considered to be non-toxic, but there is also data indicating the possibility of a toxic effect [230] [231] [232].

Factors which can alter the biocompatibility of gold nanoparticles need to be studied thoroughly. Among those belong the size and concentration of the NPs [233] [234]. The significance of the nanoparticle size was highlighted by *Jong et al*. [235], who carried out in vivo experiments by intravenously injecting gold nanospheres in rats. The NPs chosen were of various diameters ranging from 10 to 250 nm. The smaller nanospheres with a diameter of 10 nm were spotted in various organs, including blood, liver, spleen, kidney, testis, thymus, heart, lung and brain. On the other hand, larger NPs were only detected in the blood, the liver and the spleen. These results supported a size-dependent distribution of gold nanoparticles after systematic delivery in rats. A similar study with intravenous delivery of gold nanospheres of various sizes (15, 50, 100 and 200 nm) in mice was conducted by *Sonavane et al*. [236]. The smaller NPs presented again wider distribution in the mice organs, including blood, liver, lung, spleen, kidney, brain, heart, and stomach. Nanoparticles with sizes below 50 nm were able to cross the blood–brain barrier (BBB).

The repeated administration of gold nanoparticles (12.5 ± 1.7 nm) was assessed by *Lasagna-Reeves et al*. [237] in C57/BL6 mice. Gold nanoparticle solutions were given through daily intraperitoneal injections (100 µL) in various doses in different groups: 40, 200, and 400 µg/kg/day for 8 days. The gold nanoparticles were distributed into tissues and the blood levels were similar among the groups, but in other organs such as the kidneys and the spleen, the accumulation followed a dose-dependent pattern. However, no changes in the weight and the behavior of the animals were noted as well as any changes in the tissue morphology or hematological and histopathological examinations occurred.

Apart from the size and dose of the administrated nanoparticles, their surface chemistry and charge are also key factors for their biocompatibility profile. The presence of cetyltrimethylammonium bromide (CTAB), a cationic detergent utilized as a stabilizing agent for the preparation of AuNPs, has been found to cause cytotoxicity [129] [238]. To reduce this cytotoxic effect, *Niidome et al*. [239] fabricated Au nanorods modified with polyethyleneglycol (PEG) and removed CTAB, and tested their biocompatibility profile in vitro and in vivo. In vitro results using HeLa cells showed reduced cytotoxicity, when CTAB was replaced with PEG. When PEG modified Au nanorods when injected intravenously in mice, more than 50 % of the NPs were detected in the blood, whereas in the case of CTAB-stabilized Au nanorods, they were mostly spotted in the liver.

Therefore, the modification of PEG can offer stealth properties and reduce cytotoxicity and bioaccumulation. The stealth characteristics are also related to the fact that PEG obstructs the binding of plasma proteins on the NP surface, helping it avoid recognition by the reticuloendothelial system. Gold nanoparticles modified with PEG of high molecular weight (> 5000 Da) were found to provide better stability and cause less toxicity than those modified with PEG of low molecular weight (< 5000 Da) [240].

The charge of gold nanoparticles can also affect their potential toxicity. *Goodman et al*. [241] tested cationic gold nanospheres with a diameter of 2 nm and found that they were toxic in a cell line. However, nanospheres at the same concentration and of the same size which had a negatively charged surface did not cause toxicity in the same cell line.

5.3.2 Studies investigating ocular distribution and safety of gold nanoparticles

All the parameters analyzed above are important factors to be taken under consideration in in vivo and clinical applications of gold nanoparticles. The studies that have been presented in this dissertation have generally provided results of non-toxicity related to the use of AuNPs, unless indicated otherwise. However, limited research has been conducted regarding AuNP compatibility in ocular cells and tissues. The in vitro, ex vivo and in vitro experiments which consider the distribution and safety issues of AuNPs towards retinal cells and ocular tissues are presented below, with the intention of gaining a better perspective on this matter.

5.3.2.1 In vitro studies

The biocompatibility of AuNPs of different morphologies and sizes was examined by *Karakoçak et al*. [242] using a retinal pigment epithelial cell line (ARPE-19). The NPs selected for their experiments were Au spheres (5-100 nm), cubes (50 nm) or rods (10 × 90 nm) at concentrations ranging from 0.01 to 5 mg/mL. To understand the potential toxicity of the AuNPs and the effect of their shape and concentration, the lethal dose required to kill 50 % of the cells (LD_{50}) was calculated with the use of an MTT assay (3-[4, 5 dimethyl-thiazoly-2-yl] 2-5 diphenyl tetrazolium bromide).

Results indicated that Au nanospheres with diameters of 5- 30 nm as well as Au nanorods with dimensions 10 × 90 nm were capable of decreasing the viability of the cells even at concentrations of 0.05 mg/mL. On the other hand, larger nanospheres with diameters of 50 and 100 nm and nanocubes of 50 nm did not affect the viability in a significant manner. When the surface area of the nanoparticles was correlated to cell viability, it was seen that independently of the nanoparticle size, the increased surface area was associated with decreased biocompatibility of the spherical AuNPs. Interestingly, the surface area concentration that caused the death of half of the retinal cells ($LD_{50,A}$) was reported to be similar for the spheres of various dimensions (5-30 nm). The above findings

imply that adjustment of the surface area is important for the application of AuNPs in imaging or as therapeutic agents.

The proliferation of ARPE-19 cells was also studied by *Hayashi et al*. [243] in correlation with AuNP exposure. Gold nanoparticles at different concentrations (10 μM, 100 μM, and 1 mM) were added to the growth medium. They were able to verify that the presence of gold nanoparticles at the above concentrations did not affect the growth of the cells, when compared to the control.

5.3.2.2 Ex vivo studies

Kim et al. [244] studied the distribution of Au nanoparticles in the retinal layers after intravenous administration in C57BL/6 mice, ex vivo. AuNPs with diameters of 20 nm and 100 nm were studied in enucleated mice eyes for their ability to penetrate the blood-retinal barrier (BRB) and their safety and potential cytotoxicity were evaluated. A day after the AuNPs IV injection (1 g/kg), the NPs with a diameter of 100 nm were not found in the retina, whereas the 20 nm NPs were able to pass through the BRB and reached all of the retinal layers. Histological evaluation at days 1 and 7 after the injection of 20 nm AuNPs showed no signs of inflammation in the vitreous, retina, or choroid. Furthermore, no changes in the viability of astrocytes and retinoblastoma cells were observed, as well as any alterations in the expression of proteins by retinal endothelial cells. In conclusion, intravenously injected Au nanoparticles can penetrate the BRB in a size-dependent manner and were proven safe. This study proves that the size of the gold nanoparticles is determining factor for the distribution within the retina. Smaller nanoparticles present increased bioavailability and can therefore be more effective as imaging or therapeutic elements in ophthalmology. However, at the same time, wider distribution within the retinal layers can also be associated with higher possibility of toxicity. Therefore, the balance between these two events needs to be investigated, in order to achieve high bioavailability and low toxicity.

Söderstjerna et al. [245] used an ex vivo cultured mouse retina model (C3H wild-type) to analyze the effect resulting from the exposure of 20 and 80 nm Ag- and AuNPs at low concentrations. Using TEM analysis 72 after the exposure, the distribution of the nanoparticles of both dimensions was revealed across all retinal neuronal layers and the smaller NPs were also localized within the nucleus of cells and other cellular compartments. An increase in the number of pyknotic cells and vacuoles was observed in the inner plexiform layers (IPL). Apart from the above morphological changes, the nanoparticles affected glial and microglial function, as well as induced cytotoxicity, apoptosis and oxidative stress. Gold nanoparticles can, therefore, give rise to adverse effects on the mouse retina model both on a cellular and tissue level.

Gold nanorods were delivered intravitreally to Dutch-belted rabbits (N: 16, eyes: 32) by *Bakri et al*. [246], to evaluate whether they can cause toxicity to the retina ex vivo. Each rabbit had one eye injected with GNRs and the other served as a control and 8 of them received a dose of 67 μmol/0.1 mL and the rest a dose of 670 μmol/0.1 mL. From each of these groups, 4 rabbits were killed 15 days after the injection and the rest 29 days post-injection and the eyes were enucleated. Visualization of the inner layers of the retina did not indicate cellular atrophy or disorganization. In both the control and treatment group, the formation of vacuoles in the cells of the ganglion layer and disorganization of the outer segments of the photoreceptors was observed to the same extent, which was attributed to autolysis. However, no toxicity in the histological analysis of the retina and the optic nerve was detected as well as any ocular inflammation was seen with light microscopy.

5.3.2.3 In vivo studies

Kim et al. [247] used Zebrafish embryos to evaluate the effect of Au nanoparticles on ocular development in vivo. Gold nanospheres with cores of 1.3 nm were functionalized with positively charged N, N, N-trimethylammoniumethanethiol (TMAT) through covalent bonds. Zebrafish exposed to TMAT-AuNPs were found to develop eyes that were smaller and paler in color than normal. Furthermore, genes linked to apoptosis, like p53 and bax, were up-regulated, whereas genes linked with eye development, such as pax6a, pax6b, otx2, and rx1, were down-regulated. The decreased pigmentation and the repression of ocular growth in embryos indicated that TMAT-AuNPs are capable of inducing unfavorable effects on eye development in mammals.

After confirming the utility of gold nanorods as contrast agents for OCT and visualizing them in the vitreous of mice, *Sandrian et al*. [173] proceeded to examine the potential inflammatory effect of intravitreal GNR injections. Four groups of C57Bl/6 mice were examined: untreated group (n=6), phosphate-buffered saline (PBS) injected mice (n=6), GNR injected mice (n=5) and mice injected with GNRs coated with anti-CD45 antibodies, which are expressed by cells of the immune system. The last two groups were characterized by a significant increase of CD45+ cells in the eye. The increase in the number of leukocytes, predominantly neutrophils, was attributed to ocular inflammation, which could not be ascribed to either tissue injury caused by the injection or contamination from endotoxins or bacteria. Therefore, it is important to further investigate which parameters concerning gold nanoparticles could be responsible for the induction of inflammation, with the goal of altering them and enabling in vivo application of AuNPs.

Intravitreal injections were also performed by *Olson et al.* [248] with the purpose to assess the potential changes in retinal electrical activity in vivo. For their study they used brown Norway rats (N=8, eyes: 16) and suspensions of colloidal gold nanoparticles (CGN) were delivered within the vitreous of the right eyes of the animals, while the left eyes did not receive an injection and were used as controls. ERGs were carried out before and six weeks after the injections, in order to compare the results. No statistically significant difference was spotted in any of the steps of the ERGs six weeks after the injections between the two

groups. Therefore, the injection of the Au nanoparticles did not elicit any electrophysiological changes and did not affect the electrical function of the retina in rats.

Song et al. [177] delivered gold nanodisks intravitreally to mice, attempting to study their ability to work as OCT CA and inhibit neovascularization, as described previously. After having proved that GNDs could enhance imaging and inhibit neovascularization, without causing any toxicity or inflammation in vivo, they continued their experiments to evaluate the clearance of gold nanodisks in vivo. For this reason, they injected GNDs (diameter of 160 nm) within the vitreous of mice at concentrations of 10 pM. Afterward, the clearance of the NPs was estimated by using OCT. Imaging 6 hours post-injection showed, that the gold nanodisks were scattered all over the vitreous, whereas at day 7 they were only detected in the hyaloid canal. Finally, 14 days after the injection the gold nanodisks were not to be detected or accumulated any longer (Figure 43)

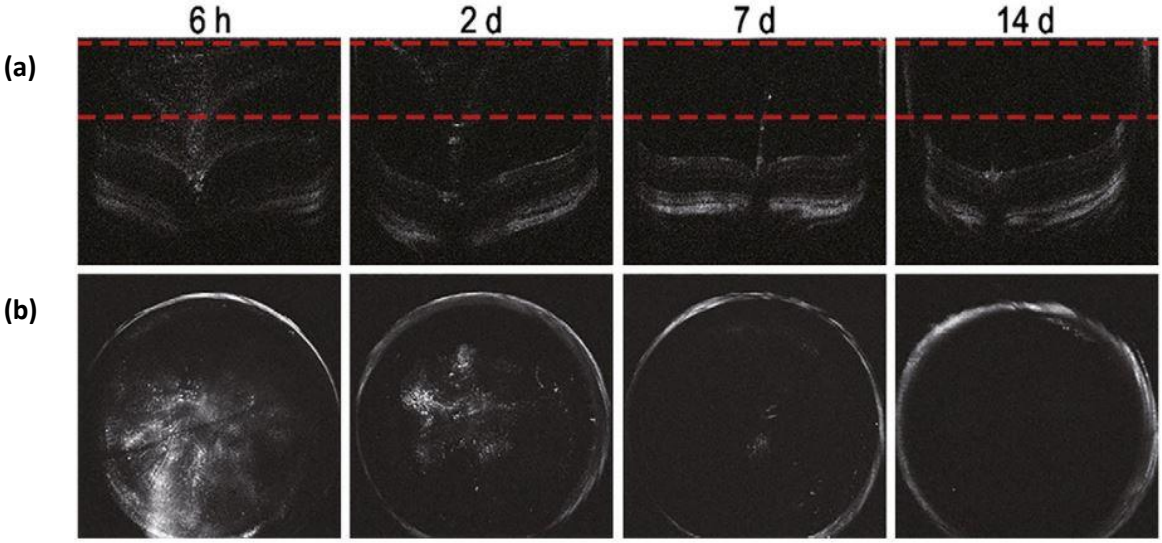

Figure 43. OCT images showing the in vivo clearance of gold nanodisks after their intravitreal injection in mice. Cross-sectional images at various time points (6 h, 2 d, 7 d and 14 d) were received (a) and Projectional images (b) from the regions defined by the red lines.

Apart from intravitreal delivery of AuNPs, subretinal injections have also been performed to study the distribution of the NPs in the retina in vivo. More specifically, *Hayashi et al*. [243] adsorbed goat IgG antibodies on gold nanoparticles (12 nm) and injected

them into the subretinal space of pigmented Dutch-belted rabbits (N=22). Fundus photographs were obtained at 7 days, 1 month and 3 months after the injection.

The image one month post-injection showed mild pigmentation in the RPE and retinal degeneration, which were more noticeable at 3 months. However, similar results were obtained when IgG with PBS or AuNPs were injected instead of IgG-adsorbed GNPs. Histological analysis of euthanized rabbits was performed at the above time points, in order to detect the presence of AuNPs within the retinal layers. One week after the injection, IgGs were found in the RPE, the photoreceptor layer, the ONL, and the OPL, and retinal degeneration was seen in the ONL and the photoreceptor layer. TEM showed that gold nanoparticles also reached the lysosomes of the RPE cells. Nevertheless, when IgG with PBS was injected, they were detected in less retinal layers and milder degeneration was observed. In conclusion, they proved that AuNPs can be delivered to photoreceptor cells and RPE, but the presence of retinal degeneration needs to be further studied.

Topical administration of gold nanoparticles is another way to deliver drugs, when aiming to reach the anterior segment of the eye [249]. *Azharuddin et al*. [250] performed in vivo experiments with guinea pig models (N= 20) and investigated whether the topical application of gold nanoparticles for therapeutic purposes is safe. For this purpose, the inertness of the corneal endothelium was tested, as well as the ability of AuNPs to penetrate the corneal layers. The treatment with the NPs (hydrodynamic diameter: 20-30 nm) lasted for 2 weeks and the histological examinations were performed after a month. TEM imaging showed the presence of gold nanoparticles in different corneal layers, primarily in keratocytes, indicating the permeability properties of the NPs. The morphology of the endothelial cells appeared normal and the intracellular organelles were intact one month after the topical application and no signs of inflammation were seen when examined with a slit lamp.

6 Discussion

Gold is a noble metal, which when designed to belong in the nanoscale, presents fascinating physical and chemical properties. Over the last decades there has been tremendous growth in scientific research exploring the unique characteristics of gold nanoparticles and their ability to augment bioimaging. AuNPs exhibit interesting optical features attributed to the localized surface plasmon resonance effect (LSPR). The LSPR phenomenon concerns the collective oscillation of conductive electrons under the excitation by an electromagnetic field. This effect involves two light-matter interactions: scattering and absorption. The extinction peaks of AuNPs can be tuned by tailoring the geometry and size of the nanostructure and can be shifted from the visible to the near-infrared region of the spectrum.

Consequently, the LSPR properties of AuNPs can be appropriately adjusted to the operating wavelength of an imaging modality. In the case of Optical Coherence Tomography, gold nanoparticles can enhance the backscattering of the light and improve image quality, and regarding Photoacoustic Imaging, they can increase the light absorption and, thus, improve photoacoustic performance. These novel imaging modalities can be used for ocular visualization and monitoring of various diseases of the anterior and posterior segments of the eye. However, early diagnosis can often be challenging in clinical practice, and molecular imaging needs to be encouraged. As a result, gold nanoparticles have been investigated through in vitro, ex vivo, and in vivo studies in animals, for their eligibility as contrast adjuvants in the above mentioned modalities. This novel idea has brought encouraging results so far, suggesting that gold nanoparticles can significantly improve ophthalmic imaging and function as contrast agents.

Apart from the exploitation of gold nanoparticles for advancements in ophthalmic imaging, these nanostructures also show great potential for therapeutic purposes. Various ocular disorders are characterized by the formation of new blood vessels, a process known as neovascularization, and current therapeutic options are not sufficient. In vitro studies on various cell lines have proved that gold nanoparticles present anti-angiogenic properties. This suppression is mainly achieved through the disruption of the interaction between VEGF 165

and its tyrosine kinase receptor, VEGFR2. Vascular Endothelial Growth Factor (VEGF) is a key molecule in the molecular pathway of angiogenesis. Therefore, inhibition of its function blocks the development of new blood vessels. Moreover, in vivo studies in animals have shown that intravitreal or intravenous injections of AuNPs suppress ocular neovascularization and CNV lesions.

The above characteristics of gold nanoparticles render them attractive candidates for the improvement of ophthalmic diagnostic and therapeutic capabilities. This dual function could potentially allow us to introduce them as “theranostic” agents in ophthalmology in the future. Gold nanoparticles have already been applied as theranostics means in other fields of medicine, primarily in oncology, for the diagnosis and therapy of cancer. Therefore, the concept of employing them also in ophthalmology, by combing the improvement of ocular imaging and management of neovascular conditions, is appealing.

However, before progressing from bench to bedside, there are challenges to be addressed and dealt with. The in vivo studies investigating the above effects have been recently introduced and are still limited in number. Further research in ocular tissues should be encouraged, in order to fully understand the capabilities of gold nanoparticles in this field and move forward to clinical translation of their promising results. Additionally, studies on the ocular distribution of AuNPs and possible toxic effects are limited and the results regarding their biocompatibility are conflicting. As a result, these unaddressed issues should be thoroughly examined before applying gold nanoparticles in the clinical practice of Ophthalmology.

7 Conclusion

Gold nanoparticles are characterized by unique physical and chemical features and present great potential as both imaging and therapeutic agents in ophthalmology. Their ability to act as contrast adjuvants for OCT and PAI has been exhibited through numerous studies, and early diagnosis and monitoring of various diseases can be improved. Additionally, gold nanoparticles present anti-angiogenic properties, which could be useful for the management of ocular diseases characterized by neovascularization. However, before combing the diagnostic and therapeutic potential of gold nanoparticles, further research is required as well as a better understanding of the ocular distribution and biocompatibility of these nanostructures.

8 References

[1] R. P. Feynman, “There’s plenty of room at the bottom,” *Eng. Sci.*, vol. 23, no. 5, pp. 22–36, 1960.

[2] G. A. Silva, “Introduction to nanotechnology and its applications to medicine,” *Surg. Neurol.*, vol. 61, no. 3, pp. 216–220, 2004, doi: 10.1016/j.surneu.2003.09.036.

[3] I. Khan, K. Saeed, and I. Khan, “Nanoparticles: Properties, applications and toxicities,” *Arab. J. Chem.*, vol. 12, no. 7, pp. 908–931, 2019, doi: 10.1016/j.arabjc.2017.05.011.

[4] Q. L. Zhu and Q. Xu, “Immobilization of Ultrafine Metal Nanoparticles to High-Surface-Area Materials and Their Catalytic Applications,” *Chem*, vol. 1, no. 2, pp. 220–245, 2016, doi: 10.1016/j.chempr.2016.07.005.

[5] M. A. Gatoo, S. Naseem, M. Y. Arfat, A. Mahmood Dar, K. Qasim, and S. Zubair, “Physicochemical properties of nanomaterials: Implication in associated toxic manifestations,” *Biomed Res. Int.*, vol. 2014, 2014, doi: 10.1155/2014/498420.

[6] S. Logothetidis, “Nanomedicine: The medicine of tomorrow,” *Nanosci. Technol.*, vol. 61, pp. 1–26, 2012, doi: 10.1007/978-3-642-24181-9_1.

[7] A. Singh and M. M. Amiji, “Application of nanotechnology in medical diagnosis and imaging,” *Curr. Opin. Biotechnol.*, vol. 74, pp. 241–246, 2022, doi: 10.1016/j.copbio.2021.12.011.

[8] M. kheirollahpour, M. Mehrabi, N. M. Dounighi, M. Mohammadi, and A. Masoudi, “Nanoparticles and Vaccine Development,” *Pharm. Nanotechnol.*, vol. 8, no. 1, pp. 6–21, 2019, doi: 10.2174/2211738507666191024162042.

[9] R. R. A. Bourne *et al.*, “Prevalence and causes of vision loss in high-income countries and in Eastern and Central Europe in 2015: Magnitude, temporal trends and projections,” *Br. J. Ophthalmol.*, vol. 102, no. 5, pp. 575–585, 2018, doi: 10.1136/bjophthalmol-2017-311258.

[10] Q. Xu, S. P. Kambhampati, and R. M. Kannan, “Nanotechnology Approaches for Ocular Drug Delivery,” *Middle East Afr. J. Ophthalmol.*, vol. 20, no. 1, pp. 26–37, 2013, doi: 10.4103/0974-9233.106384.

[11] M. A. Kamaleddin, “Nano-ophthalmology: Applications and considerations,” *Nanomedicine Nanotechnology, Biol. Med.*, vol. 13, no. 4, pp. 1459–1472, 2017, doi: 10.1016/j.nano.2017.02.007.

[12] C. E. Willoughby, D. Ponzin, S. Ferrari, A. Lobo, K. Landau, and Y. Omidi, “Anatomy and physiology of the human eye: Effects of mucopolysaccharidoses disease on structure and function - a review,” *Clin. Exp. Ophthalmol.*, vol. 38, no. SUPPL. 1, pp. 2–11, 2010,

doi: 10.1111/j.1442-9071.2010.02363.x.

[13] M. Hoon, H. Okawa, L. Della Santina, and R. O. L. Wong, “Functional architecture of the retina: Development and disease,” *Prog. Retin. Eye Res.*, vol. 42, pp. 44–84, 2014, doi: 10.1016/j.preteyeres.2014.06.003.

[14] B. D. Kels, A. Grzybowski, and J. M. Grant-Kels, “Human ocular anatomy,” *Clin. Dermatol.*, vol. 33, no. 2, pp. 140–146, 2015, doi: 10.1016/j.clindermatol.2014.10.006.

[15] C. S. McCaa, “The eye and visual nervous system: anatomy, physiology and toxicology,” *Environ. Health Perspect.*, vol. Vol. 44, no. April, pp. 1–8, 1982, doi: 10.1289/ehp.82441.

[16] F. O’Leary and M. Campbell, “The blood–retina barrier in health and disease,” *FEBS J.*, pp. 1–14, 2021, doi: 10.1111/febs.16330.

[17] R. Sharma, D. Sharma, L. D. Hazlett, and N. K. Singh, “Nano-Biomaterials for Retinal Regeneration,” *Nanomaterials*, vol. 11, no. 8, pp. 1–25, 2021, doi: 10.3390/nano11081880.

[18] D. Schmidl, A. Schlatter, J. Chua, B. Tan, G. Garhöfer, and L. Schmetterer, “Novel Approaches for Imaging-Based Diagnosis of Ocular Surface Disease,” *Diagnostics*, vol. 10, no. 8, pp. 1–23, 2020, doi: 10.3390/diagnostics10080589.

[19] T. Ilginis, J. Clarke, and P. J. Patel, “Ophthalmic imaging,” *Br. Med. Bull.*, vol. 111, no. 1, pp. 77–88, 2014, doi: 10.1093/bmb/ldu022.

[20] B. R. Hurley and C. D. Regillo, “Fluorescein angiography: General principles and interpretation,” *Retin. Angiogr. Opt. Coherence Tomogr.*, pp. 27–42, 2009, doi: 10.1007/978-0-387-68987-6_2.

[21] H. R. NOVOTNY and D. L. ALVIS, “A method of photographing fluorescence in circulating blood in the human retina.,” *Circulation*, vol. 24, no. July, pp. 82–86, 1961, doi: 10.1161/01.CIR.24.1.82.

[22] T. Olsen, “The accuracy of ultrasonic determination of axial length in pseudophakic eyes,” *Acta Ophthalmol*, vol. 67, no. 2, pp. 141–144, 1989, doi: 10.1111/j.1755-3768.1989.tb00743.x.

[23] C. J. Pavlin, M. D. Sherar, and F. S. Foster, “Subsurface Ultrasound Microscopic Imaging of the Intact Eye,” *Ophthalmology*, vol. 97, no. 2, pp. 244–250, 1990, doi: 10.1016/S0161-6420(90)32598-8.

[24] M. De La Hoz Polo, A. Torramilans Lluís, O. Pozuelo Segura, A. Anguera Bosque, C. Esmerado Appiani, and J. M. Caminal Mitjana, “Ocular ultrasonography focused on the posterior eye segment: what radiologists should know,” *Insights Imaging*, vol. 7, no. 3, pp. 351–364, 2016, doi: 10.1007/s13244-016-0471-z.

[25] D. Huang, E. A. Swanson, and C. P. Lin, “Optical coherence tomography (OCT),” vol. 254, no. 5035, pp. 1178–1181, 1991, doi: 10.1126/science.1957169.

[26] M. E. J. van Velthoven, D. J. Faber, F. D. Verbraak, T. G. van Leeuwen, and M. D. de Smet, “Recent developments in optical coherence tomography for imaging the retina,” *Prog. Retin. Eye Res.*, vol. 26, no. 1, pp. 57–77, 2007, doi: 10.1016/j.preteyeres.2006.10.002.

[27] X. Shu, L. Beckmann, and H. F. Zhang, “Visible-light optical coherence tomography: a review,” *J. Biomed. Opt.*, vol. 22, no. 12, p. 1, 2017, doi: 10.1117/1.jbo.22.12.121707.

[28] R. Weissleder, “A clearer vision for in vivo imaging: Progress continues in the development of smaller, more penetrable probes for biological imaging,” *Nat. Biotechnol.*, vol. 19, no. 4, pp. 316–317, 2001, doi: 10.1038/86684.

[29] E. A. Swanson *et al.*, “In vivo retinal imaging by optical coherence tomography,” *Opt. Lett.*, vol. 18, no. 21, p. 1864, 1993, doi: 10.1364/ol.18.001864.

[30] M. R. Hee *et al.*, “Optical Coherence Tomography of the Human Retina,” *Arch Ophthalmol.*, vol. 113, no. 3, pp. 325–32, 1995, doi: 10.1001/archopht.1995.01100030081025.

[31] W. Drexler and J. G. Fujimoto, “State-of-the-art retinal optical coherence tomography,” *Prog. Retin. Eye Res.*, vol. 27, no. 1, pp. 45–88, 2008, doi: 10.1016/j.preteyeres.2007.07.005.

[32] C. A. Puliafito *et al.*, “Imaging of Macular Diseases with Optical Coherence Tomography,” *Ophthalmology*, vol. 102, no. 2, pp. 217–229, 1995, doi: 10.1016/S0161-6420(95)31032-9.

[33] M. R. Hee *et al.*, “Optical coherence tomography of age-related macular degeneration and choroidal neovascularization,” *Ophthalmology*, vol. 103, no. 8, pp. 1260–1270, 1996, doi: 10.1016/S0161-6420(96)30512-5.

[34] J. M. B. de B. Garcia, D. L. C. Isaac, and M. Avila, “Diabetic retinopathy and OCT angiography: Clinical findings and future perspectives,” *Int. J. Retin. Vitr.*, vol. 3, no. 1, pp. 1–10, 2017, doi: 10.1186/s40942-017-0062-2.

[35] D. C. Hood, “Improving our understanding, and detection, of glaucomatous damage: An approach based upon optical coherence tomography (OCT),” *Prog. Retin. Eye Res.*, vol. 57, pp. 46–75, 2017, doi: 10.1016/j.preteyeres.2016.12.002.

[36] M. C. Skala, M. J. Crow, A. Wax, and J. A. Izatt, “Photothermal optical coherence tomography of epidermal growth factor receptor in live cells using immunotargeted gold nanospheres,” *Opt. Coherence Tomogr. Coherence Domain Opt. Methods Biomed. XIII*, vol. 7168, p. 71680S, 2009, doi: 10.1117/12.808052.

[37] N. Nassif *et al.*, “In vivo human retinal imaging by ultrahigh-speed spectral domain

optical coherence tomography," *Opt. Lett.*, vol. 29, no. 5, p. 480, 2004, doi: 10.1364/ol.29.000480.

[38] S. Makita, Y. Hong, M. Yamanari, T. Yatagai, and Y. Yasuno, "Optical coherence angiography," *Opt. Express*, vol. 14, no. 17, p. 7821, 2006, doi: 10.1364/oe.14.007821.

[39] M. Pircher, C. K. Hitzenberger, and U. Schmidt-Erfurth, "Polarization sensitive optical coherence tomography in the human eye," *Prog. Retin. Eye Res.*, vol. 30, no. 6, pp. 431–451, 2011, doi: 10.1016/j.preteyeres.2011.06.003.

[40] M. R. Ford, W. J. Dupps, A. M. Rollins, A. S. Roy, and Z. Hu, "Method for optical coherence elastography of the cornea," *J. Biomed. Opt.*, vol. 16, no. 1, p. 016005, 2011, doi: 10.1117/1.3526701.

[41] Z. Chen, T. E. Milner, D. Dave, and J. S. Nelson, "Optical Doppler tomographic imaging of fluid flow velocity in highly scattering media," *Opt. Lett.*, vol. 22, no. 1, p. 64, 1997, doi: 10.1364/ol.22.000064.

[42] Z. Ding, Y. Zhao, H. Ren, J. S. Nelson, and Z. Chen, "Real-time phase-resolved optical coherence tomography and optical Doppler tomography," *Opt. Express*, vol. 10, no. 5, p. 236, 2002, doi: 10.1364/oe.10.000236.

[43] T. S. Kirtane and M. S. Wagh, "Endoscopic optical coherence tomography (OCT): Advances in gastrointestinal imaging," *Gastroenterol. Res. Pract.*, vol. 2014, 2014, doi: 10.1155/2014/376367.

[44] G. J. Tearney and B. E. Bouma, "Atherosclerotic plaque characterization by spatial and temporal speckle pettern analysis," *Conf. Lasers Electro-Optics Eur. - Tech. Dig.*, vol. 27, no. 7, pp. 307–308, 2001, doi: 10.1364/ol.27.000533.

[45] C. M. Putnam, "Clinical imaging of macular pigment optical density and spatial distribution," *Clin. Exp. Optom.*, vol. 100, no. 4, pp. 333–340, 2017, doi: 10.1111/cxo.12500.

[46] L. V. Wang and J. Yao, "A practical guide to photoacoustic tomography in the life sciences," *Nat. Methods*, vol. 13, no. 8, pp. 627–638, 2016, doi: 10.1038/nmeth.3925.

[47] S. Zackrisson, S. M. W. Y. Van de Ven, and S. S. Gambhir, "Light In and Sound Out: Emerging Translational Strategies for Photoacoustic Imaging," *Cancer Res*, vol. 74, no. 4, pp. 979–1004, 2014, doi: 10.1158/0008-5472.CAN-13-2387.

[48] A. G. Bell, "On the production and reproduction of sound by light," *Am. J. Sci.*, vol. s3-20, no. 118, pp. 305–324, 1880, doi: 10.2475/ajs.s3-20.118.305.

[49] L. V. Wang and S. Hu, "Photoacoustic tomography: In vivo imaging from organelles to organs," *Science (80-.).*, vol. 335, no. 6075, pp. 1458–1462, 2012, doi: 10.1126/science.1216210.

[50] P. Beard, “Biomedical photoacoustic imaging,” *Interface Focus*, vol. 1, no. 4, pp. 602–631, 2011, doi: 10.1098/rsfs.2011.0028.

[51] M. Xu and L. V. Wang, “Photoacoustic imaging in biomedicine,” *Rev. Sci. Instrum.*, vol. 77, no. 4, 2006, doi: 10.1063/1.2195024.

[52] R. H. Silverman *et al.*, “High-resolution photoacoustic imaging of ocular tissues,” *Ultrasound Med. Biol.*, vol. 36, no. 5, pp. 733–742, 2010, doi: 10.1016/j.ultrasmedbio.2010.02.006.

[53] V. J. Pansare, S. Hejazi, W. J. Faenza, and R. K. Prud’Homme, “Review of long-wavelength optical and NIR imaging materials: Contrast agents, fluorophores, and multifunctional nano carriers,” *Chem. Mater.*, vol. 24, no. 5, pp. 812–827, 2012, doi: 10.1021/cm2028367.

[54] V. P. Nguyen and Y. M. Paulus, “Photoacoustic ophthalmoscopy: Principle, application, and future directions,” *J. Imaging*, vol. 4, no. 12, 2018, doi: 10.3390/jimaging4120149.

[55] X. Zhang, H. F. Zhang, and S. Jiao, “Optical coherence photoacoustic microscopy: accomplishing optical coherence tomography and photoacoustic microscopy with a single light source,” *J. Biomed. Opt.*, vol. 17, no. 3, p. 030502, 2012, doi: 10.1117/1.jbo.17.3.030502.

[56] X. Wang, Y. Pang, G. Ku, X. Xie, G. Stoica, and L. V. Wang, “Noninvasive laser-induced photoacoustic tomography for structural and functional in vivo imaging of the brain,” *Nat. Biotechnol.*, vol. 21, no. 7, pp. 803–806, 2003, doi: 10.1038/nbt839.

[57] S. Hu and L. V. Wang, “Photoacoustic imaging and characterization of the microvasculature,” *J. Biomed. Opt.*, vol. 15, no. 1, p. 011101, 2010, doi: 10.1117/1.3281673.

[58] S. Bhattacharyya, S. Wang, D. Reinecke, W. Kiser, R. A. Kruger, and T. R. DeGrado, “Synthesis and evaluation of near-infrared (NIR) dye-herceptin conjugates as photoacoustic computed tomography (PCT) probes for HER2 expression in breast cancer,” *Bioconjug. Chem.*, vol. 19, no. 6, pp. 1186–1193, 2008, doi: 10.1021/bc700482u.

[59] P. Y. Hu Z, Wang X, Liu Q, “Photoacoustic Imaging in Ophthalmology,” *Int J Ophthalmol Eye Res*, vol. 3, no. 8, pp. 126–132, 2015, doi: http://dx.doi.org/10.19070/2332-290X-1500027.

[60] H. F. Zhang, K. Maslov, G. Stoica, and L. V. Wang, “Functional photoacoustic microscopy for high-resolution and noninvasive in vivo imaging,” *Nat. Biotechnol.*, vol. 24, no. 7, pp. 848–851, 2006, doi: 10.1038/nbt1220.

[61] A. de la Zerda *et al.*, “Photoacoustic ocular imaging,” *Opt. Lett.*, vol. 35, no. 3, p. 270, 2010, doi: 10.1364/ol.35.000270.

[62] S. Jiao *et al.*, “Photoacoustic ophthalmoscopy for in vivo retinal imaging,” *Opt. Express*, vol. 18, no. 4, p. 3967, 2010, doi: 10.1364/oe.18.003967.

[63] F. Chen, P. Si, A. De La Zerda, J. V. Jokerst, and D. Myung, “Gold nanoparticles to enhance ophthalmic imaging,” *Biomater. Sci.*, vol. 9, no. 2, pp. 367–390, 2021, doi: 10.1039/d0bm01063d.

[64] E. Midena and E. Pilotto, “Emerging Insights into Pathogenesis,” *Dev. Ophthalmol.*, vol. 60, pp. 16–27, 2017, doi: 10.1159/000459687.

[65] F. E. Robles, C. Wilson, G. Grant, and A. Wax, “Molecular imaging true-colour spectroscopic optical coherence tomography,” *Nat. Photonics*, vol. 5, no. 12, pp. 744–747, 2011, doi: 10.1038/nphoton.2011.257.

[66] S. A. Boppart, A. L. Oldenburg, C. Xu, and D. L. Marks, “Optical probes and techniques for molecular contrast enhancement in coherence imaging,” *J. Biomed. Opt.*, vol. 10, no. 4, p. 041208, 2005, doi: 10.1117/1.2008974.

[67] J. Weber, P. C. Beard, and S. E. Bohndiek, “Contrast agents for molecular photoacoustic imaging,” *Nat. Methods*, vol. 13, no. 8, pp. 639–650, 2016, doi: 10.1038/nmeth.3929.

[68] J. K. Barton, J. B. Hoying, and C. J. Sullivan, “Use of microbubbles as an optical coherence tomography contrast agent,” *Acad. Radiol.*, vol. 9, no. SUPPL. 1, pp. 52–55, 2002, doi: 10.1016/S1076-6332(03)80395-1.

[69] T. M. Lee *et al.*, “Engineered microsphere contrast agents for optical coherence tomography,” *Opt. Lett.*, vol. 28, no. 17, p. 1546, 2003, doi: 10.1364/ol.28.001546.

[70] J. Yi, J. Gong, and X. Li, “Analyzing absorption and scattering spectra of micro-scale structures with spectroscopic optical coherence tomography,” *Opt. Express*, vol. 17, no. 15, p. 13157, 2009, doi: 10.1364/oe.17.013157.

[71] Z. Yaqoob, E. McDowell, J. Wu, X. Heng, J. Fingler, and C. Yang, “Molecular contrast optical coherence tomography: a pump-probe scheme using indocyanine green as a contrast agent,” *J. Biomed. Opt.*, vol. 11, no. 5, p. 054017, 2006, doi: 10.1117/1.2360525.

[72] C. Xu, J. Ye, D. L. Marks, and S. A. Boppart, “Near-infrared dyes as contrast-enhancing agents for spectroscopic optical coherence tomography,” vol. 29, no. 14, pp. 1647–1649, 2004.

[73] A. L. Oldenburg, J. R. Gunther, F. J. Toublan, D. L. Marks, K. S. Suslick, and S. A. Boppart, “Magnetic contrast agents for optical coherence tomography,” *Coherence Domain Opt. Methods Opt. Coherence Tomogr. Biomed. VIII*, vol. 5316, no. 217, p. 91, 2004, doi: 10.1117/12.529119.

[74] D. C. Adler, S.-W. Huang, R. Huber, and J. G. Fujimoto, “Photothermal detection of gold

nanoparticles using phase-sensitive optical coherence tomography," *Opt. Express*, vol. 16, no. 7, p. 4376, 2008, doi: 10.1364/oe.16.004376.

[75] R. García-Álvarez *et al.*, "Optimizing the Geometry of Photoacoustically Active Gold Nanoparticles for Biomedical Imaging," *ACS Photonics*, vol. 7, no. 3, pp. 646–652, 2020, doi: 10.1021/acsphotonics.9b01418.

[76] L. Nie and X. Chen, "Structural and functional photoacoustic molecular tomography aided by emerging contrast agents," *Chem. Soc. Rev.*, vol. 43, no. 20, pp. 7132–7170, 2014, doi: 10.1039/c4cs00086b.

[77] J. Yao, K. Maslov, S. Hu, and L. V. Wang, "Evans blue dye-enhanced capillary-resolution photoacoustic microscopy in vivo," *J. Biomed. Opt.*, vol. 14, no. 5, p. 054049, 2009, doi: 10.1117/1.3251044.

[78] K. Pu, A. J. Shuhendler, and J. V. Jokerst, "Semiconducting Polymer Nanoparticles as Photoacoustic Molecular Imaging Probes in Living Mice," *Nat Nanotechnol*, vol. 9, no. 3, pp. 233–239, 2014, doi: 10.1038/nnano.2013.302.

[79] G. Ku, M. Zhou, S. Song, Q. Huang, J. Hazle, and C. Li, "Copper sulfide nanoparticles as a new class of photoacoustic contrast agent for deep tissue imaging at 1064 nm," *ACS Nano*, vol. 6, no. 8, pp. 7489–7496, 2012, doi: 10.1021/nn302782y.

[80] A. de la Zerda, C. Zavaleta, and K. Shay, "Carbon nanotubes as photoacoustic molecular imaging agents in living mice," *Nat Nanotechnol*, vol. 3, no. 9, pp. 557–562, 2008, doi: 10.1038/nnano.2008.231.

[81] K. A. Homan *et al.*, "Silver nanoplate contrast agents for in vivo molecular photoacoustic imaging," *ACS Nano*, vol. 6, no. 1, pp. 641–650, 2012, doi: 10.1021/nn204100n.

[82] C. Kim, E. C. Cho, and J. Chen, "In vivo molecular photoacoustic tomography of melanomas targeted by bio-conjugated gold nanocages," *ACS Nano*, vol. 4, no. 8, pp. 4559–4564, 2010, doi: doi:10.1021/nn100736c.

[83] P.-C. Li *et al.*, "In vivo photoacoustic molecular imaging with simultaneous multiple selective targeting using antibody-conjugated gold nanorods," *Opt. Express*, vol. 16, no. 23, p. 18605, 2008, doi: 10.1364/oe.16.018605.

[84] L. Nie *et al.*, "In vivo volumetric photoacoustic molecular angiography and therapeutic monitoring with targeted plasmonic nanostars," *Small*, vol. 10, no. 8, pp. 1585–1593, 2014, doi: 10.1002/smll.201302924.

[85] I. H. El-Sayed, X. Huang, and M. A. El-Sayed, "Surface plasmon resonance scattering and absorption of anti-EGFR antibody conjugated gold nanoparticles in cancer diagnostics: Applications in oral cancer," *Nano Lett.*, vol. 5, no. 5, pp. 829–834, 2005, doi: 10.1021/nl050074e.

[86] K. Sokolov *et al.*, “Real-time vital optical imaging of precancer using anti-epidermal growth factor receptor antibodies conjugated to gold nanoparticles,” *Cancer Res.*, vol. 63, no. 9, pp. 1999–2004, 2003.

[87] X. Yang, M. Yang, B. Pang, M. Vara, and Y. Xia, “Gold Nanomaterials at Work in Biomedicine,” *Chem. Rev.*, vol. 115, no. 19, pp. 10410–10488, 2015, doi: 10.1021/acs.chemrev.5b00193.

[88] E. Boisselier and D. Astruc, “Gold nanoparticles in nanomedicine: preparations, imaging, diagnostics, therapies and toxicity,” *Chem. Soc. Rev.*, vol. 38, no. 6, pp. 1759–1782, 2009, doi: 10.1039/b806051g.

[89] G. J. Higby, “Gold in medicine - A review of its use in the west before 1900,” *Gold Bull.*, vol. 15, no. 4, pp. 130–140, 1982, doi: 10.1007/BF03214618.

[90] L. A. Dykman and N. G. Khlebtsov, “Gold nanoparticles in biology and medicine: recent advances and prospects,” *Acta Naturae* ., vol. 3, no. 2, pp. 34–55, 2011.

[91] J. Aaseth, M. Haugen, and Ø. Førre, “Rheumatoid arthritis and metal compounds - Perspectives on the role of oxygen radical detoxification,” *Analyst*, vol. 123, no. 1, pp. 3–6, 1998, doi: 10.1039/a704840h.

[92] A. Thako, J. Jokerst, and C. Zaveleta, “GOLD NANOPARTICLES: A REVIVAL IN PRECIOUS METAL ADMINISTRATION TO PATIENTS,” *Nano Lett*, vol. 11, no. 10, pp. 4029–4036, 2011, doi: 10.1021/nl202559p.

[93] S. A. Bansal, V. Kumar, J. Karimi, A. P. Singh, and S. Kumar, “Role of gold nanoparticles in advanced biomedical applications,” *Nanoscale Adv.*, vol. 2, no. 9, pp. 3764–3787, 2020, doi: 10.1039/d0na00472c.

[94] Y. Yang *et al.*, “Multifunctional Gold Nanoparticles in Cancer Diagnosis and Treatment,” *Int. J. Nanomedicine*, vol. 17, no. May, pp. 2041–2067, 2022, doi: 10.2147/IJN.S355142.

[95] J. Guo, K. Rahme, Y. He, L.-L. Li, J. D. Holmes, and C. M. O’driscoll, “Gold nanoparticles enlighten the future of cancer theranostics,” *Int. J. Nanomedicine*, vol. 12, pp. 6131–6152, 2017, doi: 10.2147/IJN.S140772.

[96] C. M. Cobley, J. Chen, E. Chul Cho, L. V. Wang, and Y. Xia, “Gold nanostructures: A class of multifunctional materials for biomedical applications,” *Chem. Soc. Rev.*, vol. 40, no. 1, pp. 44–56, 2011, doi: 10.1039/b821763g.

[97] M. Faraday, “The Bakerian Lecture : Experimental Relations of Gold (and Other Metals) to Light Author (s): Michael Faraday Source : Philosophical Transactions of the Royal Society of London , Vol . 147 , No . (1857), pp . 145-181 Published by : The Royal Society,” *Philos. Trans. R. Soc. London*, vol. 147, no. 1857, pp. 145–181, 1857.

[98] G. Mie, “Beiträge zur Optik trüber Medien, speziell kolloidaler Metallösungen,” *Ann.*

Phys., vol. 330, no. 3, pp. 377–445, 1908, doi: 10.1002/andp.19083300302.

[99] J. Turkevich, P. C. Stevenson, and J. Hillier, "A study of the nucleation and growth processes in the synthesis of colloidal gold," *Discuss. Faraday Soc.*, vol. 11, pp. 55–75, 1951, doi: 10.1039/df9511100055.

[100] K. K. Bharadwaj *et al.*, "Green synthesis of gold nanoparticles using plant extracts as beneficial prospect for cancer theranostics," *Molecules*, vol. 26, no. 21, 2021, doi: 10.3390/molecules26216389.

[101] M. C. Daniel and D. Astruc, "Gold Nanoparticles: Assembly, Supramolecular Chemistry, Quantum-Size-Related Properties, and Applications Toward Biology, Catalysis, and Nanotechnology," *Chem. Rev.*, vol. 104, no. 1, pp. 293–346, 2004, doi: 10.1021/cr030698+.

[102] M. Giersig and P. Mulvaney, "Preparation of Ordered Colloid Monolayers by Electrophoretic Deposition," *Langmuir*, vol. 9, no. 12, pp. 3408–3413, 1993, doi: 10.1021/la00036a014.

[103] M. Brust, M. Walker, D. Bethell, D. J. Schiffrin, and R. Whyman, "Synthesis of Thiol-derivatised Gold Nanoparticles in a Two-phase Liquid-Liquid System," *J. Chem. Soc., Chem. Commun.*, pp. 801–802, 2000, doi: 10.1039/C39940000801.

[104] R. Arvizo, R. Bhattacharya, and P. Mukherjee, "Gold nanoparticles: Opportunities and Challenges in Nanomedicine," *Expert Opin Drug Deliv*, vol. 7, no. 6, pp. 753–763, 2010, doi: 10.1517/17425241003777010.

[105] N. Li, P. Zhao, and D. Astruc, "Anisotropic gold nanoparticles: Synthesis, properties, applications, and toxicity," *Angew. Chemie - Int. Ed.*, vol. 53, no. 7, pp. 1756–1789, 2014, doi: 10.1002/anie.201300441.

[106] A. M. Alkilany and C. J. Murphy, "Toxicity and cellular uptake of gold nanoparticles: What we have learned so far?," *J. Nanoparticle Res.*, vol. 12, no. 7, pp. 2313–2333, 2010, doi: 10.1007/s11051-010-9911-8.

[107] J. H. Park, D. S. Dumani, A. Arsiwala, S. Emelianov, and R. S. Kane, "Tunable aggregation of gold-silica janus nanoparticles to enable contrast-enhanced multiwavelength photoacoustic imaging in vivo," *Nanoscale*, vol. 10, no. 32, pp. 15365–15370, 2018, doi: 10.1039/c8nr03973a.

[108] M. Ovais *et al.*, "Current state and prospects of the phytosynthesized colloidal gold nanoparticles and their applications in cancer theranostics," *Appl. Microbiol. Biotechnol.*, vol. 101, no. 9, pp. 3551–3565, 2017, doi: 10.1007/s00253-017-8250-4.

[109] J. Pérez-Juste, I. Pastoriza-Santos, L. M. Liz-Marzán, and P. Mulvaney, "Gold nanorods: Synthesis, characterization and applications," *Coord. Chem. Rev.*, vol. 249, no. 17-18 SPEC. ISS., pp. 1870–1901, 2005, doi: 10.1016/j.ccr.2005.01.030.

[110] Y. C. Wang, É. Rhéaume, F. Lesage, and A. Kakkar, “Synthetic methodologies to gold nanoshells: An overview,” *Molecules*, vol. 23, no. 11, pp. 1–28, 2018, doi: 10.3390/molecules23112851.

[111] S. E. Skrabalak *et al.*, “Gold Nanocages: Synthesis, Properties, and Applications,” *Acc Chem Res.*, vol. 41, no. 12, pp. 1587–1595, 2008, doi: 10.1021/ar800018v.

[112] S. M. Mousavi *et al.*, “Gold nanostars-diagnosis, bioimaging and biomedical applications,” *Drug Metab. Rev.*, vol. 52, no. 2, pp. 299–318, 2020, doi: 10.1080/03602532.2020.1734021.

[113] A. Mendoza-Galván, K. Järrendahl, A. Dmitriev, T. Pakizeh, M. Käll, and H. Arwin, “Optical response of supported gold nanodisks,” *Opt. Express*, vol. 19, no. 13, p. 12093, 2011, doi: 10.1364/oe.19.012093.

[114] T. H. Ha, H. J. Koo, and B. H. Chung, “Shape-controlled syntheses of gold nanoprisms and nanorods influenced by specific adsorption of halide ions,” *J. Phys. Chem. C*, vol. 111, no. 3, pp. 1123–1130, 2007, doi: 10.1021/jp066454l.

[115] H. Chen, X. Kou, Z. Yang, W. Ni, and J. Wang, “Shape- and size-dependent refractive index sensitivity of gold nanoparticles,” *Langmuir*, vol. 24, no. 10, pp. 5233–5237, 2008, doi: 10.1021/la800305j.

[116] U. Kreibig and M. Vollmer, *Optical Properties of Metal Clusters*. 1995.

[117] C. Kohout, C. Santi, and L. Polito, “Anisotropic gold nanoparticles in biomedical applications,” *Int. J. Mol. Sci.*, vol. 19, no. 11, 2018, doi: 10.3390/ijms19113385.

[118] K. S. Lee and M. A. El-Sayed, “Dependence of the enhanced optical scattering efficiency relative to that of absorption for gold metal nanorods on aspect ratio, size, end-cap shape, and medium refractive index,” *J. Phys. Chem. B*, vol. 109, no. 43, pp. 20331–20338, 2005, doi: 10.1021/jp054385p.

[119] L. M. Liz-marza, “Tailoring Surface Plasmons through the Morphology and Assembly of Metal Nanoparticles,” *Langmuir*, vol. 22, no. 1, pp. 32–41, 2006, doi: 10.1021/la0513353.

[120] E. C. Dreaden, A. M. Alkilany, X. Huang, C. J. Murphy, and M. A. El-Sayed, “The golden age: Gold nanoparticles for biomedicine,” *Chem. Soc. Rev.*, vol. 41, no. 7, pp. 2740–2779, 2012, doi: 10.1039/c1cs15237h.

[121] P. N. Njoki *et al.*, “Size correlation of optical and spectroscopic properties for gold nanoparticles,” *J. Phys. Chem. C*, vol. 111, no. 40, pp. 14664–14669, 2007, doi: 10.1021/jp074902z.

[122] M. F. Tsai *et al.*, “Au nanorod design as light-absorber in the first and second biological near-infrared windows for in vivo photothermal therapy,” *ACS Nano*, vol. 7, no. 6, pp. 5330–5342, 2013, doi: 10.1021/nn401187c.

[123] J. L. West and N. J. Halas, “Engineered nanomaterials for biophotonics applications: Improving sensing, imaging, and therapeutics,” *Annu. Rev. Biomed. Eng.*, vol. 5, pp. 285–292, 2003, doi: 10.1146/annurev.bioeng.5.011303.120723.

[124] P. Dey, I. Blakey, and N. Stone, “Diagnostic prospects and preclinical development of optical technologies using gold nanostructure contrast agents to boost endogenous tissue contrast,” *Chem. Sci.*, vol. 11, no. 33, pp. 8671–8685, 2020, doi: 10.1039/d0sc01926g.

[125] Y. Xia and N. J. Halas, “Shape-Controlled Synthesis and Surface Plasmonic Properties of Metallic Nanostructures,” *MRS Bull.*, vol. 30, no. 5, pp. 338–348., 2005, doi: 10.1557/mrs2005.96.

[126] M. Hu *et al.*, “Gold nanostructures: Engineering their plasmonic properties for biomedical applications,” *Chem. Soc. Rev.*, vol. 35, no. 11, pp. 1084–1094, 2006, doi: 10.1039/b517615h.

[127] E. C. Cho, C. Kim, and F. Zhou, “Measuring the Optical Absorption Cross-sections of Au-Ag Nanocages and Au Nanorods by Photoacoustic Imaging,” *J Phys Chem C Nanomater Interfaces*, vol. 113, no. 21, pp. 9023–9028, 2009, doi: 10.1021/jp903343p.

[128] X. Huang, S. Neretina, and M. A. El-Sayed, “Gold nanorods: From synthesis and properties to biological and biomedical applications,” *Adv. Mater.*, vol. 21, no. 48, pp. 4880–4910, 2009, doi: 10.1002/adma.200802789.

[129] Y.-Y. Yu, S.-S. Chang, and C.-L. Lee, “Gold Nanorods: Electrochemical Synthesis and Optical Properties,” *J. Phys. Chem. B*, vol. 101, no. 34, pp. 661–678, 1997, doi: 10.1002/chin.199744015.

[130] R. Gans, “Über die Form ultramikroskopischer Goldteilchen,” *Ann. Phys. (N. Y).*, vol. 342, no. 5, pp. 881–900, 1912, doi: 10.1002/andp.19123420503.

[131] C. J. Murphy *et al.*, “Chemical sensing and imaging with metallic nanorods,” *Chem. Commun.*, vol. 8, no. 5, pp. 544–557, 2002, doi: 10.1039/b711069c.

[132] A. E. Neeves and M. H. Birnboim, “Composite structures for the enhancement of nonlinear optical materials,” *Opt. Lett.*, vol. 13, no. 12, p. 1087, 1988, doi: 10.1364/ol.13.001087.

[133] R. D. Averitt, D. Sarkar, and N. J. Halas, “Plasmon resonance shifts of au-coated Au2S nanoshells: Insight into multicomponent nanoparticle growth,” *Phys. Rev. Lett.*, vol. 78, no. 22, pp. 4217–4220, 1997, doi: 10.1103/PhysRevLett.78.4217.

[134] S. J. Oldenburg, R. D. Averitt, S. L. Westcott, and N. J. Halas, “Nanoengineering of optical resonances,” *Chem. Phys. Lett.*, vol. 288, no. 2–4, pp. 243–247, 1998, doi: 10.1016/S0009-2614(98)00277-2.

[135] Y. Sun and Y. Xia, “Shape-Controlled Synthesis of Gold and Silver Nanoparticles,” *Am.*

Assoc. Adv. Sci., vol. 298, no. 5601, pp. 2176–2179, 2002, doi: 10.1126/science.1077229.

[136] X. Xia and Y. Xia, "Gold nanocages as multifunctional materials for nanomedicine," *Front. Phys.*, vol. 9, no. 3, pp. 378–384, 2014, doi: 10.1007/s11467-013-0318-8.

[137] J. Chen *et al.*, "Gold nanocages: Engineering their structure for biomedical applications," *Adv. Mater.*, vol. 17, no. 18, pp. 2255–2261, 2005, doi: 10.1002/adma.200500833.

[138] F. Hao, C. L. Nehl, J. H. Hafner, and P. Nordlander, "Plasmon resonances of a gold nanostar," *Nano Lett.*, vol. 7, no. 3, pp. 729–732, 2007, doi: 10.1021/nl062969c.

[139] L. E. Cole, R. D. Ross, J. M. Tilley, T. Vargo-Gogola, and R. K. Roeder, "Gold nanoparticles as contrast agents in X-ray imaging and computed tomography," *Nanomedicine*, vol. 10, no. 2, pp. 321–341, 2015, doi: 10.2217/nnm.14.171.

[140] C. A. S. Dunning and M. Bazalova-Carter, "Sheet beam x-ray fluorescence computed tomography (XFCT) imaging of gold nanoparticles," *Med. Phys.*, vol. 45, no. 6, pp. 2572–2582, 2018, doi: 10.1002/mp.12893.

[141] M. F. Kircher, A. de la Zerda, and J. V Jokerst, "A Brain Tumor Molecular Imaging Strategy Using A New TripleModality MRI-Photoacoustic-Raman Nanoparticle," *Nat Med*, vol. 18, no. 5, pp. 829–834, 2012, doi: 10.1038/nm.2721.

[142] H. Arya, Z. Kaul, R. Wadhwa, K. Taira, T. Hirano, and S. C. Kaul, "Quantum dots in bio-imaging: Revolution by the small," *Biochem. Biophys. Res. Commun.*, vol. 329, no. 4, pp. 1173–1177, 2005, doi: 10.1016/j.bbrc.2005.02.043.

[143] L. C. Estrada and E. Gratton, "Spectroscopic properties of gold nanoparticles at the single-particle level in biological environments," *ChemPhysChem*, vol. 13, no. 4, pp. 1087–1092, 2012, doi: 10.1002/cphc.201100771.

[144] W. Li and X. Chen, "Gold nanoparticles for photoacoustic imaging," *Nanomedicine*, vol. 10, no. 2, pp. 299–320, 2015, doi: 10.2217/nnm.14.169.

[145] V. Sebastián, S.-K. Lee, and C. Zhou, "One-step Continuous Synthesis of Biocompatible Gold Nanorods for Optical Coherence Tomography," *Chem Commun*, vol. 48, no. 53, pp. 6654–6656, 2012, doi: 10.1039/c2cc32969g.

[146] J. Chen *et al.*, "Gold nanocages: Bioconjugation and their potential use as optical imaging contrast agents," *Nano Lett.*, vol. 5, no. 3, pp. 473–477, 2005, doi: 10.1021/nl047950t.

[147] P. K. Jain, K. S. Lee, I. H. El-Sayed, and M. A. El-Sayed, "Calculated absorption and scattering properties of gold nanoparticles of different size, shape, and composition: Applications in biological imaging and biomedicine," *J. Phys. Chem. B*, vol. 110, no. 14, pp. 7238–7248, 2006, doi: 10.1021/jp057170o.

[148] V. P. Nguyen *et al.*, “Contrast Agent Enhanced Multimodal Photoacoustic Microscopy and Optical Coherence Tomography for Imaging of Rabbit Choroidal and Retinal Vessels in vivo,” *Sci. Rep.*, vol. 9, no. 1, pp. 1–17, 2019, doi: 10.1038/s41598-019-42324-5.

[149] T. S. Troutman, J. K. Barton, and M. Romanowski, “Optical coherence tomography with plasmon resonant nanorods of gold,” *Opt. Lett.*, vol. 32, no. 11, p. 1438, 2007, doi: 10.1364/ol.32.001438.

[150] Y. S. Chen, Y. Zhao, S. J. Yoon, S. S. Gambhir, and S. Emelianov, “Miniature gold nanorods for photoacoustic molecular imaging in the second near-infrared optical window,” *Nat. Nanotechnol.*, vol. 14, no. 5, pp. 465–472, 2019, doi: 10.1038/s41565-019-0392-3.

[151] Y. Jia *et al.*, “Spectral fractionation detection of gold nanorod contrast agents using optical coherence tomography,” *Opt. Express*, vol. 23, no. 4, p. 4212, 2015, doi: 10.1364/oe.23.004212.

[152] W. Al Rawashdeh *et al.*, “Differential contrast of gold nanorods in dual-band OCT using spectral multiplexing,” *J. Nanoparticle Res.*, vol. 17, no. 3, 2015, doi: 10.1007/s11051-015-2949-x.

[153] O. Liba, E. D. Sorelle, D. Sen, and A. De La Zerda, “Contrast-enhanced optical coherence tomography with picomolar sensitivity for functional in vivo imaging,” *Sci. Rep.*, vol. 6, no. January, pp. 1–12, 2016, doi: 10.1038/srep23337.

[154] E. D. SoRelle, O. Liba, Z. Hussain, M. Gambhir, and A. De La Zerda, “Biofunctionalization of Large Gold Nanorods Realizes Ultrahigh-Sensitivity Optical Imaging Agents,” *Langmuir*, vol. 31, no. 45, pp. 12339–12347, 2015, doi: 10.1021/acs.langmuir.5b02902.

[155] J. K. Barton, N. J. Halas, J. L. West, and R. A. Drezek, “Nanoshells as an optical coherence tomography contrast agent,” *Coherence Domain Opt. Methods Opt. Coherence Tomogr. Biomed. VIII*, vol. 5316, p. 99, 2004, doi: 10.1117/12.529235.

[156] C. Loo *et al.*, “Nanoshell-Enabled Photonics-Based Imaging and Therapy of Cancer,” *Technol. Cancer Res. Treat.*, vol. 3, no. 1, pp. 33–40, 2004, doi: 10.1177/153303460400300104.

[157] A. Agrawal *et al.*, “Quantitative evaluation of optical coherence tomography signal enhancement with gold nanoshells,” *J. Biomed. Opt.*, vol. 11, no. 4, p. 041121, 2006, doi: 10.1117/1.2339071.

[158] E. V. Zagaynova *et al.*, “Contrasting properties of gold nanoparticles for optical coherence tomography: Phantom, in vivo studies and Monte Carlo simulation,” *Phys. Med. Biol.*, vol. 53, no. 18, pp. 4995–5009, 2008, doi: 10.1088/0031-9155/53/18/010.

[159] H. Cang *et al.*, “Gold nanocages as contrast agents for spectroscopic optical coherence tomography,” *Opt. Lett.*, vol. 30, no. 22, p. 3048, 2005, doi: 10.1364/ol.30.003048.

[160] Y. R. Ponce-de-Leon, J. A. Lopez-Rios, J. L. Pichardo-Molina, and N. Alcalá Ochoa, “Optical coherence tomography image enhancement by using gold nanoparticles,” *22nd Congr. Int. Comm. Opt. Light Dev. World*, vol. 8011, p. 80118W, 2011, doi: 10.1117/12.902773.

[161] O. Bibikova *et al.*, “Plasmon-Resonant Gold Nanostars with Variable Size as Contrast Agents for Imaging Applications,” *IEEE J. Sel. Top. Quantum Electron.*, vol. 22, no. 3, pp. 13–20, 2016, doi: 10.1109/JSTQE.2016.2526602.

[162] B. Wang *et al.*, “Gold nanorods as a contrast agent for Doppler optical coherence tomography,” *PLoS One*, vol. 9, no. 3, pp. 1–7, 2014, doi: 10.1371/journal.pone.0090690.

[163] H. A. Quigley, “Number of people with glaucoma worldwide,” *Br. J. Ophthalmol.*, vol. 80, no. 5, pp. 389–393, 1996, doi: 10.1136/bjo.80.5.389.

[164] S. Prabhulkar, J. Matthews, S. Rawal, and R. M. Awdeh, “Molecular histopathology using gold nanorods and optical coherence tomography,” *Investig. Ophthalmol. Vis. Sci.*, vol. 54, no. 2, pp. 1192–1200, 2013, doi: 10.1167/iovs.12-10794.

[165] S. Squamous, I. Gurses, S. Doganay, and B. Mizrak, “Expression of Glucose Transporter Protein-1 (Glut-1),” *Ocul. Surf.*, vol. 1, pp. 826–830, 2007.

[166] S. V. Kumar and D. Joshi, “Ocular surface squamous neoplasia,” *Med. J. Armed Forces India*, vol. 74, no. 3, pp. 273–275, 2018, doi: 10.1016/j.mjafi.2017.01.006.

[167] D. J. Faber *et al.*, “NAOMI: nanoparticle assisted optical molecular imaging,” *Coherence Domain Opt. Methods Opt. Coherence Tomogr. Biomed. X*, vol. 6079, no. 2006, p. 607905, 2006, doi: 10.1117/12.645316.

[168] H. Lee, E. K. Kim, H. Y. Kim, and T. I. Kim, “Effects of exposure to ozone on the ocular surface in an experimental model of allergic conjunctivitis,” *PLoS One*, vol. 12, no. 1, pp. 1–18, 2017, doi: 10.1371/journal.pone.0169209.

[169] X. Jiang, P. Tang, P. Gao, Y. S. Zhang, C. Yi, and J. Zhou, “Gold Nanoprobe-Enabled Three-Dimensional Ozone Imaging by Optical Coherence Tomography,” *Anal. Chem.*, vol. 89, no. 4, pp. 2561–2568, 2017, doi: 10.1021/acs.analchem.6b04785.

[170] X. Jiang *et al.*, “Controllably tuning the near-infrared plasmonic modes of gold nanoplates for enhanced optical coherence imaging and photothermal therapy,” *RSC Adv.*, vol. 5, no. 98, pp. 80709–80718, 2015, doi: 10.1039/c5ra15204f.

[171] A. De La Zerda, S. Prabjulkar, and V. L. Perez, “Optical coherence contrast imaging using gold nanorods in living mice eyes,” *Clin Exp. Ophthalmol.*, vol. 43, no. 4, pp. 358–366, 2015, doi: 10.1111/ceo.12299.

[172] D. Sen *et al.*, “High-resolution contrast-enhanced optical coherence tomography in mice retinae,” *J. Biomed. Opt.*, vol. 21, no. 06, p. 1, 2016, doi: 10.1117/1.jbo.21.6.066002.

[173] M. Gabriele Sandrian *et al.*, “Inflammatory response to intravitreal injection of gold nanorods.,” *Br. J. Ophthalmol.*, vol. 96, no. 12, pp. 1522–1529, 2012, doi: 10.1136/bjophthalmol-2012-301904.

[174] A. Y. Gordon, “Contrast-Enhanced Optical Coherence Tomography Using Gold Nanorods,” Vanderbilt University, 2019.

[175] S. J. Ryan, “The development of an experimental model of subretinal neovascularization in disciform macular degeneration,” *Trans. Am. Ophthalmol. Soc.*, vol. VOL. 77, pp. 707–745, 1979.

[176] M. Lapierre-Landry, A. Y. Gordon, J. S. Penn, and M. C. Skala, “In vivo photothermal optical coherence tomography of endogenous and exogenous contrast agents in the eye,” *Sci. Rep.*, vol. 7, no. 1, pp. 1–9, 2017, doi: 10.1038/s41598-017-10050-5.

[177] H. B. Song *et al.*, “Intraocular application of gold nanodisks optically tuned for optical coherence tomography : inhibitory effect on retinal neovascularization without unbearable toxicity,” *Nanomedicine Nanotechnology, Biol. Med.*, vol. 13, no. 6, pp. 1901–1911, 2017, doi: 10.1016/j.nano.2017.03.016.

[178] W. S. Chang, J. W. Ha, L. S. Slaughter, and S. Link, “Plasmonic nanorod absorbers as orientation sensors,” *Proc. Natl. Acad. Sci. U. S. A.*, vol. 107, no. 7, pp. 2781–2786, 2010, doi: 10.1073/pnas.0910127107.

[179] Y. Chemla *et al.*, “Gold nanoparticles for multimodal high-resolution imaging of transplanted cells for retinal replacement therapy,” *Nanomedicine*, vol. 14, no. 14, pp. 1857–1871, 2019, doi: 10.2217/nnm-2018-0299.

[180] M. K. Jones, B. Lu, S. Girman, and S. Wang, “Cell-based therapeutic strategies for replacement and preservation in retinal degenerative diseases,” *Prog. Retin. Eye Res.*, vol. 58, pp. 1–27, 2017, doi: 10.1016/j.preteyeres.2017.01.004.

[181] V. Raghavan, H. Subhash, A. Breathnach, M. Leahy, P. Dockery, and M. Olivo, “Dual plasmonic gold nanoparticles for multispectral photoacoustic imaging application,” *Photons Plus Ultrasound Imaging Sens. 2014*, vol. 8943, p. 89434J, 2014, doi: 10.1117/12.2042079.

[182] C. L. Bayer, Y. Chen, S. Kim, S. Mallidi, K. Sokolov, and S. Emelianov, “Multiplex photoacoustic molecular imaging using targeted silica-coated gold nanorods,” vol. 2, no. 7, pp. 6583–6588, 2011.

[183] S. Raveendran, H. T. Lim, T. Maekawa, M. Vadakke Matham, and D. Sakthi Kumar, “Gold nanocages entering into the realm of high-contrast photoacoustic ocular

imaging," *Nanoscale*, vol. 10, no. 29, pp. 13959–13968, 2018, doi: 10.1039/c8nr02866d.

[184] H. Kim *et al.*, "Doxorubicin-fucoidan-gold nanoparticles composite for dualchemo-photothermal treatment on eye tumors," *Oncotarget*, vol. 8, no. 69, pp. 113719–113733, 2017, doi: 10.18632/oncotarget.23092.

[185] J. S. Wi, J. Park, H. Kang, D. Jung, S. W. Lee, and T. G. Lee, "Stacked Gold Nanodisks for Bimodal Photoacoustic and Optical Coherence Imaging," *ACS Nano*, vol. 11, no. 6, pp. 6225–6232, 2017, doi: 10.1021/acsnano.7b02337.

[186] C. Langhammer, B. Kasemo, and I. Zorić, "Absorption and scattering of light by Pt, Pd, Ag, and Au nanodisks: Absolute cross sections and branching ratios," *J. Chem. Phys.*, vol. 126, no. 19, 2007, doi: 10.1063/1.2734550.

[187] V. P. Nguyen *et al.*, "Plasmonic Gold Nanostar-Enhanced Multimodal Photoacoustic Microscopy and Optical Coherence Tomography Molecular Imaging to Evaluate Choroidal Neovascularization," *ACS Sensors*, vol. 5, no. 10, pp. 3070–3081, 2020, doi: 10.1021/acssensors.0c00908.

[188] V. P. Nguyen *et al.*, "Chain-like gold nanoparticle clusters for multimodal photoacoustic microscopy and optical coherence tomography enhanced molecular imaging," *Nat. Commun.*, vol. 12, no. 1, pp. 1–14, 2021, doi: 10.1038/s41467-020-20276-z.

[189] T. Okamoto, H. Usuda, T. Tanaka, K. Wada, and M. Shimaoka, "The functional implications of endothelial gap junctions and cellular mechanics in vascular angiogenesis," *Cancers (Basel).*, vol. 11, no. 2, 2019, doi: 10.3390/cancers11020237.

[190] J. Folkman and Y. Shing, "Angiogenesis," *J. Biol. Chem.*, vol. 267, no. 16, pp. 10931–10934, 1992, doi: 10.1016/s0021-9258(19)49853-0.

[191] P. Carmeliet and R. K. Jain, "Angiogenesis in cancer and other diseases," *Nature*, vol. 407, no. 6801, pp. 249–257, 2000, doi: 10.1038/35025220.

[192] J. A. Nagy *et al.*, "Vascular permeability factor/vascular endothelial growth factor induces lymphangiogenesis as well as angiogenesis," *J. Exp. Med.*, vol. 196, no. 11, pp. 1497–1506, 2002, doi: 10.1084/jem.20021244.

[193] L. Lamalice, F. Houle, and J. Huot, "Phosphorylation of Tyr1214 within VEGFR-2 triggers the recruitment of Nck and activation of Fyn leading to SAPK2/p38 activation and endothelial cell migration in response to VEGF," *J. Biol. Chem.*, vol. 281, no. 45, pp. 34009–34020, 2006, doi: 10.1074/jbc.M603928200.

[194] L. Lamalice, F. Le Boeuf, and J. Huot, "Endothelial cell migration during angiogenesis," *Circ. Res.*, vol. 100, no. 6, pp. 782–794, 2007, doi: 10.1161/01.RES.0000259593.07661.1e.

[195] H. M. W. Verheul and H. M. Pinedo, "Vascular endothelial growth factor and its

inhibitors," *Drugs of Today*, vol. 39, no. SUPPL. C, pp. 81–93, 2003.

[196] B. I. Terman *et al.*, "Identification of the KDR tyrosine kinase as a receptor for vascular endothelial cell growth factor," *Biochem. Biophys. Res. Commun.*, vol. 187, no. 3, pp. 1579–1586, 1992, doi: 10.1016/0006-291X(92)90483-2.

[197] N. Ferrara, "Vascular endothelial growth factor: Basic science and clinical progress," *Endocr. Rev.*, vol. 25, no. 4, pp. 581–611, 2004, doi: 10.1210/er.2003-0027.

[198] M. J. Cross and L. Claesson-Welsh, "FGF and VEGF function in angiogenesis: Signalling pathways, biological responses and therapeutic inhibition," *Trends Pharmacol. Sci.*, vol. 22, no. 4, pp. 201–207, 2001, doi: 10.1016/S0165-6147(00)01676-X.

[199] C. W. Pugh and P. J. Ratcliffe, "Regulation of angiogenesis by hypoxia: Role of the HIF system," *Nat. Med.*, vol. 9, no. 6, pp. 677–684, 2003, doi: 10.1038/nm0603-677.

[200] N. Ferrara, "VEGF and intraocular neovascularization: From discovery to therapy," *Transl. Vis. Sci. Technol.*, vol. 5, no. 2, 2016, doi: 10.1167/tvst.5.2.10.

[201] W. L. Wong *et al.*, "Global prevalence of age-related macular degeneration and disease burden projection for 2020 and 2040: A systematic review and meta-analysis," *Lancet Glob. Heal.*, vol. 2, no. 2, pp. e106–e116, 2014, doi: 10.1016/S2214-109X(13)70145-1.

[202] L. K. Cheung and A. Eaton, "Age-related macular degeneration.," *Pharmacotherapy*, vol. 33, no. 8, pp. 838–855, 2013, doi: 10.1002/phar.1264.

[203] A. W. Stitt, N. Lois, R. J. Medina, P. Adamson, and T. M. Curtis, "Advances in our understanding of diabetic retinopathy," *Clin. Sci.*, vol. 125, no. 1, pp. 1–17, 2013, doi: 10.1042/CS20120588.

[204] R. Hennig and A. Goepferich, "Nanoparticles for the treatment of ocular neovascularizations," *Eur. J. Pharm. Biopharm.*, vol. 95, pp. 294–306, 2015, doi: 10.1016/j.ejpb.2015.02.027.

[205] L. E. H. Smith, "Pathogenesis of retinopathy of prematurity," *Growth Horm. IGF Res.*, vol. 14, no. SUPPL. A, pp. 140–144, 2004, doi: 10.1016/j.ghir.2004.03.030.

[206] K. M. Farjo and J. X. Ma, "The potential of nanomedicine therapies to treat neovascular disease in the retina," *J. Angiogenes. Res.*, vol. 2, no. 1, p. 21, 2010, doi: 10.1186/2040-2384-2-21.

[207] E. Duh and L. P. Aiello, "Vascular endothelial growth factor and diabetes: the agonist versus antagonist paradox," *Diabetes*, vol. 48, no. 10, pp. 1899–906, 1999, doi: 10.2337/diabetes.48.10.1899.

[208] R. D. Jager, W. F. Mieler, and J. W. Miller, "Age-Related Macular Degeneration," *N Engl J Med.*, vol. 358, no. 24, pp. 2606–17, 2008, doi: 10.1056/NEJMra0801537.

[209] P. A. Campochiaro, “Molecular Pathogenesis of Retinal and Choroidal Vascular Diseases,” *Prog Retin Eye Res*, vol. 49, pp. 67–81, 2015, doi: 10.1016/j.preteyeres.2015.06.002.

[210] A. Hellström, L. E. H. Smith, and O. Dammann, “Retinopathy of prematurity,” *Lancet*, vol. 382, no. 9902, pp. 1445–1457, 2013, doi: 10.1016/S0140-6736(13)60178-6.

[211] I. Bhutto and G. Lutty, “Understanding age-related macular degeneration (AMD): Relationships between the photoreceptor/retinal pigment epithelium/Bruch’s membrane/choriocapillaris complex,” *Mol Asp. Med.*, vol. 33, no. 4, pp. 295–317, 2012, doi: 10.1016/j.mam.2012.04.005.

[212] N. S. Abdelfattah *et al.*, “Clinical correlates of common corneal neovascular diseases: A literature review,” *Int. J. Ophthalmol.*, vol. 8, no. 1, pp. 182–193, 2015, doi: 10.3980/j.issn.2222-3959.2015.01.32.

[213] S. Feizi, A. A. Azari, and S. Safapour, “Therapeutic approaches for corneal neovascularization,” *Eye Vis.*, vol. 4, no. 1, pp. 1–10, 2017, doi: 10.1186/s40662-017-0094-6.

[214] Z. Sharif and W. Sharif, “Corneal neovascularization: updates on pathophysiology, investigations & management,” *Rom. J. Ophthalmol.*, vol. 63, no. 1, pp. 15–22, 2019, doi: 10.22336/rjo.2019.4.

[215] Z. F. Bashshur, A. Bazarbachi, A. Schakal, Z. A. Haddad, C. P. El Haibi, and B. N. Noureddin, “Intravitreal Bevacizumab for the Management of Choroidal Neovascularization in Age-related Macular Degeneration,” *Am. J. Ophthalmol.*, vol. 142, no. 1, pp. 1–9, 2006, doi: 10.1016/j.ajo.2006.02.037.

[216] S. B. Bressler, W. T. Beaulieu, and A. R. Glassman, “Factors Associated with Worsening Proliferative Diabetic Retinopathy in Eyes Treated with Panretinal Photocoagulation or Ranibizumab,” *Ophthalmology*, vol. 124, no. 4, pp. 431–439, 2017, doi: 10.1016/j.ophtha.2016.12.005.

[217] T. Pincus *et al.*, “Evidence from clinical trials and long-term observational studies that disease-modifying anti-rheumatic drugs slow radiographic progression in rheumatoid arthritis: Updating a 1983 review,” *Rheumatology*, vol. 41, no. 12, pp. 1346–1356, 2002, doi: 10.1093/rheumatology/41.12.1346.

[218] S. R. Montezuma, D. Vavvas, and J. W. Miller, “Review of the ocular angiogenesis animal models,” *Semin. Ophthalmol.*, vol. 24, no. 2, pp. 52–61, 2009, doi: 10.1080/08820530902800017.

[219] R. Bhattacharya, P. Mukherjee, Z. Xiong, A. Atala, S. Soker, and D. Mukhopadhyay, “Gold nanoparticles inhibit VEGF165-induced proliferation of HUVEC cells,” *Nano Lett.*, vol. 4, no. 12, pp. 2479–2481, 2004, doi: 10.1021/nl0483789.

[220] P. Mukherjee *et al.*, "Antiangiogenic properties of gold nanoparticles," *Clin. Cancer Res.*, vol. 11, no. 9, pp. 3530–3534, 2005, doi: 10.1158/1078-0432.CCR-04-2482.

[221] K. Kalishwaralal, S. Sheikpranbabu, S. Barathmanikanth, R. Haribalaganesh, S. Ramkumarpandian, and S. Gurunathan, "Gold nanoparticles inhibit vascular endothelial growth factor-induced angiogenesis and vascular permeability via Src dependent pathway in retinal endothelial cells," *Angiogenesis*, vol. 14, no. 1, pp. 29–45, 2011, doi: 10.1007/s10456-010-9193-x.

[222] Y. Pan, H. Ding, L. Qin, X. Zhao, J. Cai, and B. Du, "Gold nanoparticles induce nanostructural reorganization of VEGFR2 to repress angiogenesis," *J. Biomed. Nanotechnol.*, vol. 9, no. 10, pp. 1746–1756, 2013, doi: 10.1166/jbn.2013.1678.

[223] Y. Pan, Q. Wu, L. Qin, J. Cai, and B. Du, "Gold nanoparticles inhibit VEGF165-induced migration and tube formation of endothelial cells via the Akt pathway," *Biomed Res. Int.*, vol. 2014, 2014, doi: 10.1155/2014/418624.

[224] C. M. Chan, C. Y. Hsiao, H. J. Li, J. Y. Fang, D. C. Chang, and C. F. Hung, "The inhibitory effects of gold nanoparticles on VEGF-A-induced cell migration in choroid-retina endothelial cells," *Int. J. Mol. Sci.*, vol. 21, no. 1, 2020, doi: 10.3390/ijms21010109.

[225] R. R. Arvizo, S. Rana, O. R. Miranda, R. Bhattacharya, V. M. Rotello, and P. Mukherjee, "Mechanism of anti-angiogenic property of gold nanoparticles: Role of nanoparticle size and surface charge," *Nanomedicine Nanotechnology, Biol. Med.*, vol. 7, no. 5, pp. 580–587, 2011, doi: 10.1016/j.nano.2011.01.011.

[226] Y. J. Roh, C. R. Rho, W. K. Cho, and S. Kang, "The antiangiogenic effects of gold nanoparticles on experimental choroidal neovascularization in mice," *Investig. Ophthalmol. Vis. Sci.*, vol. 57, no. 15, pp. 6561–6567, 2016, doi: 10.1167/iovs.16-19754.

[227] R. Singh, J. C. Batoki, M. Ali, V. L. Bonilha, and B. Anand-Apte, "Inhibition of choroidal neovascularization by systemic delivery of gold nanoparticles," *Nanomedicine Nanotechnology, Biol. Med.*, vol. 28, p. 102205, 2020, doi: 10.1016/j.nano.2020.102205.

[228] N. Shen *et al.*, "Inhibition of retinal angiogenesis by gold nanoparticles via inducing autophagy," *Int. J. Ophthalmol.*, vol. 11, no. 8, pp. 1269–1276, 2018, doi: 10.18240/ijo.2018.08.04.

[229] W. K. Cho, S. Kang, H. Choi, and C. R. Rho, "Topically administered gold nanoparticles inhibit experimental corneal neovascularization in mice," *Cornea*, vol. 34, no. 4, pp. 456–459, 2015, doi: 10.1097/ICO.0000000000000343.

[230] B. Merchant, "Gold, the Noble metal and the paradoxes of its toxicology," *Biologicals*, vol. 26, no. 1, pp. 49–59, 1998, doi: 10.1006/biol.1997.0123.

[231] N. Pernodet *et al.*, “Adverse effects of citrate/gold nanoparticles on human dermal fibroblasts,” *Small*, vol. 2, no. 6, pp. 766–773, 2006, doi: 10.1002/smll.200500492.

[232] G. S. Terentyuk *et al.*, “Circulation and distribution of gold nanoparticles and induced alterations of tissue morphology at intravenous particle delivery,” *J. Biophotonics*, vol. 2, no. 5, pp. 292–302, 2009, doi: 10.1002/jbio.200910005.

[233] D. H. Jo, T. G. Lee, and J. H. Kim, “Nanotechnology and nanotoxicology in retinopathy,” *Int. J. Mol. Sci.*, vol. 12, no. 11, pp. 8288–8301, 2011, doi: 10.3390/ijms12118288.

[234] Y. Pan *et al.*, “Size-dependent cytotoxicity of gold nanoparticles,” *Small*, vol. 3, no. 11, pp. 1941–1949, 2007, doi: 10.1002/smll.200700378.

[235] W. H. De Jong, W. I. Hagens, P. Krystek, M. C. Burger, A. J. A. M. Sips, and R. E. Geertsma, “Particle size-dependent organ distribution of gold nanoparticles after intravenous administration,” *Biomaterials*, vol. 29, no. 12, pp. 1912–1919, 2008, doi: 10.1016/j.biomaterials.2007.12.037.

[236] G. Sonavane, K. Tomoda, and K. Makino, “Biodistribution of colloidal gold nanoparticles after intravenous administration: Effect of particle size,” *Colloids Surfaces B Biointerfaces*, vol. 66, no. 2, pp. 274–280, 2008, doi: 10.1016/j.colsurfb.2008.07.004.

[237] C. Lasagna-Reeves *et al.*, “Bioaccumulation and toxicity of gold nanoparticles after repeated administration in mice,” *Biochem. Biophys. Res. Commun.*, vol. 393, no. 4, pp. 649–655, 2010, doi: 10.1016/j.bbrc.2010.02.046.

[238] X. Huang, I. H. El-Sayed, W. Qian, and M. A. El-Sayed, “Cancer cell imaging and photothermal therapy in the near-infrared region by using gold nanorods,” *J. Am. Chem. Soc.*, vol. 128, no. 6, pp. 2115–2120, 2006, doi: 10.1021/ja057254a.

[239] T. Niidome *et al.*, “PEG-modified gold nanorods with a stealth character for in vivo applications,” *J. Control. Release*, vol. 114, no. 3, pp. 343–347, 2006, doi: 10.1016/j.jconrel.2006.06.017.

[240] G. Zhang *et al.*, “Influence of anchoring ligands and particle size on the colloidal stability and in vivo biodistribution of polyethylene glycol-coated gold nanoparticles in tumor-xenografted mice,” *Biomaterials*, vol. 30, no. 10, pp. 1928–1936, 2009, doi: 10.1016/j.biomaterials.2008.12.038.

[241] C. M. Goodman, C. D. McCusker, T. Yilmaz, and V. M. Rotello, “Toxicity of gold nanoparticles functionalized with cationic and anionic side chains,” *Bioconjug. Chem.*, vol. 15, no. 4, pp. 897–900, 2004, doi: 10.1021/bc049951i.

[242] B. B. Karakoçak *et al.*, “Biocompatibility of gold nanoparticles in retinal pigment epithelial cell line,” *Toxicol. Vitr.*, vol. 37, pp. 61–69, 2016, doi: 10.1016/j.tiv.2016.08.013.

[243] A. Hayashi, A. Naseri, M. E. Pennesi, and E. De Juan, “Subretinal delivery of immunoglobulin G with gold nanoparticles in the rabbit eye,” *Jpn. J. Ophthalmol.*, vol. 53, no. 3, pp. 249–256, 2009, doi: 10.1007/s10384-009-0655-x.

[244] J. H. Kim, J. H. Kim, K. W. Kim, M. H. Kim, and Y. S. Yu, “Intravenously administered gold nanoparticles pass through the blood-retinal barrier depending on the particle size, and induce no retinal toxicity.,” *Nanotechnology*, vol. 20, no. 50, p. 505101, 2009, doi: 10.1088/0957-4484/20/50/505101.

[245] E. Söderstjerna, P. Bauer, T. Cedervall, H. Abdshill, F. Johansson, and U. E. Johansson, “Silver and gold nanoparticles exposure to in Vitro cultured retina - Studies on nanoparticle internalization, apoptosis, oxidative stress, glial- and microglial activity,” *PLoS One*, vol. 9, no. 8, 2014, doi: 10.1371/journal.pone.0105359.

[246] S. J. Bakri, J. S. Pulido, P. Mukherjee, R. J. Marler, and D. Mukhopadhyay, “Absence of histologic retinal toxicity of intravitreal nanogold in a rabbit model,” *Retina*, vol. 28, no. 1, pp. 147–149, 2008, doi: 10.1097/IAE.0b013e3180dc9360.

[247] K. T. Kim, T. Zaikova, J. E. Hutchison, and R. L. Tanguay, “Gold nanoparticles disrupt zebrafish eye development and pigmentation,” *Toxicol. Sci.*, vol. 133, no. 2, pp. 275–288, 2013, doi: 10.1093/toxsci/kft081.

[248] J. L. Olson, R. Velez-Montoya, and N. Nghiem, “Intraocular Biocompatibility of Gold-Nanoparticles,” *J Nanomater Mol Nanotechnol*, vol. 2, no. 2, pp. 1–5, 2013, doi: 10.4172/2324-8777.1000111.

[249] A. Vaneev *et al.*, “Nanotechnology for topical drug delivery to the anterior segment of the eye,” *Int. J. Mol. Sci.*, vol. 22, no. 22, 2021, doi: 10.3390/ijms222212368.

[250] M. Azharuddin, S. Sahana, H. Datta, and A. K. Dasgupta, “Corneal penetration of gold nanoparticles - Therapeutic implications,” *J. Nanosci. Nanotechnol.*, vol. 14, no. 8, pp. 5669–5675, 2014, doi: 10.1166/jnn.2014.8884.